Università degli Studi di Padova
Department of Biomedical Sciences

School of Bioscience and Biotechnology
Curriculum: Biotechnology
XXV Cycle

STRUCTURAL AND FUNCTIONAL CHARACTERIZATION OF SARCOENDOPLASMIC RETICULUM Ca^{2+}-ATPases (SERCA)

Director of PhD School: Ch.mo Prof. Giuseppe Zanotti

Coordinator of the curriculum: Ch.mo Prof. Giorgio Valle

Supervisor: Ch.mo Prof. Giuseppe Zanotti

PhD candidate: Sara Giannetti

December 2012

CONTENTS

SUMMARY

Ca^{2+} is the most versatile among the second messengers and is responsible for controlling several cellular processes. From cell growth and proliferation to programmed cell death, its versatility is employed to regulate processes as diverse as muscle contraction, secretion, energetic metabolism and synaptic plasticity. Therefore, the involvement of calcium in controlling several aspects of cell physiology demands the use of a sophisticated mechanism based on a wide set of protein components (toolkit), able to use oscillations in calcium concentration as a signal to regulate a variety of *Ca^{2+}-sensitive processes.* Nonetheless, cells are unable to sustain prolonged increase of intracellular calcium. For this motif eukaryotic cells have evolved an efficient transport system (*Ca^{2+} homeostasis*) to maintain the intracellular concentration of calcium within a range 20-100 nM. As a response to a specific extracellular stimulus, a rapid increase of free Ca^{2+} (500-1000 nM) results in an immediate tissue specific cellular response, thanks to the ability of ***Ca^{2+}- binding proteins*** to bind calcium by the EF-hand motif and activate several downstream effectors involved in other signaling pathway. The coordinated removal of cytosolic free Ca^{2+} out of the plasma membrane and into internal organelles (ER/SR) via the ***PMCA*** pump (plasma membrane Ca^{2+}-ATPase) and the *Na^{+}/Ca^{2+}exchanger*, and via the ***SERCA*** pump (sarcoplasmic reticulum Ca^{2+}-ATPase) restores Ca^{2+} to its resting level.

The most specialized mechanism of coordination of calcium signaling network can possibly be found in skeletal muscle, where the increase in cytosolic Ca^{2+} results in muscle contraction and removal of Ca^{2+} induces muscle relaxation. Since in human about 70% of cytosolic Ca^{2+} returns to the sarcoplasmic reticulum (SR) and since it represents the major source of Ca^{2+} store, the SERCA pump is consequently involved in regulating the excitation-contraction coupled mechanism in skeletal and cardiac muscle.

The SERCA protein shares the catalytic properties of ion-motive ATPases of the P-type family, characterized by the formation of an energized intermediate, resulting from the auto-

phosphorylation of a key invariant aspartate residue in a highly conserved sequence. Basically, the P-type family members couple the active transport of ions across the membrane to the hydrolysis of ATP through a reaction cycle proposed more than 30 years ago, called *Post-Albers cycle*. With respect to other members of P-type family, the SERCA pump differs in tissue distribution, regulation, transport specificities and role in Ca^{2+} homeostasis. It is encoded by a family of three genes, SERCA 1, 2, 3 and its isoforms diversity is highly increased by alternative splicing of the transcripts, principally at the COOH-terminal. At present, more than 10 different SERCA isoforms have been detected at the protein level, but only the 3D structure of isoform 1a from rabbit has been determined.

The first X-ray crystal structure of SERCA solved by the group of Toyoshima about 13 years ago represents a milestone in the understanding of the molecular machine responsible for calcium pumping. It has established the basement for the building of all the following knowledge about the P-type ATPase family. Since then, crystallographers have worked very hard trying to elucidate the P-type pump catalytic cycle. In particular, two research groups (the groups of C. Toyoshima in Japan and P. Nissen in Denmark) have moved their efforts towards the understanding of the ATP-driven ion transport mechanism, producing and analyzing at atomic resolution (2,3-3 Å) the 3D crystals of several intermediates of SERCA1a. Their studies have opened the way to the recent advances in membrane proteins crystallography. In fact, about 44 crystal structures of rabbit SERCA1a, possibly mimicking all the conformational states of the enzyme cycle, have been so far deposited in the Protein Data Bank (PDB) and the three-dimensional structure of SERCA1a from rabbit skeletal muscle continues to be considered the archetype of the P-type ATPases family.

Since SERCA pumps play a key role in the regulation of calcium homeostasis, alteration of their activity has been investigated in relation to two human diseases associated with SERCA pump gene defects: the Brody's and Darier's disease. The former is a rare recessive muscular condition characterized by an exercise-induced impairment of muscle relaxation. The underlying cause for muscle contracture has been found to be associated to a SERCA

reduced activity, resulting from a defect in the gene coding for SERCA1a isoform (ATP2A1). Nonetheless, the origin of the SERCA deficiency is still controversial. The second genetic pathology known as Darier's disease is a rare autosomal dominant skin disorder characterized by loss of cell-to-cell adhesion and abnormal keratinization of the epidermis. More than 130 mutations in the gene coding for the SERCA2 isoforms (ATP2A2) have been identified in human patients. Differently from Brody's disease, the clinical symptoms are restricted to the epidermis and specific area of the skin and it is thought that this localization reflects genetic mosaicism.

Our structural contribution to the understanding of the effects of point mutations on the protein conformation come from the crystal structure of bovine SERCA pump, recently solved at 2.9 Å resolution. Since an R164H substitution has been identified in cows affected by congenital pseudomiotonia and a Hungarian patient affected by Brody's disease was found to carry the same mutation, this animal could be used as a suitable model for studying human pathology. In addition, this protein represents the first crystal structure of SERCA1a from a source different from rabbit.

The protein was extracted from a portion of *Cutaneus trunci* muscle and homogenized and solubilized with deoxycholate or C12E8 detergent. Crystals were obtained by using the hanging drop vapor diffusion technique and the structure solved by molecular replacement. X-ray data collection was performed at the European Synchrotron Radiation Facility (ESRF) in Grenoble, France. The crystallographic R factor of the refined final structure is 0.23. The overall molecular model is very similar to that of the rabbit enzyme, as expected by the high amino acid sequence identity. Nevertheless, the bovine enzyme has reduced catalytic activity with respect to the rabbit enzyme. Subtle structural modifications, in particular in the region of the long loop that protrudes into the SR lumen connecting transmembrane α-helices M7 and M8, explain the difference.

About the pathological mutant, since the mutation is located in the A domain of the pump, which is involved in large movements of the pump during its reaction cycle, it is

possible to speculate about the effect of the mutation on the protein conformation, on the basis of our structure. In the E1.AMPPCP state, the negatively charged Glu2 counterbalances the protonated side chain of Arg164 that acts as a central 'anchor point' for three different stretches of the A-domain fold. The substitution of the side chain of the arginine with the imidazole of the His residue could destabilize the conformation of the pump during the E1-E2 transition, probably enhancing the sensibility of the protein to proteolytic degradation.

Since the aim of my PhD project is the study of the SERCA pump gene defects responsible for human genetic disease, the SERCA 2a isoform represents another important target for our structural investigations. This protein is the major player involved in the regulation of the excitation-contraction coupling of the heart. Evidences from human and experimental models of heart failure have demonstrated that alterations in SR calcium handling are associated with an impaired contractility. Other evidences also seem to suggest that mutations of the isoform 2a may predispose to cardiac diseases. Recently, SERCA2a pump gene transfer was demonstrated to be safe and effective in restoring contractile function via over-expression of SERCA2a under physiological and patho-physiological conditions. The determination of the crystal structure of the SERCA2a could help to elucidate the molecular mechanisms responsible for Ca^{2+} signaling dysfunction as well as to design and study specific inhibitors of the heart SERCA2a enzyme.

In our work, the human SERCA2a was expressed in *Saccharomyces cerevisiae* as a recombinant protein with a biotin acceptor domain (BAD) linked to the C-terminus (hSERCA2a-BAD) by a thrombin cleavage site. Owing to the presence of a thrombin cleavage site within the protein sequence, a point mutant (R863G) was generated and the protein was successfully expressed. In vivo yeast biotinylation of BAD added as a tag to SERCA2a has offered both a fast and efficient affinity purification strategy and a positive selection of the properly folded enzyme. To obtain sufficient amount of protein to perform crystallization trials, a protocol for batch fermentation of *S. cerevisiae* was optimized in a home made bioreactor. The protein was solubilized with a buffer containing n-dodecyl β-D-maltoside

(DDM) at the appropriate CMC. Finally, the enzyme was purified by avidin-affinity strategy, using two different purification tools (the avidin resin and the avidin magnetic nanoparticles).

Finally, a new protein target has been the object of structural investigations: the EFhd2 calcium-binding protein. This protein represents a novel tau-associated protein identified in the JNPL3 tauopathy mouse model, which develops neurodegeneration in age-dependent manner. This evidence has been also validated in human affected by Alzheimer's disease, where the association between tau and the novel calcium-binding protein was found enhanced. The tau protein plays a key role in the appearance of tauophathies, which are described as a group of neurological disorders characterized by the aggregation of hyperphosphorylated and filamentous tau proteins organized in neurofibrillary tangles. Despite the tau phosphorylation process has been intensely studied, the molecular mechanism underlying the tau-mediated neurodegeneration is poorly understood. The identification of the new tau-associated protein EFhd2 and its structural characterization could help to elucidate the mechanisms responsible for tauopathies. In our work, the recombinant EFHD2 protein was expressed in *Escherichia coli* as a poly-histidine-tagged fusion protein. The protein has been purified, concentrated and used for crystallization trials. Despite diffracting crystals have not been obtained yet, preliminary tests appear quite promising.

RIASSUNTO

Il Ca^{2+} è il più versatile tra i secondi messaggeri ed è responsabile del controllo di numerosi processi cellulari. Dalla crescita e proliferazione cellulare alla morte programmata, la sua versatilità è impiegata per regolare diverse tipologie di processi quali la contrazione muscolare, la secrezione, il metabolismo energetico e la plasticità sinaptica. Il coinvolgimento del calcio nel controllo di diversi aspetti della fisiologia cellulare richiede, pertanto, l'utilizzo di un sofisticato meccanismo basato su un set di componenti proteici (toolkit), in grado di usare le oscillazioni nella concentrazione del calcio come segnale per regolare una varietà di processi Ca^{2+} sensibili (*Ca^{2+} sensitive processes*). Tuttavia, le cellule non sono in grado di sostenere incrementi prolungati di calcio intracellulare. Per questo motivo le cellule eucariote hanno evoluto un efficiente sistema di trasporto (*Ca^{2+} homeostasis*) per mantenere la concentrazione intracellulare di calcio entro un intervallo tra i 20-100 nM. In risposta ad uno stimolo extracellulare, un rapido incremento del Ca^{2+} libero (500-1000 nM) produce un'immediata risposta cellulare tessuto-specifica, grazie all'abilità delle *proteine che legano il calcio* (*Ca^{2+} sensitive proteins*) di attivare diverse proteine bersaglio coinvolte in altre vie di segnalazione, in seguito al loro legame attraverso il motivo strutturale a mani EF. La coordinata rimozione del Ca^{2+} citosolico fuori dalla membrana plasmatica e dentro gli organelli interni (ER/SR) attraverso la pompa PMCA (Ca^{2+}-ATPase della membrana plasmatica) e lo scambiatore Na^{+}/Ca^{2+} e attraverso la pompa SERCA (Ca^{2+}-ATPase del reticolo sarcoendoplasmatico) ripristina il livello basale del Ca^{2+}. Il più specializzato meccanismo di coordinazione della rete di segnalazione del calcio può essere probabilmente trovato nel muscolo scheletrico, dove un aumento della concentrazione del Ca^{2+} produce la contrazione muscolare mentre la sua rimozione induce il rilassamento muscolare. Poiché negli umani circa il 70% del Ca^{2+} citosolico ritorna nel reticolo sarcoplasmatico (SR) e poiché quest'ultimo rappresenta la maggiore riserva di Ca^{2+}, la pompa SERCA è conseguentemente coinvolta nella regolazione del meccanismo accoppiato di contrazione e rilassamento nel muscolo scheletrico e cardiaco.

La proteina SERCA condivide le proprietà catalitiche del motivo ionico della famiglia delle P-type ATPasi, caratterizzata dalla formazione di un intermedio fosforilato, derivante dall'autofosforilazione di un residuo di aspartato nella loro sequenza altamente conservata. In sintesi, i membri della famiglia P-Type accoppiano il trasporto attivo di ioni attraverso la membrana all'idrolisi dell'ATP tramite un ciclo di reazione proposto 30 anni fa, chiamato *Post-Albers cycle*. Rispetto agli altri membri, la pompa SERCA si differenzia per la sua distribuzione tissutale, la regolazione, la specificità e il ruolo nell'omeostasi del calcio. Essa è codificata da una famiglia di tre geni, SERCA 1, 2, 3 e la variabilità delle sue isoforme è legata ad uno splicing alternativo del trascritto primario, specialmente al COOH-terminale. Finora, più di 10 isoforme sono state identificate a livello proteico, ma solo la struttura tridimensionale dell'isoforma1a di coniglio è stata determinata.

La prima struttura cristallografica della SERCA, risolta dal gruppo di Toyoshima circa 13 anni fa, rappresenta una pietra miliare nella comprensione della macchina molecolare responsabile del trasporto attivo del calcio. Essa ha stabilito le basi per la costruzione di tutte le attuali conoscenze relative alla famiglia delle P-type ATP-asi. Da allora, i cristallografi hanno lavorato faticosamente nel cercare di chiarire il ciclo catalitico della pompa P-type. In particolare, due gruppi di ricerca (il gruppo di C. Toyoshima in Giappone e quello di Nissen in Danimarca) hanno mosso i loro sforzi verso la comprensione del meccanismo di trasporto ionico attivato dall'ATP, producendo e analizzando a livello atomico (2,3-3 A) le strutture cristallografiche di diversi intermedi della SERCA1a. I loro studi hanno aperto la strada ai recenti progressi nella cristallografia delle proteine di membrana. Infatti, circa 44 strutture della SERCA1a di coniglio, che cercano di simulare tutti gli stati conformazionali del ciclo enzimatico, sono state depositate nella Banca Dati Proteica (PDB) e la struttura tridimensionale della SERCA1a dal muscolo scheletrico continua ad essere considerata l'archetipo della famiglia della P-type ATPasi.

Poiché le pompe SERCA svolgono un ruolo chiave nella regolazione dell'omeostasi del calcio, variazioni nella loro attività proteica sono state identificate in due malattie umane

associate a difetti nei geni codificanti per la pompa SERCA: la malattie di Brody e di Darier. La prima è una rara e recessiva condizione muscolare caratterizzata da una riduzione nel rilassamento muscolare indotta dall'esercizio. La causa della contrattura è associata ad una riduzione nell'attività della SERCA, derivante da un difetto nel gene codificante l'isoforma 1a (ATP2A1). Tuttavia, l'origine di questa riduzione è ancora controversa. La seconda patologia genetica, nota come malattia di Darier, è un raro disturbo autosomico dominante della pelle, caratterizzato da un'assenza di adesione tra le cellule e un'anomala cheratinizzazione dell'epidermide. Sono state identificate più di 130 mutazioni nel gene codificante per le isoforme 2a (ATP2A2) in pazienti umani. A differenza della malattia di Brody, i sintomi clinici, ristretti all'epidermide e a specifiche aree della pelle, probabilmente riflettono un mosaicismo di tipo genetico. Il nostro contributo strutturale alla comprensione degli effetti delle mutazioni puntiformi sulla conformazione proteica deriva dalla struttura cristallografica della pompa SERCA1a bovina, recentemente risolta a 2.9 Å di risoluzione. Poiché una mutazione da arginina a istidina nella posizione 164 è stata identificata in una mucca affetta da pseudo miotonia congenita e la stessa mutazione è stata identificata in un paziente ungherese affetto dalla malattia di Brody, questo animale potrebbe essere usato come modello compatibile allo studio delle patologie umane.

La proteina è stata estratta da una porzione del muscolo *Cutaneus trunci*, che è stato omogeneizzato e solubilizzato con i detergenti deossicolato e C12E8. I cristalli proteici sono stati ottenuti tramite la tecnica dell'hanging drop con il metodo della diffusione di vapore e la struttura è stata risolta con il metodo della sostituzione molecolare. La raccolta dei dati cristallografici è stata eseguita nella struttura del sincrotrone europeo (ESRF) a Grenoble, Francia. Il fattore cristallografico R del modello strutturale raffinato è 0.23. Nel complesso il modello è simile a quello dell'enzima di coniglio, come atteso dall'alta identità della sequenza amminoacidica. Tuttavia, l'enzima bovino mostra una ridotta attività catalitica rispetto a quella del coniglio. Qualche piccola modificazione, in particolare nella regione del loop che protrude

nel lume del reticolo sarcoplasmatico e che connette le α-eliche M7 e M8, potrebbe spiegare la differenza.

Riguardo alle forme patologiche, poiché la mutazione è localizzata nel dominio A della pompa, cruciale nel ciclo di reazione, sulla base della nostra struttura è stato possibile fare delle speculazioni sugli effetti che la mutazione potrebbe produrre sulla conformazione proteica. Nello stato E1- AMMPPCP, il residuo di acido glutammico carico negativamente controbilancia la catena laterale protonata dell'Arg164 che agisce come perno centrale per tre differenti stiramenti del dominio A. La sostituzione della catena laterale dell'arginina con l'imidazolo del residuo d'istidina potrebbe destabilizzare la conformazione della pompa durante la transizione tra gli stadi E1-E2, aumentando probabilmente la suscettibilità della proteina alla degradazione proteolitica.

Poiché lo scopo del mio progetto di dottorato è lo studio dei difetti genici responsabili delle malattie umane, l'isoforma SERCA2a rappresenta un altro importante bersaglio dei nostri studi strutturali. Questa proteina svolge un ruolo chiave nella regolazione del meccanismo accoppiato di contrazione e rilassamento del muscolo cardiaco. Risultati ottenuti da pazienti colpiti da infarto cardiaco e da modelli sperimentali hanno dimostrato che alterazioni nella regolazione del flusso di calcio sono associate a una ridotta contrattilità. Altre evidenze sembrano, inoltre, suggerire che alcune mutazioni nell'isoforma2a possono predisporre a malattie cardiache. Recentemente, la terapia di trasferimento genico della SERCA2a si è dimostrata sicura ed efficace nel ripristinare la funzione contrattile del cuore, attraverso l'over espressione della SERCA2a in condizioni fisiologiche e pato-fisiologiche. La determinazione della struttura cristallografica della SERCA2a potrebbe quindi aiutare a chiarire i meccanismi molecolari responsabili della disfunzione nel processo di segnalazione del calcio, così come aprire la possibilità di identificare e studiare gli inibitori proteici specifici per la SERCA2a.

Nel nostro lavoro, l'isoforma2a umana è stata espressa in *Saccharomyces cerevisiae* come proteina ricombinante con un dominio accettore di biotina (BAD) legato al C-terminale (hSERCA2a-BAD) da un sito di taglio per la trombina. Poiché quest'ultimo era presente anche

dentro la sequenza proteica, una mutazione puntiforme (R863G) è stata generata e la proteina è stata espressa con successo. In vivo, la biotinilazione del BAD aggiunto come sito "bersaglio" alla SERCA2a ha offerto sia una veloce ed efficiente strategia di purificazione che una selezione positiva dell'enzima propriamente foldato. Per ottenere una sufficiente quantità di enzima purificato in modo da realizzare prove di cristallizzazione, in un reattore costruito in laboratorio, è stato ottimizzato un protocollo per la fermentazione in batch in *S. cerevisiae*. La proteina è stata quindi solubilizzata in un tampone con DDM alla appropriata concentrazione critica micellare. Alla fine, l'enzima è stato purificato attraverso la purificazione per affinità all'avidina, usando due differenti sistemi di purificazione (avidina coniugata alla resina e nano particelle rivestite di avidina).

Per finire, un nuovo target è stato oggetto dei nostri studi strutturali: la proteina che lega il calcio EFHD2. Questa rappresenta una nuova proteina associata alla tau che è stata identificata nel modello sperimentale di topo (JNPL3), specifico per lo studio delle tauopatie. Il modello sperimentale sviluppa infatti neuro degenerazione in maniera dipendente dagli anni. Questa evidenza è stata anche riscontrata in pazienti affetti da Alzheimer, nei quali è risultata più elevata l'associazione tra la tau e la EFHD2. La proteina tau svolge un ruolo chiave nella comparsa delle tauopatie, che sono descritte come un gruppo di malattie neurologiche caratterizzate dall'aggregazione di proteine tau iperfosforilate e filamentose, organizzate in gomitoli di neurofibrille. Nonostante il processo di fosforilazione sia stato studiato intensivamente, il meccanismo molecolare alla base della neuro degenerazione mediato dalla tau è ancora poco studiato. L'identificazione della nuova proteina EFhd2 associata alla tau e la sua caratterizzazione strutturale potrebbero aiutare a chiarire i meccanismi responsabili delle tauopatie. Nel nostro lavoro, la proteina ricombinante EFhd2 umana è stata espressa in *E. coli* come proteina di fusione con un tag di istidine. La proteina è stata purificata, concentrata e usata per le prove di cristallizzazione. Nonostante non siano ancora stati ottenuti cristalli diffrangenti, le prove preliminari appaiono veramente promettenti.

CHAPTER I

INTRODUCTION

CONTENTS

1.1 CALCIUM SIGNALING

Cells need to communicate to survive. During the evolution, multi-cellular organisms have adopted sophisticated mechanisms to generate and elaborate information through messengers carrying primary signals to cells (***first messengers***) and decoding their information inside them (***second messengers***) (Carafoli, 2001). Ca^{2+} is among the most versatile second messengers, since it triggers a wide range of spatial and temporal intracellular signals. Thanks to its abilities to alter local electrostatic fields and protein conformations of specific molecular targets, it controls several cellular processes (Clapham, 1995). From cell growth and proliferation to programmed cell death, its versatility is employed to regulate processes as diverse as muscle contraction, secretion, energetic metabolism and synaptic plasticity during learning and memory (Berridge, 1997).

To coordinate each of these functions, Ca^{2+} signal must be efficiently and precisely controlled. Two broad classes of specialized proteins perform this task, the **Ca^{2+} buffer and the Ca^{2+} sensor proteins**. Both of them bind calcium with great specificity and affinity in intracellular environment maintaining its cytosolic concentration around 100 nM (Brini, Carafoli, 2009). Nonetheless, they play a different role in the Ca^{2+} signaling network. The former includes intrinsic membrane proteins that move calcium ions across the membrane, modulating the Ca^{2+} signal both spatially and temporally. They belong to several subclasses of Ca^{2+}-pumps and exchangers that differ in affinity for Ca^{2+} and transport mechanisms. Since they control Ca^{2+} concentration without processing its message, they are named ***Ca^{2+} buffer proteins***. On the contrary, Ca^{2+} sensor proteins decode the intracellular Ca^{2+} signal into several cellular responses and are generally characterized by a helix–loop–helix structural motif termed the EF-hand. These proteins belong to the EF-hand *Ca^{2+}- binding proteins family* that contains over 600 members.

The functional relationship between all these proteins suggests a sophisticated Ca^{2+} signaling mechanism based on a wide set of protein components (toolkit), able to work in

cooperation to ensure the punctual and exact transmission of Ca^{2+} signal inside the cell. This toolkit is also able to interact with other signaling pathway. Thanks to the plurality of combination that can be generated, different cell types can select a unique set of components in order to create their own appropriate system of calcium signaling (Berridge, 2003). Finally, the accurate combination and the precise assembly of this extensive Ca^{2+} signaling toolkit and its interaction with other signaling pathway allows calcium signal to play a pivotal role in cell biology (Berridge, 2000).

1.1.1 HOW DOES THE Ca^{2+}-SIGNAL WORK?

Considering a single functional unit, for instance a non-stimulated cell, the distribution of calcium signal can be easily depicted in terms of concentration varying in time. In fact, in resting cells the intracellular concentration of calcium is maintained within the range 20-100 nM. A rapid increase of Ca^{2+} through the coordinated opening of specific **Ca^{2+}-channels** on the plasma membrane (*VOCs: voltage-operated channels; ROCs: receptor-operated channels; SOCs: store-operated channels; see keywords for definitions)* and by its release from internal stores (*ER/SR*) through the **Ca^{2+}-release channels** results in an immediate cellular response that depends on cell type and context (Berridge, 2003).

Two families of intracellular calcium channels control the release of calcium from internal stores: the ryanodine receptor (*RyR*) and the inositol 1,4,5-triphosphate receptor (I*nsP$_3$R*) families. Several second messengers derived from the activation of different signaling pathway on the plasma membrane activate them. Nonetheless, the primary activator of these channels is the calcium itself through the auto-regulatory mechanism known as Ca^{2+}-induced Ca^{2+}-release (*CIRC*). This positive feedback system converts an elementary signal event in a global calcium response (*Ca^{2+} transient*), responsible for controlling of diverse types of cellular processes (Berridge, 1997). As a consequence, signals from several cellular pathways can activate and modulate one or more cellular processes. In our case, thanks to the ability of *Ca^{2+}- binding proteins* to bind calcium by the EF-hand motif and activate several

downstream effectors involved in other signaling pathway, the calcium signal is able to modulate a variety of *Ca^{2+}-sensitive processes* that operate over a wide temporal spectrum.

Nonetheless, cells are unable to sustain an extensive and persistent increase of calcium concentration. Prolonged elevation of cytosolic Ca^{2+} result in mitochondrial overloading, activation of proteases, and activation of DNA-fragmenting enzymes. To avoid these cytotoxic effects, eukaryotic cells have evolved an efficient transport system to maintain adequate intracellular concentration of calcium, the so-called Ca^{2+} homeostasis. This mechanism results from the coordinated removal of cytosolic Ca^{2+} out of the plasma membrane and into internal organelles (ER/SR). The main proteins involved in the control of Ca^{2+} homeostasis are: the *Na^{+}/Ca^{2+}exchanger* and the *PMCA* pump (plasma membrane Ca^{2+}-ATPase) on the plasma membrane, and the *SERCA* pump (sarcoplasmic reticulum Ca^{2+}-ATPase) responsible for the calcium reuptake into the sarcoplasmic reticulum (SR). As a result, the perfect balance between the entry of calcium in the cytoplasm and the constant removal either by its extrusion across PM or by its storage in the sarcoplasmic allows cells to use oscillation in calcium concentration as a signaling mechanism to regulate and coordinate each instant of cellular life.

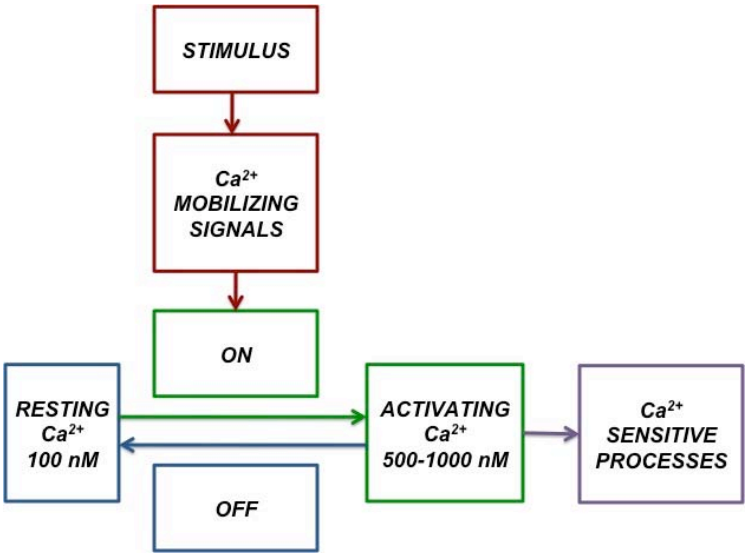

Fig 1. Schematic representation of functional units of Ca^{2+} signaling network. Adapted from, Berridge, M. et al, 2000.

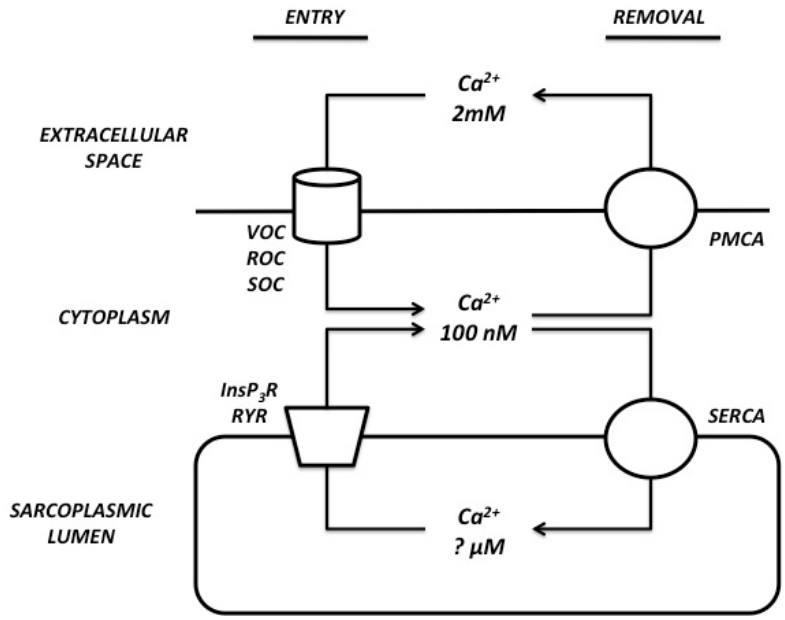

Fig. 2. Schematic representation of Ca^{2+} signaling toolkit. Intracellular Ca^{2+} homeostasis is achieved by balancing the entry and removal of Ca^{2+}ion. VOC, voltage-operated channels; ROC, receptor operated channels; SOC, store-operated channels; $InsP_3Rs$, inositol 1,4,5-trisphosphate receptors; RyRs, ryanodine receptors, PMCA, plasma membrane Ca^{2+}-ATPase; SERCA, sarcoplasmic reticulum Ca^{2+}-ATPase. Adapted from Berridge, M. et al, 1997.

1.1.2 THE CORE OF CALCIUM SIGNALING NETWORK

The most specialized mechanism of coordination of calcium signaling toolkit can possibly be found in skeletal muscle, where the L-type Voltage-Operated Channels are directly coupled to the RYR1, so that the transmission of Ca^{2+}-signal occurs by an allosteric variation of protein conformations (Tsugorka et a1996; Klein et al.1996). Consequently, the membrane depolarization causes the release of calcium from SR through the well-known *Ca^{2+}-induced Ca^{2+}-release* mechanism. This increase in calcium concentration is recognized by specific *Ca^{2+}-sensors* in skeletal muscle: the *TroponinC* (TpC) and the *Calmodulin (CaM).* They are considered prototypes of the *Ca^{2+} binding protein family.* Both of them have four EFhand structural motifs for binding calcium and they regulate different steps of the excitation-relaxation coupled mechanism. The TpC controls the key event of muscle contraction, the myosin-actin interaction. This is locked by the presence of tropomyosin-troponin complex, which is removed in response to conformational changes of troponin as a consequence of the

calcium binding. In this way, the actin-binding site becomes available and myosin can move on filaments at the expense of ATP hydrolisis. On the other hand, CAM stimulates the enzyme phosphorylase kinase to ensure a parallel increase in ATP production via mitochondria, confirming the thesis that the same cell can use different sensors to regulate separately coordinated processes. Reuptake of cytosolic calcium into SR by SERCA pump and removal to the extracellular space by NCX and PMCA pump results in muscle relaxation. This mechanism is more conserved in other type of eukaryotic cells such as heart cells, where in response of membrane depolarization a small amount of calcium enters through the L-type channel and actives the release from internal store through RYR2. A proportion of this Ca^{2+} travels through the mitochondria, and during this time it stimulates the metabolism to provide the ATP that is necessary to maintain contraction.

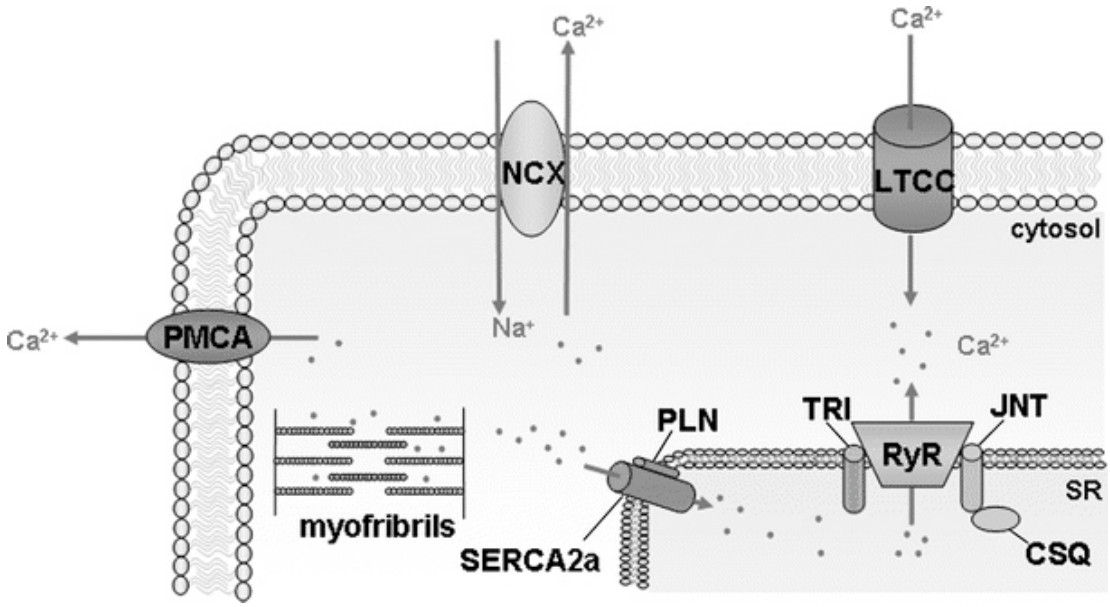

Fig. 3. Schematic representetion of the major players implicated in exitation-contraction coupling of the heart. L-type Ca^{2+} channel (LTCC), the ryanodine receptor (RyR), the sarco(endo)plasmic reticulum Ca^{2+} ATPase (SERCA2a) pump and the plasma-membrane Ca^{2+} ATPase (PMCA) and the Na^{+}/ Ca^{2+} exchanger (NCX). PLN phospholamban, JNT junction, TRI triadin, CSQ calsequestrin. Adapted from Vafiadaki, E. et al, 2008.

1.2 THE SERCA PUMP

1.2.1 THE P-TYPE ATPASE FAMILY

In mammals, three calcium pumps have been described: the sarcoplasmic reticulum (SERCA), plasma membrane (PMCA) and the Golgi network (SPCA) pumps. All three pumps belong to the P-type ATPases family, characterized by the formation of an energized intermediate, resulting from the auto-phosphorylation of a key invariant aspartate residue in a highly conserved sequence: S**D**KTGTLT.

A sequence alignment of four main representatives of the family from unrelated organisms (Kuhlbrandt, 2004) shows conserved regions in cytoplasmic domains, such as the site where the phosphorylated intermediate is formed, the ATP-binding pocket, and the region involved in the dephosphorylation of the enzyme. Despite the low degree (15%) of general identities, these conserved regions are structurally and functionally significant and are conserved throughout the P-type ATP-ase family. In addition to these features, the family members share the essential properties of membrane topology (from 6 to 11 transmembrane helices, where the ion-binding sites are located) and reaction mechanism, but they can differ in regulation processes, inhibition mechanisms and transport specificities. Basically, they couple the active transport of ions across the membrane to the hydrolysis of ATP through a reaction cycle proposed more than 30 years ago. Originally, the cycle was described as two distinct conformational states, based on the different affinity of the enzyme for transported ions: E1 state (high affinity, faced on cytoplasm) and E2 state (ion low affinity, faced on extracellular space) (Albers, 68). Later, kinetic data showed that the energy required for the coupling of hydrolytic and vectorial transport processes resulted from two phosphorylated intermediate states: E1~P (high-energy intermediate) and E2-P (low-energy intermediate) (Whittam, 1970).

Based on kinetics data observed from Na^+/K^+-ATPase experiments, Post and Albers (Albers, 1967; Post et al., 1969) proposed a general ion-translocation cycle of P-type ATPases.

According to the model (see box1), phosphorylation and dephosphorylation processes exclusively occurred when the enzyme was linked to Na^+, and to K^+ respectively, while the ion movement across the membrane took place during the E_1-P to E_2-P and the E_2 to E_1 transitions, simultaneously. In this way, the right sequence of molecular events, whereby the pump transported ions at the expense of ATP, were described. Nonetheless, these evidences were insufficient to reconstruct with reasonable confidence the molecular mechanisms that convert the chemical energy, derived from ATP hydrolysis, into a vectorial transport, or to describe this processes at the atomic detail. Finally, the molecular understanding of the ATP-driven ion transport mechanism had a turning point thanks to the determination of the three-dimensional structure of SR Ca^{2+}-ATPase (SERCA) from rabbit skeletal muscle, which is now considered the archetype of the P-type ATPases (Toyoshima, 2000).

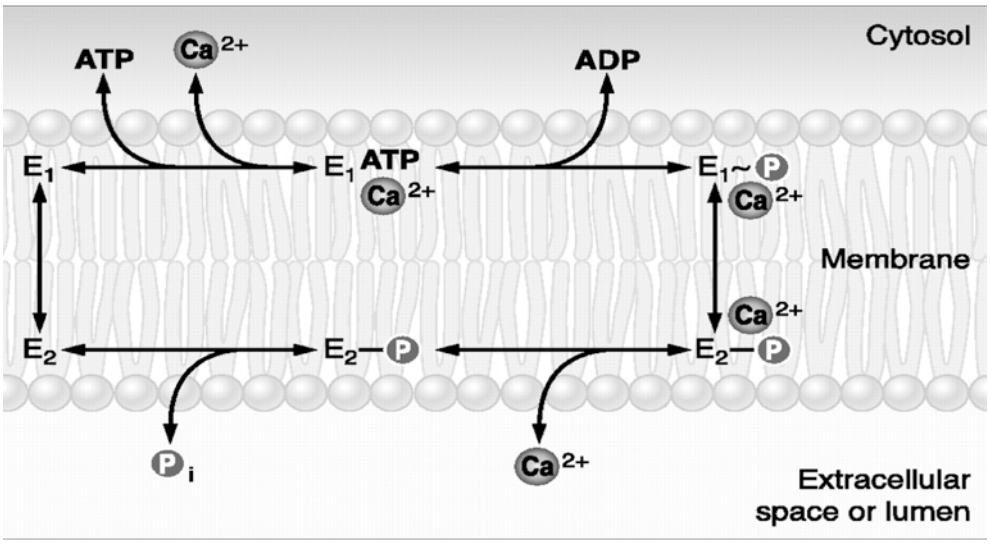

Fig. 4. The Post-Albers cycle. The catalytic cycle can be described as follow: in the E1 state, the high affinity ion-binding site is accessible from cytoplasm. Ca^{2+} binding triggers the phosphorylation of the catalytic D-residue by the Mg^{2+} coordinated g-phosphate of ATP and the subsequent transition to the E1~P state. This is one of the rate-limiting steps of the cycle, and under favorable conditions the intermediate can transfer the phosphoryl group back to ADP. The fast transition to the E2-P state induces the Ca^{2+} release into the extracellular site. At this point, the ion-binding site has a high affinity for H^+, which can bind from the outside. The next hydrolysis of the enzyme regenerates the conformation E2 and the dissociation of the inorganic phosphate and magnesium reverts to the E1 state, where the H^+ is release into the cells. The free ion-enzyme can thus start and another cycle. Taken from Brini, M. et al, 2010.

1.2.2 *ISOFORMS OF THE SERCA PUMP*

In mammals, a family of three conserved genes, SERCA 1, 2, and 3, encodes three main SERCA pumps and the alternative splicing at the COOH-terminal of transcripts enhances the number of protein variants. Developmentally alternative splicing of SERCA1 gene results in two transcript variants encoding different isoforms: the SERCA1a and SERCA1b proteins, which are expressed in adult and in neonatal fast-twitch skeletal muscle, respectively. For the SERCA2 gene, a tissue-dependent processing of primary transcript is responsible for the expression of two main isoforms: the SERCA2a and the SERCA2b proteins. The first is expressed predominantly in cardiac and slow-twitch skeletal muscle, while the second is considered the housekeeping isoform, because it is expressed at low levels in muscle and non-muscle cells. Another variant of the SERCA 2 gene (SERCA2c) has been found in human monocytes and fetal heart. Finally, six possible variants (a-f) of SERCA3 gene have been described, but only 3 isoforms (a-c) have been detected in humans at protein level. These latter are expressed in a number of non-muscle cells. The expression pattern of SERCA isoforms, which changes during development and tissue differentiation, suggests that each SERCA isoform plays a specific function inside the tissue in which it is expressed. In addition, some regulatory molecules of the SERCA pump could enhance these functional differences.

1.2.3 *SERCA REGULATORY PROTEINS*

Two endogenous molecules modulate the activity of the SERCA pump: phospholamban (PLB) and sarcolipin (SLN), which are expressed in cardiac and skeletal muscles, respectively. While the mechanism of action of PLB on SERCA is well characterized, that of SLN only begins to be understood.

Phospholamban is a small protein of only 52 amino acids, which has been found on the SR membrane in two different conformations: the unphosphorylated PLB monomer of 6 kDa, responsible for the SERCA pump inhibition, and the phosphorylated PLB homopentamer of about 22kDa working as a reservoir. Each monomer has been predicted to be divided into

two wide domains: a hydrophilic domain (amino acids residues 1-30), which contains the regulatory sites, and a hydrophobic domain (amino acids 31-52), which is anchored into the cardiac sarcoplasmic reticulum membrane. Detailed cross-linking and site-direct mutagenesis studies have identified the interaction sites between the PLB and the SERCA protein. The first interaction was identified by the cross-linking of Lys3 in the PLN domain to the Lys397 and Lys400 of the sequence KDDKPV in the cytosolic N domain of the SERCA pump (James, P., 1989). This sequence is conserved in the SERCA 1 and 2 proteins and probably is responsible for the exclusion of SERCA 3 isoforms from the PLB inhibitory system. The second site has been found in specific residues of the PLN trans-membrane domain (28-52 residues) that are responsible for the pump inhibition, reducing its apparent calcium affinity. This inhibitory function of trans-membrane domain has been found using PLB molecules in which the cytosolic domains were deleted, suggesting that PLN-SERCA trans-membrane interaction has a key inhibitory role (Kimura, Y., 1996).

The homologue of PLN is Sarcolipin (SNL) that exclusively inhibits the SERCA1a isoform in skeletal muscle cells. From sequence alignment, the trans-membrane domain of SLN shares nearly 30% identity with that of phospholamban (PLN), confirming its role as an inhibitory site. Recent observations have demonstrated that SLN is co-expressed with SERCA2a in model cells and this is related to a super-inhibition of the pump. In addition, NMR studies have suggested that the two regulatory proteins bind to SERCA in a similar manner. However, the physiological significance of the SERCA pump regulation by SLN remains to be elucidated.

1.2.4 REGULATION OF SERCA2A ACTIVITY

As mentioned, PLN is the major regulator of SERCA2a activity and so far is the only one that was proven to be involved in cardiac development, including heart failure. The PLN-mediated inhibition of SERCA2a is finely regulated by phosphorylation of three distinct phosphorylation sites (Ser 10, Ser 16, Thr 17) in the regulatory domain of PLN, which are controlled by three different protein kinases (protein kinase C (PKC), cAMP-dependent protein kinase (PKA) and Ca^{2+}-calmodulin protein kinase (CaMKII). Phosphorylation of each

residue is related to an increase in SERCA2a activity as a result of the association of PLB monomers into pentamer. On the other end, dephosphorylation via protein phosphatase I (PPI) restores the inhibitory effects of PLN on SERCA2a. This results in a decrease in Ca^{2+} affinity as a consequence of SERCA2a/PLN interaction, which stabilizes the enzyme in the E2 conformation, causing the inhibition and the aggregation of the pump. The activity of the SERCA pump is modulated by β adrenergic signalling pathway through the phosphorylation of inhibitor I via protein kinase A. Adrenaline and other β-agonists initiate an important signal-transduction pathway, where the increase in the cAMP concentration activates cAMP-dependent protein kinase (PKA), which then phosphorylates and alters the function of a few cardiac proteins. In fact, the serine16 site appears to be the most important mediator to enhance cardiac contractility and has been suggested to be the main regulator of the activity of phospholamban.

1.3 STRUCTURAL PROPERTIES OF SERCA PUMP. A DETAILED OVERVIEW

1.3.1 E1 VERSUS E2: THE FIRST STEPS INSIDE THE MOLECULAR UNDERSTANDING OF REACTION CYCLE

Since the first prediction of the structure of the SR Ca^{2+}-ATPase (SERCA) has been proposed more than 20 years, a huge number of biochemical and mutational analyses have been accumulate to clarify the molecular aspects of the reaction cycle and the region involved in the enzymatic catalysis. From this scenario, the SERCA emerged like an integral membrane protein of about 110 KDa, consisting of three cytoplasmic domains joined to a group of 10 transmembrane (TM) helices (M1-M10) by a short *stalk* segment (MacLennan et al., 1985; Brandl et al., 1986; Taylor and Green, 1989). The critical residues for Ca^{2+} binding and those for ATP hydrolysis, identified by mutagenesis studies, have been located in the middle of the transmembrane helices (Clarke et al., 1989; Chen et al., 1996), and in the cytoplasmic domain between the M4 and M5 helices (Maruyama et al., 1989; Clarke et al., 1990a; Vilsen et al., 1991), respectively. A number of biochemical data have been collected to propose a structural arrangement of the ATP binding pocket (Taylor and Green, 1989),

formed by two distinct domains connected by a hinge. A smaller cytoplasmic domain between M2 and M3 has been postulated to be responsible for the coupling of ATP hydrolysis to ion transport (Andersen et al., 1989; Clarke et al., 1990b).

All these data have been completed and confirmed by the description of the first X-ray crystal structure of Ca^{2+}-bound SERCA at 2.6 Å resolution, solved by Toyoshima's group (Toyoshima, C. et al, 2000). It has represented a milestone in the understanding of the molecular machine responsible for the calcium pumping and it has put the basement for the building of all the following knowledge about the P-type ATPase family. SERCA crystal structure has confirmed the general architecture of the pump, consisting in three cytoplasmic domains, N (nucleotide binding), P (phosphorylation residue), and A (actuator), and 10 transmembrane helices (M1-M10) surrounding two calcium-binding site.

In the crystallographic structure of **Ca-E1** state three cytoplasmic domains are well separated to form an *open headpiece*, in which the central part of the cytoplasmic region is occupied by domain P, containing the conserved phosphorylation residue (Asp351). Around this site, the residues critical for ATP hydrolysis is clustered, forming a highly negatively charged surface, accessible to the solvent. The domain N is the largest of the three cytoplasmic domains, and contains the nucleotide-binding site (Phe 487). Domain A, the so-called *actuator domain*, is the smallest of the three and is connected to the M1-M3 trans-membrane helices by long flexible loops. In addition, it contains another signature sequence of P-type ATP-ase family, the TGES motif. The two Ca^{2+} binding sites (I and II) are indeed embedded side by side in the trans-membrane domain. Site I is located in the space between helices M5 and M6, with contribution from M8 at a rather distal position; the side chain oxygen atoms of Asn768, Glu771 (M5), Thr799, Asp800 (M6) and Glu908 (M8) contribute to this site, in agreement with mutational studies. Site II is formed almost on helix M4 by the main-chain carbonyl oxygen atoms of Val304, Ala305 and Ile307 (M4) and the side-chain oxygen atoms of Asn796, Asp800 (M6) and Glu309 (M4) (8). The M4 and M5 helices are the largest of trans-membrane domain and their cytoplasmic moiety are directly connected to

the catalytic core of the P-domain. In fact, the M5 helix is considered the backbone of the SERCA structure.

Surprisingly, the long distance between the nucleotide-binding and phosphorylation sites (25 Å), and that between the phosphorylation and ion-binding sites in the membrane (about 45 Å) opened unsolved questions about the molecular mechanism that couple the phosphorylation process to the calcium release. How does the ATP binding on the N domain transfer the phosphate to the Asp351 located in another domain? And how can this reaction be associated with the calcium release in the lumen of sarcoplasmic reticulum? As the P domain present structural similarity with the catalytic core of haloacid dehalogenase, it was suggested that a possible rearrangement of the overall structure, in the presence of Ca^{2+}, could shape an N/P domain interface where the phosphorylation process can take place. As a consequence of this interaction, the A domain could transmit the mechanical signal to the trans-membrane domain, that in turn releases the Ca^{2+} bound in the SR lumen.

Structural evidences, resulting from the comparison of this structure with a low-resolution electron density map of the same enzyme in the vanadate-inhibited E2–P conformation (Zhang, P., 1998), have suggested that rigid-body rearrangements of cytoplasmic domains take place during active transport, in agreement with biochemical data. This interpretation was finally confirmed by the crystal structure of Ca^{2+} free SR Ca^{2+}-ATPase in the thapsigargin-stabilized E2 state, solved at 3.1Å resolution (Toyoshima, 2002). With respect to Ca^{2+}-bound E1 molecular model, it displays a different arrangement of the three cytoplasmic domains, organised as a *compact headpiece*, and large-scale rearrangements of six trans-membrane helices (M1-M6), ensuring the Ca^{2+} release into the SR lumen. The latter also generates a pathway for the entry of new calcium ions from the cytoplasmic side.

1.3.2 E1-P PHOSPHO-INTERMEDIATE STRUCTURES AS A RESPONSE TO ATP-BINDING SITE CONTROVERSY

Biochemical studies had well established that the catalytic cycle of SERCA pump takes place through two phosphorylated intermediates and that the energy demanded for ion-translocation results from the hydrolysis of a phospho-intermediate enzyme. Structures in E1

and E2 states have confirmed the general architecture of the pump and postulated a possible reaction mechanism, whereby rearrangements of three cytoplasmic domains is mechanically transmitted to the trans-membrane domain in order to release the calcium into the SR lumen, as response to phosphoryl transfer. On the other hand, they have also sparked a debate about the structural basis of the ATP binding pocket and have left unsolved the molecular understanding of mechanisms that couple the phosphoryl transfer reaction to the Ca^{2+} occlusion in the E1-P state.

The first structural evidence that tried to bridge these gaps resulted from two crystal structures of SERCA, solved by Nissen's group at 2.6 and 2.9 Å, respectively: the Ca^{2+} bound SERCA (**Ca_2E1-AMPPCP**) in complex with a non-hydrolysable ATP analogue, AMPPCP [adenosine (β-γ methylene)-triphosphate], and that (**Ca_2E1-ADP:AlF_4^-**) in complex with adenosine diphosphate plus aluminium fluoride, an inorganic phosphate analogue (Sorensen, 2004). They mimic the conformational state of the enzyme with the ATP bound and the transition state of phosphoryl transfer, respectively. The overall conformation of the pump in these two forms is almost the same, except for local adjustments at the catalytic site, and is characterized by tight association of cytoplasmic domains linked to the transiently occlusion of Ca^{2+} bound in trans-membrane region, as it was suggested by biochemical data. Structural comparison of Ca_2-E1 and Ca_2-E1-AMPPCP molecular models enabled to enter into atomic details of these cytoplasmic rearrangements, showing how the binding of ATP to the invariant residue Phe487 results in the assembling of the nucleotide-binding pocket, by a 90° rotation of the N domain toward the P domain. This rearrangement brings the 576-581 loop of the N domain close to the 720-725 loop of the P domain in order to form a crevice, where the 155-160 loop of the A domain can insert, as response to a subsequent rotation of 45°. As the A domain is joined to trans-membrane helices M1-M3, this rotation results in two coordinated effects that occlude the Ca^{2+} bound in the trans-membrane domain: the stretching of the M2 helix towards the cytoplasm, and the bending of the M1 in a parallel position to the membrane surface (kink at Leu60), respectively. Local differences in coordination of the

AMPPCP and AlF_4^- analogues at the catalytic core enabled to identify critical residues for nucleotide binding, suggesting a possible chemical reaction mechanism for the phosphoryl transfer, in agreement with mutational data. As the nucleotide-binding pocket is assembled at the interface between the N and P domains, as a response to the π stacking interaction between aromatic rings of adenine and Phe487, three Arginine (489, 560, 687) residues stabilize the α- and β-phosphate groups of AMPPCP in a bent conformation. The γ-phosphate, far 3 Å from Asp351, is in turn stabilized both by the coordination of Mg^{2+} with the carbonyl of Thr353 and the side chains of Asp703 and Asp351 plus two water molecules, and by the side chains of Lys684, Thr353 and Thr625 as well as by the main chain of Gly626. On the other hand, in the Ca_2E1-ADP:AlF_4^- structure another Mg^{2+} ion takes part in the stabilization of the α- and β-phosphates of ADP at the nucleotide binding pocket. The planar aluminium fluoride molecule bridges between the β-phosphate and the side chain of Asp351, modifying the interactions of the amino acid residues involved in phosphoryl transfer, by the coordination of two Mg^{2+} ions. Surprisingly, bonding distances (~2 Å) of the atoms that cross-link aluminium with β-phosphate and Asp351 oxygen atoms are in agreement with the hypothesis of a possible nucleophilic reaction mechanism (SN2) that was finally suggested to be responsible for the aspartyl-phosphorylated intermediate formation.

In addition, Toyoshima's group published the crystal structure of Ca^{2+} bound SERCA in a complex with AMPPCP (**E1•AMPPCP**) at 2.9 Å in the same year (Toyoshima, 2004). In this paper, the structure is very similar to that previously described, but the authors used evidences derived from structural superimposition to emphasize the role of ATP as the primary modifier of the protein conformation, and those of Glu309, as the gating residue responsible for cytoplasmic occlusion of transmembrane Ca^{2+} binding-site. By the superimposition of the E1*2Ca^{2+} and E1*AMPPCP conclusions about the protein rearrangements that mediated interactions between cytoplasmic and transmembrane domains were drawn, suggesting a mechanism for the occlusion of the cytoplasmic gate.

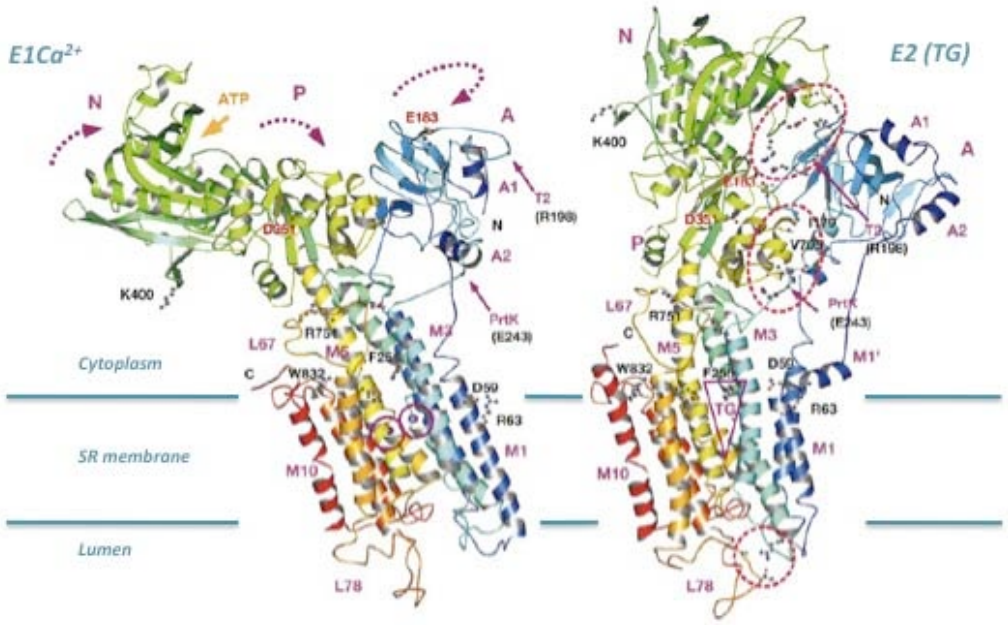

Fig. 5. Structural comparison between E1Ca^{2+} and E2(TG) structures. Colours change from the amino terminus (blue) to the carboxy terminus. In E1Ca^{2+}, two Ca^{2+} ions are shown as purple spheres, whereas in E2(TG) red cycles indicate extra hydrogen bound. Purple arrows in E1Ca^{2+} represent the direction of rearrangements of cytoplasmic domains during the transition from E1 to E2 states. Adapted from Toyoshima, C. et al 2002.

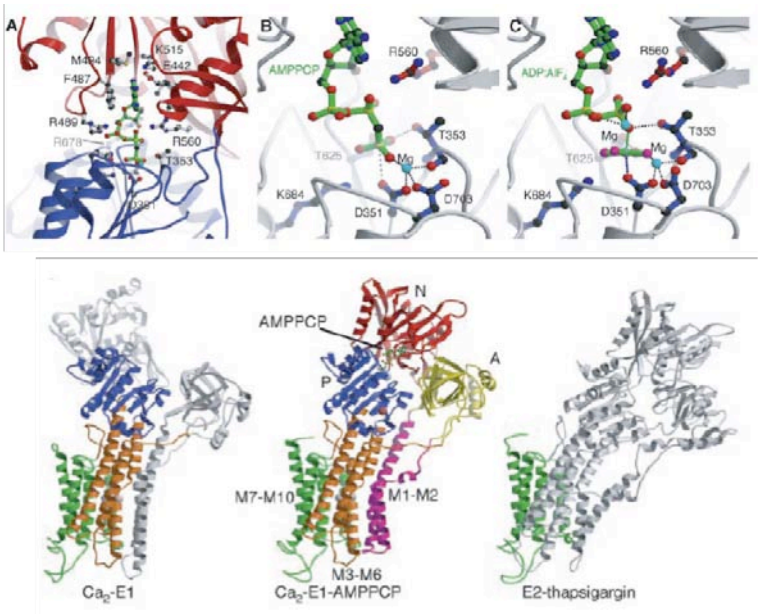

Fig. 6. Coordination of the two types of nucleotide analogues by Mg^{2+} (A, B, C). Comparison of E1AMP-PCP SERCA1a structure with the E1Ca^{2+} form and the E2TG form (D). Adapted from Sørensen, T. L.-M. et al, 2004.

1.3.3 E2-P PHOSPHO-INTERMEDIATE STRUCTURES AND THE CATALYTIC CYCLE IS COMPLETED

Structural evidence about low energy intermediates involved in Ca^{2+} release and counter-transport arrived immediately after. In 2004, Toyoshima presented the crystal structure of Ca^{2+}-free rabbit SERCA (**E2-MgF_4^{2-}**) in a complex with magnesium fluoride, a stable phosphate analogue, and tapsigargin (TG), an inhibitor, at 2.3 Å resolution (Toyoshima, 2004). This structure can be considered to represent the E2-P state of the enzyme after the hydrolysis of aspartyl-phosphate, but before the release of the inorganic phosphate. With respect to the Ca^{2+}-bound E1-AlF_4*ADP structure, solved by the same group in the same years, this molecular model shows a tight association between the A and P domains as result of the A domain rotation by 110° around an axis perpendicular to the membrane. Consequently, rearrangements of six (M1-M6) transmembrane helices destroy the high affinity Ca^{2+} binding site and open the luminal gate, formed by M1 and M2 helices. The drastic change with respect to the earlier structures is related to the release of ADP from the nucleotide-binding pocket. This dissociation modifies the N and P domains interactions, creating a space for the subsequent insertion of the A domain by the TGES signature loop. The latter now contributes to the coordination between Mg^{2+} and aspartyl-phosphate, avoiding the dephosphorylation of the enzyme. The trans-membrane helices linked to the A domain, in particular M1 and M2, reflect these cytoplasmic rearrangements pushing on M5 and M4. This movement result in the release of Ca^{2+} bound into the lumen, as a consequence of two coordinated effects: the destruction of the high affinity conformation of the Ca^{2+} binding site, as a consequence of the bending of M5 towards M1 and of one turn of M4 α-helix, and the opening of its luminal gate. The role of the A domain, as the actuator of transmembrane gate, was clarified once again.

In the same work, the **E2-MgF_4^{2-}** molecular model was superimposed to that of E2 (TG) structure in order to clarify the molecular rearrangements that take place during the E2-P→E2 transition. The most important evidence was found in the trans-membrane domain. Particularly, the structure around the Ca^{2+}-binding sites was found hardly changed, as a

response to a further tilting of the A domain by 30° caused by the release of Mg^{2+}. The lumenal half of the M4 helix (M4L) is turned by ~20° in E2(TG) and shows a change in the orientation of the loop containing Glu309 that closes the luminal gate. Finally, a schematic reaction of the complete cycle based on five representative crystal structures has been proposed.

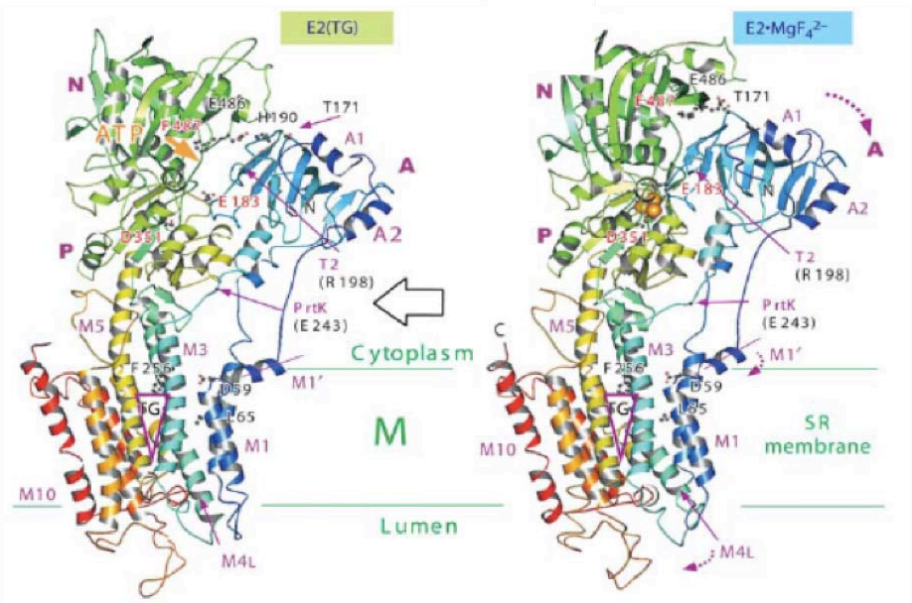

Fig. 7. Structural comparison between E2TG and E2-MgF42- structures. Colours change from the amino terminus (blue) to the carboxy terminus. In both the structures, thapsigargin is represented as purple ttriangle. Purple arrows in E2-MgF42- represents the direction of A domain rearrangement during the transition from E2-P to E2 states. Adapted from Toyoshima, C. et al, 2004.

1.3.4 INSIGHT INTO THE TRANSPORT MECHANISM COUPLED TO ATP HYDROLYSIS

To understand the dephosphorylation mechanism that concludes the ATP hydrolysis, in 2004 Nissen et al. determined the crystal structure of the proton-bound E2 rabbit SERCA, stabilized by aluminum fluoride (AlF_4^-) and tapsigargin (TG), at 3Å resolution (Olesen, C. et al, 2004) With respect to the other stable phosphate analogue (MgF_4^{2-}), the coordination of residues involved in the phosphorylation process was quite different, demonstrating that the **E2-AlF_4^-** structure represent the transition state of the low energy phospho-enzyme (E2-P) with occluded cation-binding sites in a protonated state. (E2-P→E2-P: H2O→E2 transition).

Compared to **$Ca_2E1{\sim}ADP{:}AlF_4^-$**, the phosphorylated residue (Asp351) in the **$E2{-}AlF_4^-$** structure interacts with the TGES motif of the A domain, as a consequence of an A domain rotation by 110° due to the ADP release. The phosphate analogue coordination with the carboxyl group of Glu183 and the main chain carbonyl of Thr181 *via* a water molecule is in agreement with the associative SN2 reaction proposed for dephosphorylation, confirming Glu183 as a catalytic base, able to extract a proton from a water molecule. Its subsequent attack to the phosphate group is in agreement with mutational data. A similar associative reaction mechanism has been proposed also for the phosphoryl transfer from ATP and represents the key element for explaining the coupling mechanisms of SERCA. It restricts the field of possible conformational states in which the phospho/dephosphorylation reactions could occur.

In addition, structural rearrangements of the enzyme in the **$E2{-}AlF_4^-$** molecular model with respect to those in **$Ca_2E1{\sim}ADP{:}AlF_4^-$** revealed the important role of the A domain as the actuator of the translocation/dephosphorylation coupled mechanism. Rearrangements of a five helices cluster, formed by the residues of the C-terminal part of the P-domain and by A-M2 and A-M3 chains and the corresponding segments of the A-domain, together with the K^+ ion bound at Glu732 (Levy, D. et al, 1990) were found critical for coupling the Ca^{2+}/H^+ exchange and the dephosphorylation events. Evidences about occluded protons could not be observed directly, because the atomic interactions with the tapsigargin inhibitor produced a structural artifact, but the were deduced from several biochemical data. For instance, the four carboxylate residues involved in the ion-conducting pathway (Glu771, Asp800, Glu908 and Glu309) seem to be in a protonated state, resulting in a hydrophobic barrier that could explain the occlusion of the luminal gate. Moreover, these residues are separated from the luminal space by five positive charged residues (Lys297, Lys958, Lys972, Lys960, arg290) that probably inhibit the backflow of luminal Ca^{2+} by electrostatic repulsion.

On the basis of structural analysis and biochemical data, the authors proposed a general mechanism of Ca^{2+} transport and H^+ counter-transport coupled to phosphorylation

and dephosphorylation, respectively, focused on the transient formation of occluded ion-binding sites, controlled by the piston-like movements of the A domain. Two gates faced on cytoplasm and sarcoplasmic lumen, respectively, were identified. Structurally, the formation of a high-energy phospho-enzyme intermediate was related to that of the occluded intermediate with Ca^{2+} bound in the trans-membrane domain as a result of the cytoplasmic gate locking. Release of ADP induces the opening of the luminal gate with subsequent Ca^{2+}/H^{+} exchange. Finally, the hydrolysis reaction closes the luminal gate, occluding the H^{+} inside the membrane; the subsequent release of the inorganic phosphate opens the cytoplasmic gate for the H^{+}/Ca^{2+} exchange.

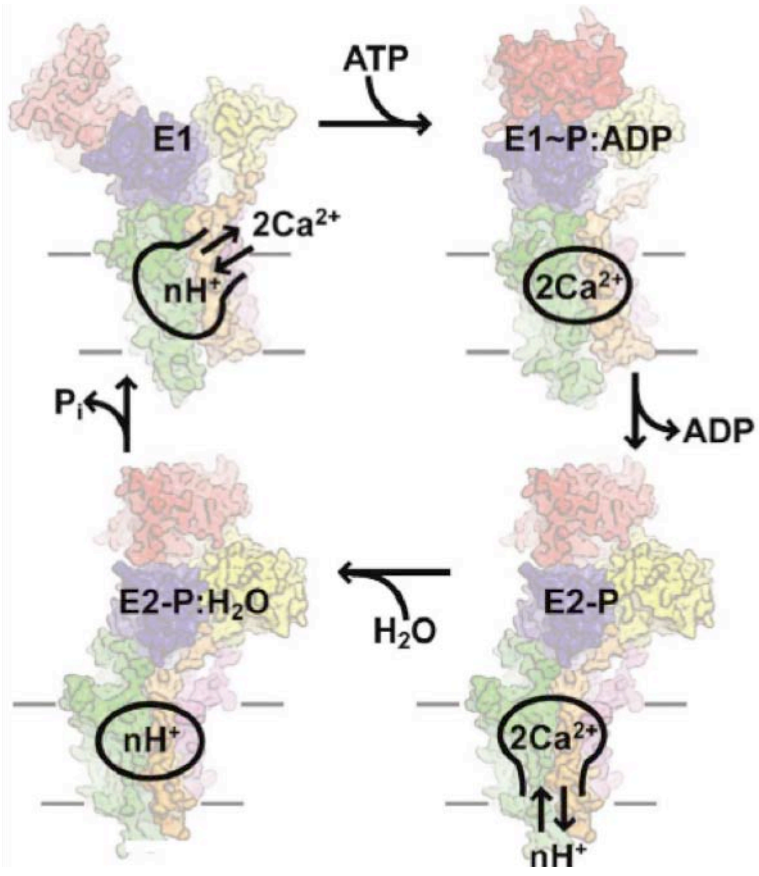

Fig. 8. Schematic representation of general mechanism of Ca^{2+} transport and H^{+} counter-transport coupled to phosphorylation and dephosphorylation, respectively, on the basis of key functional intermediates of SERCA. Red, N domain; blue, P domain; yellow, A domain; purple, transmembrane segments 1 and 2 (M1–M2) with their cytosolic extensions; orange, M3–M4; green, M5–M10. Taken from Moller, J. P. et al, 2005.

1.4 THE HUMAN SERCA PUMPS GENE MUTATIONS

Two human diseases associated with the SERCA pump gene defects have been described until now, Brody's and Darier's disease. The former is a rare recessive muscular condition characterized by an exercise-induced impairment of muscle relaxation (Brody IA, 1969). The underlying cause for muscle contracture has been found to be associated to a SERCA reduced activity, resulting from a defect of the gene coding for SERCA1a isoform (ATP2A1). Nonetheless, the origin of the SERCA deficiency is still controversial (Karpati G, 1986; Benders AAGM, 1994). Clinically, the diagnosis is made difficult owing to the genetic heterogeneity of the symptoms. Originally, three mutations have been identified in the ATP2A1 gene of Brody myopathy-affected members families as responsible for the pathology. These mutations lead to premature stop codons, truncating the pump and thus deleting essential domains (Odetterman A. et al, 1996), or to a missense substitution of Pro789 to Leu (Odetterman A. et al, 2000). However, all these data seem to agree with the suggestion that the reduction in the SERCA1a activity could be compensated at cellular level by the expression of the isoforms 2 and 3 in fast-twitch skeletal muscle and/or by the coordinated Ca^{2+} removal out of the plasma membrane via the PMCA pump and Na^{+}/Ca^{2+} exchanger (Brini et al, 2010). Recently, a mutation leading to the R164H replacement in the gene coding for the SERCA1a protein has been identified in cattle belonging to the Chianina family affected by congenital pseudomyotonia (PMT) (Sacchetto et al, 2009). This mutation induces symptoms very similar to those of the Brody syndrome, suggesting that this animal can be used as a suitable model for studying human pathology. The SERCA1a protein content has been found to be significantly reduced in the affected muscle despite the mRNA was present in equivalent amounts with respect to wild-type counterpart. This evidence could suggest that a defect in transcription is not involved in the aetiology of the disease. Since the mutation is located in the A domain of the pump, which is involved in large movements of the pump during its reaction cycle, the replacement of R with H side chain could destabilize the conformation of the pump during the E1-E2 transition, probably enhancing the vulnerability

of the protein to proteolytic degradation (Sacchetto et al, 2012). In addition, a Hungarian patient affected by Brody's disease was found to carry a missense mutation in the same position of the protein sequence. This evidence once again confirms Chianina cattle as a model for studying this genetic disease.

The second genetic pathology associated with SERCA pump gene mutations is known as Darier's disease. This is a rare autosomal dominant skin disorder characterized by loss of cell-to-cell adhesion and abnormal keratinization of the epidermis (REF). The clinical phenotype is characterized by persistent eruption of kerotopic papules in seborrhoic regions and flexures, palmitar pits and nail dystrophy. More than 130 mutations in the gene coding for the SERCA2 isoforms (ATP2A2) have been identified in human patients. These mutations have a widespread distribution and they are principally located in regions that are common to the 2a and 2b isoforms. Differently from Brody's disease, the clinical symptoms are restricted to the epidermis and specific area of the skin and it is thought that this localization reflects genetic mosaicism. The classical genotype reported in three families affected by Darier's disease is heterozygous for a mutation located in a region that is specific for SERCA2b. This mutation leads to premature stop codons that result in a misfolded and inactive pump. There is not evidence about possible compensation for its expression, and the suppression in SERCA2b activity is able to determine skin disorders (Brini et al, 2012). Although it not very clear how the loss of SERCA function causes Darier's disease, significant advances have been made in elucidating the molecular basis of this disorder during the last decade. Because of the wide genetic variability found in family members that exhibit differences in the clinical severity of the disease, probably other genes or environmental factors could influence the expression of the pathology.

1.5 THE EF-HAND AS THE STRUCTURAL MOTIF OF THE CA^{2+}-BINDING PROTEINS FAMILY

As described in this chapter, the effectors of the Ca^{2+} signaling network are represented by Ca^{2+}-binding proteins, which respond to changes in the intracellular calcium concentration

by associating and activating several downstream proteins involved in different signaling pathway. Calmodulin represents a well-characterized example of a calcium “sensor”. Moreover, Ca^{2+}-binding proteins can exhibit a modulator role, spatially and temporally controlling the cytoplasmic Ca^{2+} concentration. The calbindin D9K protein is a classical calcium “buffer” example. Anyway, these two classes of proteins are linked through a common structural feature, the EF-hand motif. This motif represents an evolutionary choice related to the possibility of playing several functions at low energy cost. According to the general consensus, Ca^{2+}-induced conformational changes represent one of the hallmarks of the signal transduction. This property is strictly related to the ability to bind Ca^{2+} through an EF-hand structural motif: the latter is defined by its helix-loop-helix secondary structure as well as by the loop that binds the Ca^{2+} ion. This motif is conserved among the members of a large and functionally diverse protein family, which owes its name to it. The structural unit of these proteins consist of two helices of about 10 amino acids, linked by a loop of 12 amino acid residues that coordinates the Ca^{2+} binding ion. Some sequence variability can be only tolerated in the region not involved in Ca^{2+} binding. The most canonical EF-hand Ca^{2+}-binding loop starts with an invariant aspartic acid and ends with a glutamic acid. Seven oxygen atoms organized in a pentagonal bypyramid form the preferred co-ordination geometry of calcium ions. The side chains of four conserved residues located at the vertices of an octahedron in position 1, 3, 5, and 12 provide the oxygen residues, with a double contribution from the carboxyl group of the Glu residue in the last position of the loop. The carbonyl oxygen of variable residues at position 7 along with the side chain oxygen of a glutamic acid in position 9 or a water oxygen contribute to the remaining two coordinating atoms. This Ca^{2+} coordination scheme characterizes the canonical EF-loop, which characterizes the majority of the EF-hand proteins. Variations in the ways the pentagonal bypyramidal coordination is achieved characterize the non-canonical EF-hand loops that have been found in a variety of family members. The EF-hand motifs always occur in pairs and the helix-loop-helix motif can be repeated from 2 to 12 times. The smallest functional EF-hand unit is dimeric, where the

two structural motifs are stabilized by an antiparallel β-sheet formed between the two loops and by numerous hydrophobic contacts between the helices. Binding of Ca^{2+} further stabilizes the structure in a four-helix bundle, formed by a hydrophobic core and a hydrophilic surface that make contacts with solvent molecules. The two EF-hands in the domain are not identical, as suggested by the preferential formation of a stable heterodimer. However, an approximate 2-fold symmetry axis relates them. Structural additions to the N-terminus of the Ca^{2+}-binding domain and modifications of the length and composition of the linker connecting the two EF-hands enhance the structural variability within the protein family. In addition, the organization of the EF-hand domains in a protein increases the level of diversity.

1.5.1 SWIPROSIN-1/EFHD2 AND SWIPROSIN-2/EFHD1

Recently a new class of EF-hand proteins has been described. According to their respective gene symbols, it has been proposed to refer to Swiprosin-1/EFhd2 and Swiprosin-2/EFhd1 as EFhd2 and EFhd1, respectively. These proteins are related to another EF-hand protein, allograft inflammatory factor-1. Secondary structure predictions for both proteins suggest disordered regions at the N-terminus, potential SH3-domain binding sites, two EF-hands motifs and a coiled-coil domain at the C-terminus. Despite the predicted overall structure is similar (about 65% of sequence identity), they exhibit a significant difference in a stretch of 60 amino acids close to the EF-hand motif, which probably is responsible for specify distinct functions of EFhd2 and EFhd1. These proteins have been identified both in nervous and immune cell lines, but until now there are not evidences about a possible interaction between the two proteins. Several functions have been proposed for them, but until now none of them is supported by conclusive evidence. The EFhd2 protein was proposed to act as a cytoskeleton associated adaptor protein involved in immune and brain cell function under basal and inflammatory conditions (Dutting et al, 2011). Other evidences draw the attention on the possible role of EFhd2 as a mediator of BCR-induced apoptosis (Avramidou et al. 2007). On the other end, the EFhd1 protein is involved in neuronal differentiation, probably through an association with mitochondria. Furthermore, EFhd1 could be part of a cellular

response to the oxidative stress (Dutting et al, 2011). However, the physiological role of these proteins is so far poorly understood and several investigators are trying to elucidate their involvement in pathological dysfunctions.

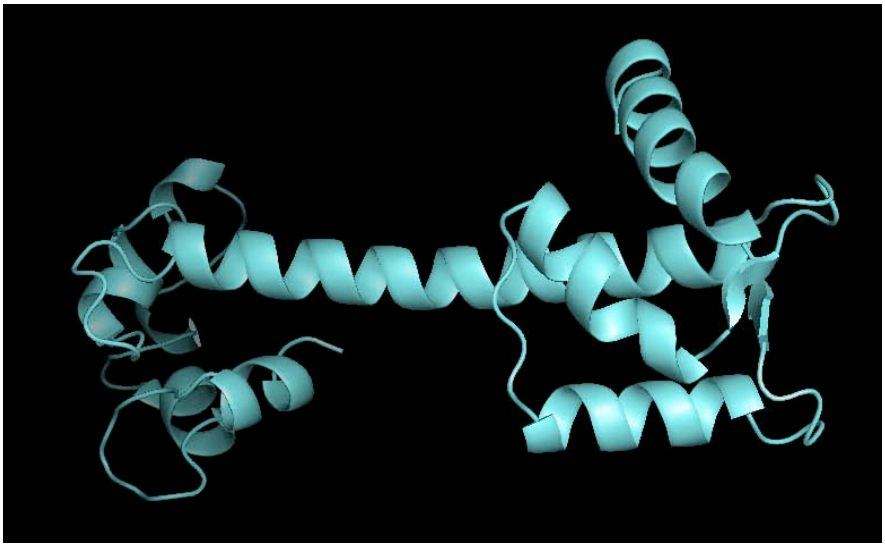

Fig. 9. Secondary structure prediction of Swiprosin-1/EFhd2. This prediction suggests disordered regions at the N-terminus, potential SH3-domain binding sites, two EF-hands motifs and a coiled-coil domain at the C-terminus.

CHAPTER II

CRYSTAL STRUCTURE OF ENDOPLASMIC RETICULUM CA^{2+}-ATPASE (SERCA) FROM BOVINE MUSCLE

ROBERTA SACCHETTO, ILENIA BERTIPAGLIA, SARA GIANNETTI, LAURA CENDRON, FRANCESCO MASCARELLO, ERNESTO DAMIANI, ERNESTO CARAFOLI AND GIUSEPPE ZANOTTI

Journal of Structural Biology 178 (2012) 38-44

CONTENTS

2.1 INTRODUCTION

The Ca^{2+}-ATPase of sarco(endo)plasmic reticulum (SERCA pump, E.C. 3.6.3.8) is a protein of about 110 kDa (MacLennan et al., 1985). It transports two Ca^{2+} ions from the cytoplasm to the lumen of the sarcoplasmic reticulum at the expense of the hydrolysis of one ATP molecule (for a review, see Brini and Carafoli, 2009). The mechanism of the transport has been explained in terms of a cycle characterized by two major conformational states, called E1 and E2. Conformation E1, which is the form with the highest affinity for calcium, binds Ca^{2+} from the cytoplasm, whilst conformation E2, which has lower affinity for the ion, releases it into the lumen (De Meis and Hasselbach, 1971).

The three-dimensional structure of SERCA1a, the isoform present mainly in fast twitch skeletal muscle, was solved by Toyoshima et al. (2000), and has been extensively characterized in rabbit: 44 crystal structures, possibly mimicking all the conformational states of the enzyme cycle, have been deposited in the Protein Data Bank (PDB) (Toyoshima and Nomura, 2002; Xu et al., 2002; Toyoshima and Mizutani, 2004; Sorensen et al., 2004; Obara et al., 2005; Jensen et al., 2006; Olesen et al., 2007; Takahashi et al., 2007; Moncoq et al., 2007; Laursen et al., 2009; Winther et al., 2010; Toyoshima et al., 2011). The protein consists of three cytoplasmic domains, called A, N and P, and a domain M, which includes the transmembrane helices and the short luminal loops. Domain A is referred to as the actuator domain of Ca^{2+} binding and release. The N domain contains the nucleotide-binding site. Domain P includes Asp351, the residue that is phosphorylated during the reaction cycle. The nucleotide is bound in between domains N and P, in such a way that its γ-phosphate is close to Asp351. The two Ca^{2+}-binding sites are located in α-helices M4, M5, M6 and M8 of domain M. The three cytoplasmic domains undergo a drastic rearrangement following aspartate phosphorylation, an event that is the key to Ca^{2+} release into the lumen (Toyoshima and Inesi, 2004).

SERCA structures of species different from rabbit are not known, and in this paper we present the structure of the Ca^{2+}-ATPase from bovine muscle. Our interest in the bovine

enzyme stems from the work in progress in our laboratory on spontaneous SERCA pump mutations responsible for genetic diseases in cows (Sacchetto et al., 2009). The bovine ATPase is a protein of 993 amino acids that shares 98% sequence identity with the rabbit enzyme. Despite the very high similarity, the bovine pump has a lower catalytic activity with respect to the rabbit SERCA. Here we describe the crystal structure of bovine SERCA and try to correlate this reduced activity to the molecular model.

2.2 MATERIALS AND METHODS

2.2.1 PROTEIN EXTRACTION, PURIFICATION AND CRYSTALLIZATION

The *cutaneus trunci* muscle was used as a representative bovine fast-twitch skeletal muscle (Totland and Kryvi, 1991). Sarcoplasmic reticulum microsomes were prepared according to the method previously described by De Meis and Hasselbach (1971). Partially purified Ca^{2+} pump protein was obtained by partial extraction of sarcoplasmic reticulum vesicles with low concentration of deoxycholate, according to the method described by Meissner et al., (1973). To obtain E1 Ca^{2+}-ATPase protein, this preparation was solubilized in 22 mg/ml octaethyleneglycol mono-*n*-dodecyl ether ($C_{12}E_8$) in 88 mM MOPS-KOH pH 6.8, 70 mM KCl, 17% glycerol (v/v), 10 mM $CaCl_2$, 3 mM $MgCl_2$, 1mM AMPPCP. The solubilisation was followed by ultracentrifugation at 72.000 x g for 35 min at 4°C (Supplementary Fig. S1). The hanging drop vapor-diffusion technique was used for crystallization. Crystals grew in a few days at 19°C starting from a solution of SERCA of about 10-12 mg/ml, using as precipitant a solution containing 220mM sodium acetate, 4% t-butanol, 5mM β-mercaptoethanol, 15% glycerol, 6-7%PEG 6000. The ATPase activity was measured after every purification step. Rabbit sarcoplasmic reticulum microsomes were isolated from *adductor magnus* by the method of Chu et al., (1987). This procedure yields mainly vesicles derived from nonjunctional sarcoplasmic reticulum as previously described (Sacchetto et al., 2005). Protein concentration of fractions was determined by the method of Lowry et al. (1951), using bovine serum albumin as a standard.

2.2.2 *STRUCTURE DETERMINATION AND REFINEMENT*

Crystals diffract to 2.95Å resolution and belong to the monoclinic space group C2, with unit cell parameters **a**=156.35, Å, **b**=75.36, Å, **c**=152.98, Å, β=108.6°. This corresponds to the same space group of one of the forms of the rabbit enzyme (PDB ID 1T5S and 1T5T), with small differences in unit cell dimensions. The asymmetric unit is comprised of one SERCA monomer, with a solvent content of approximately 68%. The data sets used in the final refinement were measured from two crystals at the ID29 beamline of the European Synchrotron Radiation Facility, Grenoble, France. Before freezing crystals in liquid nitrogen for data collection, glycerol concentration was increased in the reservoir to protect them for cryo-cooling. Data were indexed and integrated with software Mosflm (Leslie, 2006) and merged and scaled with Scala (Evans, 2006), contained in the CCP4 crystallographic package (Collaborative Computational Project, Number 4, 1994). The structure was solved by molecular replacement using software Phaser (McCoy et al., 2007) starting from the structure of the monoclinic E1 form (PDB ID code 1T5S (Sorensen et al., 2004)). Refinement was carried out using software CNS (Brunger et al., 1998). Several steps of manual rebuilding, performed with graphic software Coot (Emsley and Cowtan, 2004), were necessary in order to reach the final model. Solvent molecules were added with the automated procedure of Phenix (Adams et al., 2010).

The final model contains 7621 protein atoms, 35 ligands atoms and 34 water molecules. The final crystallographic R factor is 0.205 (R_{free} 0.277). Geometrical parameters of the model, checked with Procheck (Laskowski et al., 1993), are as expected or better for this resolution.

See Table 1 for statistics on data collection and refinement.

Table 1
Data collection and refinement statistics.

Data collection[a]	
Space group	C2
Cell dimensions	
a, b, c (Å), β(°)	156.35, 75.36, 152.98, 108.6
Resolution (Å)	76.61-2.95 (3.11-2.95)
R_{sym} or R_{merge}	0.106 (0.692)
$\langle I/\sigma(I)\rangle$	14.1 (3.5)
Completeness (%)	99.1 (98.4)
Redundancy	7.4 (7.5)
Refinement	
No. reflections	35.546
R_{work}/R_{free}	0.205/0.277
No. atoms	
Protein	7621
Ions/ligand	36
Water	34
B-factors	
Protein	80
Ligand/ion	49
Water	52
R.m.s deviations	
Bond lengths (Å)	0.007
Bond angles (°)	1.3
Ramachandran plot (%)	
Allowed	97.3
Generously allowed	1.7
Disallowed	1.0
Overall G factor	0.2

[a] *Two crystals were used to collect all diffraction data. Highest-resolution shell is shown in parentheses. A wavelength of 1.1271 Å was used.*

2.2.3 *ACTIVITY MEASUREMENTS*

ATPase activity was measured by spectrophotometric determination of NADH oxidation coupled to an ATP regenerating system, as previously described (Sacchetto et al., 2009). The assay was performed at 37°C, in a final volume of 1 ml of a mixture containing 20 mM histidine, pH 7.2, 5 mM $MgCl_2$, 0.5 mM EGTA, 0.1 M KCl, 0.5 mM phosphoenolpyruvate, 0.15 mM NADH, 1.4 units of pyruvate kinase/lactic dehydrogenase, 2 mM ATP, 0.1% NaN_3, in the

presence of 2 μg/ml A23187 Ca^{2+}-ionophore, at pCa5. The ATPase activity, detected at 340 nm (DU640 Spectrophotometer, Beckman Coulter), was normalized to Ca^{2+} pump expression levels in sarcoplasmic reticulum vesicles and was expressed in micromoles of Pi/min/mg of Ca^{2+}-ATPase protein (moles of phosphate originated from the ATP hydrolysis).

The Ca^{2+}-ATPase protein content in bovine and rabbit sarcoplasmic reticulum microsome fractions, prepared as described above, was quantified by densitometry. Fractions were separated by electrophoresis on SDS polyacrylamide gradient gels (5-10%) and the gels were stained with Coomassie blue (Supplementary Fig. S1). In each series of experiments, a calibration curve was constructed using commercial bovine serum albumin. Densitometric scanning of Ca^{2+}-ATPase protein band was carried out using an Amersham Pharmacia Biotech Image Scanner, equipped with appropriate software.

2.3 RESULTS

2.3.1 SERCA1A ISOFORM

The enzyme was purified from bovine *cutaneus trunci*, a fast-twitch muscle used for fast skin twitching. Immunoblotting experiments with antibodies against SERCA1a and SERCA2a isoforms (Fig. 1) clearly showed that the purified enzyme corresponds nearly entirely to the SERCA1a isoform, the SERCA2a presence being limited to less than 5%. This was confirmed by confocal microscopy images of muscle cryosections immune-labeled with monoclonal antibodies against SERCA1, SERCA2 and phospholamban (Supplementary figure S2)

2.3.2 SERCA1A ACTIVITY

The specific activity of bovine SERCA1a was 6.55 ± 0.26 μmoles/min/mg. That of rabbit SERCA1a measured under the same experimental conditions was 10.06 ± 0.61 μmoles/min/mg. The $K_{0.5}$ for the Ca^{2+} activation of the ATPase (Supplementary Fig. S3) was similar for bovine and rabbit membrane samples (pCa 6.61±0.05, Sacchetto et al., 2009, and

pCa around 6, Gould et al., 1986, Maruyama and MacLennan, 1988, respectively), and similar to that of the human SERCA1 protein (pCa 6.46±0.05, Odermatt et al., 2000).

2.3.3 *CRYSTAL STRUCTURE OF BOVINE SERCA1A*

The crystal structure of the Ca^{2+}-bound form of bovine SERCA includes residues from 1 to 992, with the exception of few disordered amino acids in the stretch 876 to 880 (due to the occurrence of a deletion in the bovine enzyme, corresponding to rabbit position 504, the numbering system is shifted by -1 as compared to the rabbit enzyme. We will use bovine numbering throughout this paper). Despite the relatively limited resolution, 2.95 Å, the electron density was well defined (as an example, see Supplementary Fig. S4), with the exception of few loops and connecting regions that are flexible. A molecule of AMPPCP, three divalent ions (Ca^{2+} or Mg^{2+}) and one K^{+} ion are bound to the protein in the same sites as in the rabbit enzyme (Fig. 2). In the final Fourier-difference map, two electron densities higher than 4σ were still present. One was on the protein surface close to side chain of Gln108, in a partially hydrophobic patch lined by the side chains of Phe808, Trp107 and 931 and Val104 (Supplementary Fig. S5). The other was close to the side chain of Asn989. In both cases we were unable to state if they corresponded to a post-translational modification, or to the binding of small ligands, taken from the tissue before purification or present in the crystallization medium. The only post-translational modification of SERCA1a detected so far is nitrosylation at Tyr122 (Sharov et al., 2002), whilst several, including nitrosylation, glutathiolation and sumoylation, have been found in SERCA2a from heart muscle (Knyushko et al., 2005; Adachi et al., 2004; Kho et al., 2011). An electron density in the cleft formed by M2, M4, M6 and M9 helices at the cytosol-membrane interface, i.e. in a position close to the former of our additional electron densities, was observed in the rabbit E1.AMPPCP monoclinic crystal form and it was interpreted as a phosphatidylcholine headgroup (Picard et al., 2007). This region has also been proposed to represent the binding site of the regulatory peptide sarcolipin (Asahi et al., 2003, Buffy et al., 2003), supporting the hypothesis of the binding of a small ligand.

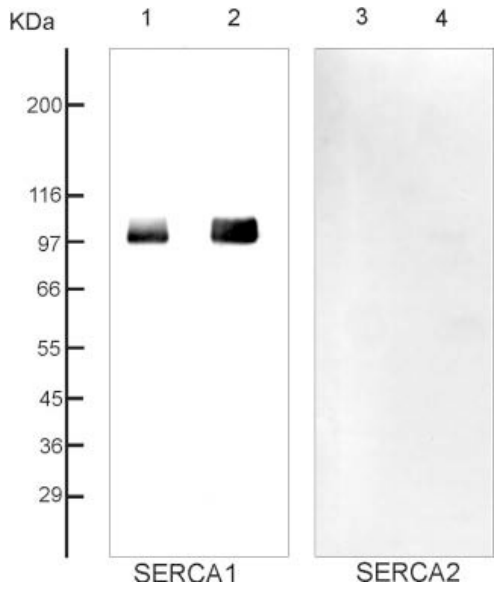

Fig. 1. Immunodetection of SERCA1 and SERCA2 proteins in rabbit and bovine sarcoplasmic reticulum membranes. Equal quantities of highly purified sarcoplasmic reticulum membrane fractions (0.5 mg/lane) were separated by 5-10% SDS-PAGE and blotted onto nitrocellulose. The blots were incubated with monoclonal antibodies to SERCA1 and SERCA2 isoforms (Thermo scientific), as indicated. Lanes 1 and 3: sarcoplasmic reticulum membranes extracted from rabbit muscle, following the procedure previously described (Sacchetto et al., 2005); lanes 2 and 4 represent sarcoplasmic reticulum membranes of bovine SERCA extracted according to (De Meis and Hasselbach, 1971).

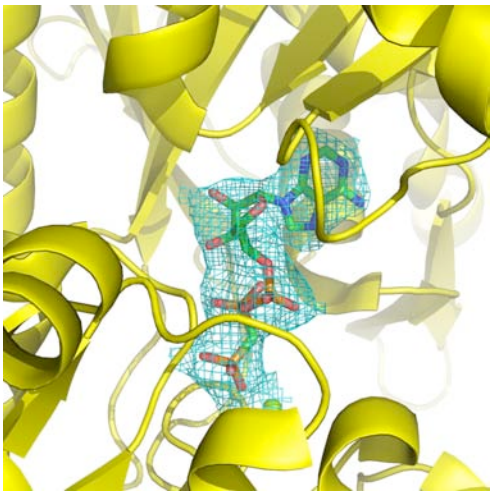

Fig. 2. Detail of the AMPPCP binding site in bovine SERCAa1. The protein is shown as a cartoon, the ligand as a stick model. Electron density from a (2Fobs-Fcalc) map was contoured at 1.2σ around the ligand.

2.4 DISCUSSION

The crystal structure presented here, with bound Ca^{2+} and AMPPCP, can be classified as corresponding to the E1.AMPPCP state of SERCA1a. In fact, it compares quite well with the corresponding crystal structures of the rabbit enzyme in the same conformational state (Sorensen et al., 2004; Toyoshima and Mizutani, 2004). Compared to the rabbit enzyme crystallized in the same monoclinic form (PDB ID 1T5S) or crystallized in the $P2_1$ space group with two molecules in the asymmetric unit (PDB ID 1VFP), the crystal structure of bovine SERCA1a presents a r.m.s.d. between equivalent Cα atoms of the core structure of 0.85 Å in both cases. Significant differences are observed only in three regions: loop 501-507, which connects strands N8 to N9; loop 80-83, which connects α-helix M1 to M2; and finally, region 874-881, that is part of a long stretch which connects helices M7 and M8 (Fig. 3)

Twenty-two residues differ in the amino acid sequence of the bovine with respect to the rabbit enzyme (Supplementary Fig. S6). In addition, an amino acid deletion occurs at position 503, in a loop connecting α-helices N8 and N9, exposed to the solvent (Fig. 4A) and therefore with probably no functional effect. This loop is disordered in model 1T5S, whilst it is well defined in the bovine enzyme. Among the 22 substitutions, 12 are conservative, mainly Ser <--> Thr or Leu, Ile <--> Val. Only 10 are non-conservative replacements and all but two are clustered in two areas of the C-terminal domain that protrudes in the lumen of the sarcoplasmic reticulum (Fig. 5). The two isolated replacements are Gly937 and Val922, which replace a Cys in the first portion of α-helix M9 and a Met in the loop region before α-helix M9, respectively. Both substitutions appear to be irrelevant from the conformational point of view, i.e. the structures of the bovine and rabbit enzymes are superimposable in these areas. A small cluster of differences is represented by the consecutive substitutions T964Y and Q965H. They occur at the end of α-helix M9, at the final end of the lipidic bilayer: again, they do not seem to perturb the three-dimensional structure of the enzyme. His 965 side chain points internally to the bundle of helices, whilst the more cumbersome Thr -> Tyr replacement can be easily accommodated, since the side chain points towards the solvent.

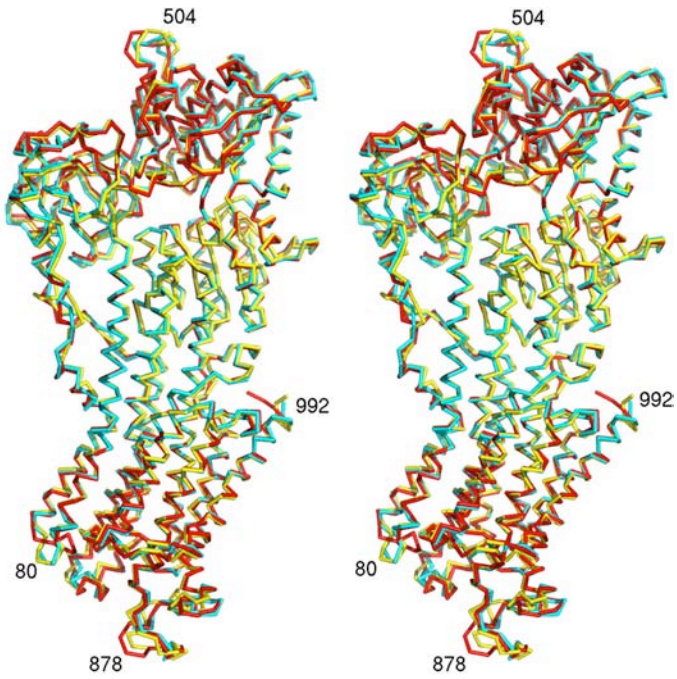

Fig. 3. Stereo view of Cα atoms of bovine muscle SERCA (cyan, this paper) superimposed to two models of rabbit muscle E1.AMPPCP form (red, PDB ID 1T5S, Sorensen et al. 2004; yellow, PDB ID 1VPF, Toyoshima and Mizutani, 2004). Regions where our model differs significantly from the others are labeled. In this Figure and in Figure 6 all Cα atoms were superimposed.

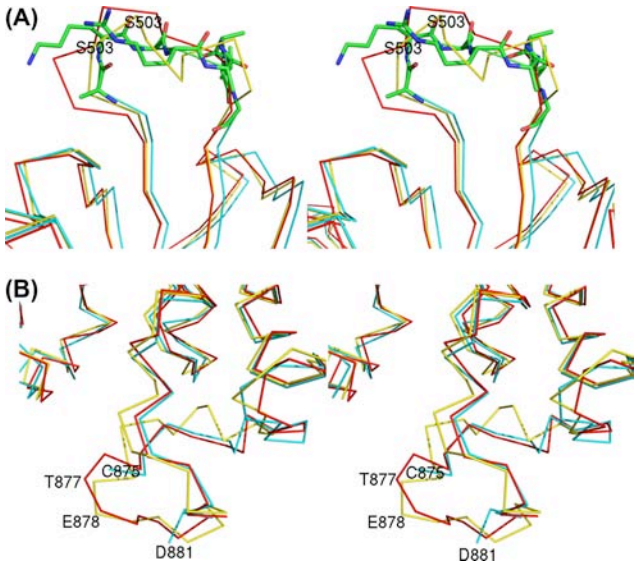

Fig. 4. (A) Stereo view of a detail of loops 501-508. Colors are as in Fig. 3. Only Cα atoms are shown, with the exception of side chains of the bovine enzyme (C atoms in green). Ser503, the amino acid absent in the bovine enzyme, is labeled in the other two models. (B) Same as (A) for loop and 863-881.

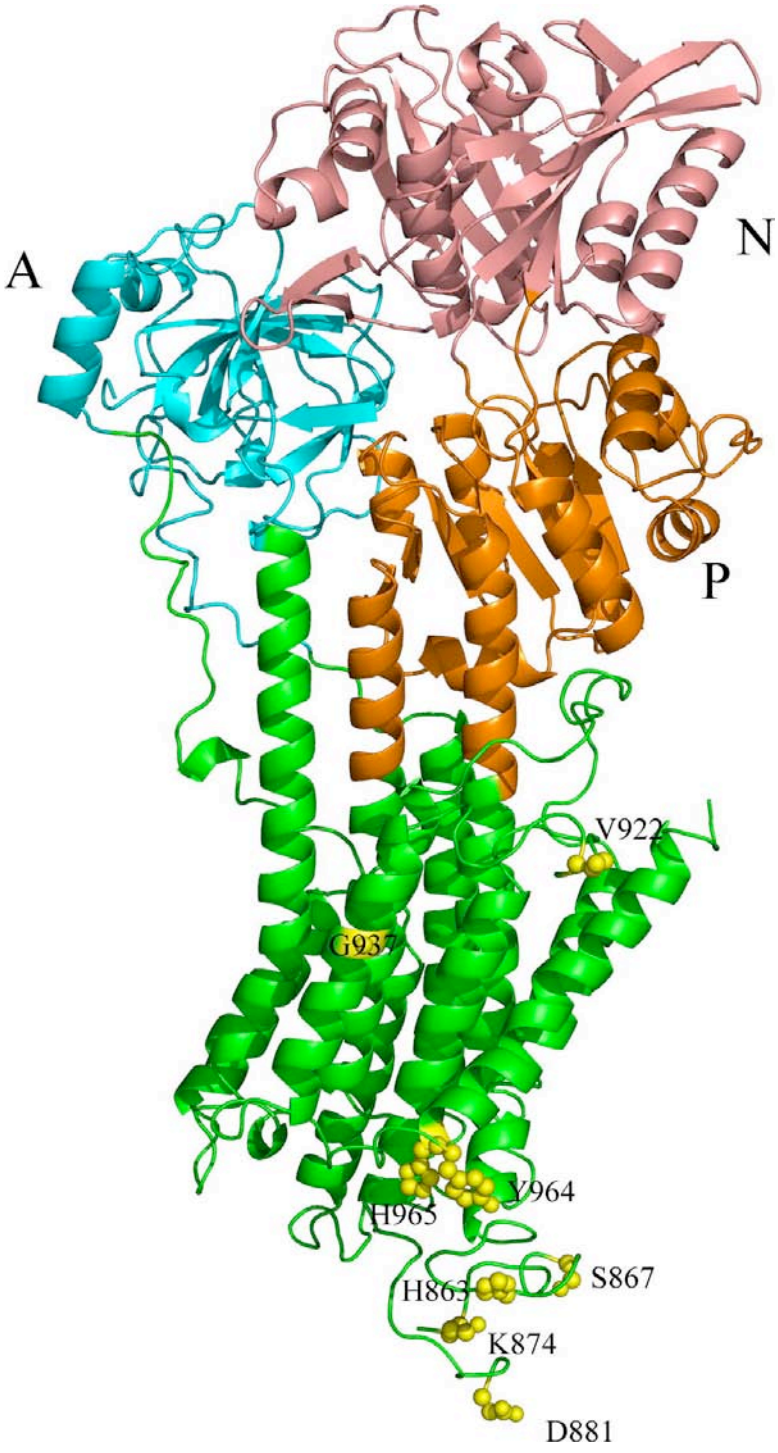

Fig. 5. Cartoon representation of bovine SERCA. Domains A, N and P, defined according to Toyoshima and Inesi (2004), are colored cyan, light red and orange, respectively. Side chains of amino acids that represent non-conserved mutations in the bovine with respect to the rabbit protein are shown in yellow.

Finally, the remaining six differences are grouped from residues 863 to 881, one of the areas where we observe a conformational difference in the two structures (Fig. 4B). No electron density is visible for residues from 874 to 881, indicating that substitutions induce conformational flexibility. It is worth noticing that two Cys residues are present in this area. It has been shown that a disulfide bond between these two Cys residues (C875-C887 in the bovine, C876-C888 in the rabbit enzyme) is required for activity (Daiho et al., 2001). Its reduction in our crystal structure is likely due to reducing agents in the buffers used for crystallization.

Given the great similarity between the structures of the E1.AMPPCP forms of bovine and rabbit SERCA, the explanation for the significantly different specific activities of the two enzymes does not appear to be obvious. We cannot exclude the possibility that part of this difference reflects a potentially different phospholipid environment of the two preparations, since the procedures used to extract the rabbit and bovine enzymes differed slightly. However, the possibility that the environment would be responsible for such a large difference seems remote, in particular since the $K_{0.5}$ for Ca^{2+} activation in the two ATPases was essentially the same. We can thus confidently conclude that the enzyme structure must play a role in the difference. Amino acids that differ significantly in the two enzymes and that perturb the three-dimensional structure are practically confined to one specific region, the long loop hat protrudes into the SR lumen and which connects α-helices M7 and M8. This area is not involved in the binding of ATP or of Ca^{2+}, nor in the large shifts that involve the cytoplasmic domains and that are the basis for the transfer of Ca^{2+} from the cytoplasm to the lumen. Nevertheless, a superposition of bovine E1 to the rabbit E2 conformation of SERCA (Fig. 6) shows that in the E2 state the large movements of the cytoplasmic domains perturb also the region of the intermembrane helices and induce a conformational rearrangement of the area protruding into the lumen. In particular, the shift of position of the long α-helix M2 and of helix M1 is transmitted to helix M3, causing a shift of the loop connecting helices M3-M4. In parallel, the long stretch connecting helices M8 and M9, which is the region that

contains most of the residues that differs in the bovine protein, undergoes a parallel rearrangement, coming closer to the previous loop, so that the side chain of Glu877 becomes close to Ser287, forming a H-bond interaction. Glu877 is conserved, but residues preceding and following it in the sequence are mutated (Q874K, T876S, D878H, H879S, H881D). These differences in the sequence, which are also reflected in the electrostatic potential surface (Supplementary Figure S7), could influence the transition from the E1 to the E2 conformation, making it slightly less favoured with respect to the rabbit enzyme. This could justify the reduced specific activity of the bovine enzyme.

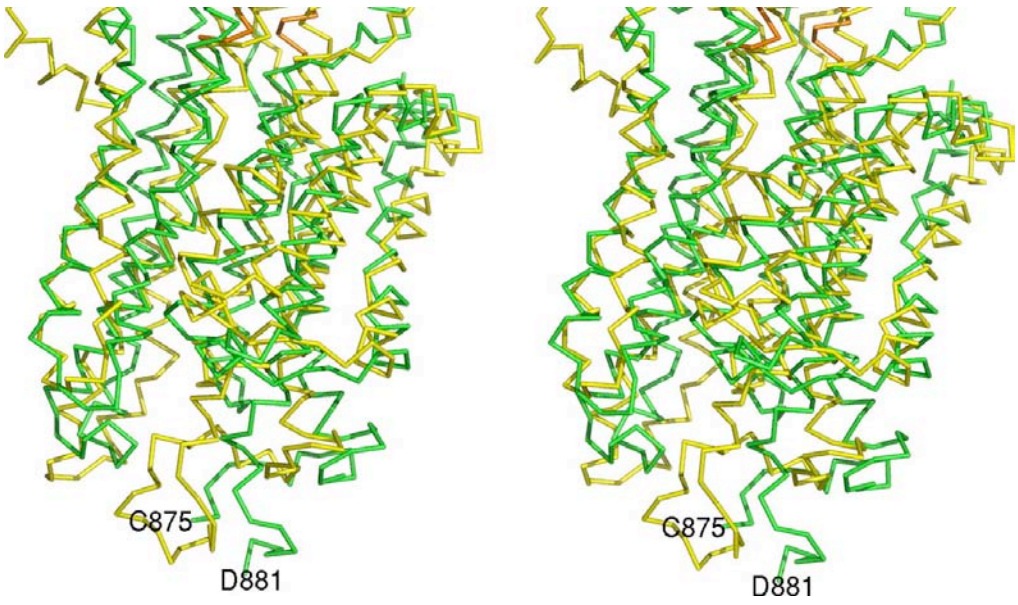

Fig. 6. Stereo ribbon drawing of the superposition of Cα atoms of the transmembrane and cytosolic portions of E2 conformation of rabbit SERCA (yellow, PDB ID 2C8L, (Jensen et al. 2006)) and of conformation E1 of the bovine enzyme. The region 863-861, which contains most of the differences between bovine and rabbit enzyme, is labeled.

2.4.1 SERCA MUTATIONS

In Chianina cattle, the Arg to His substitution at position 164 of SERCA1 leads to a pseudomyotonia (Sacchetto et al., 2009). Cattle pseudomyotonia associated with ATP2A1 gene mutations has been described also in Belgian Blue breed (named congenital muscular dystonia1) (Charlier et al., 2008) and as a single case in a Dutch improved Red and White cross-breed calf (Grünberg et al., 2010) in which the DNA sequencing revealed an Arg to Cys substitution at position 559 (corresponding to rabbit 560). In the latter, Arg559 directly interacts with the nucleotide and its mutation affects the binding of the nucleotide. In Chianina cattle, the amount of protein present in the SR reticulum in the diseased animals is significantly decreased with respect to wild type counterparts, despite the fact that the mRNA coding for SERCA1a is present in equivalent amounts. The mutated R164H amino acid belongs to the A domain of SERCA, which is critical in the dephosphorylation process, during which it rotates and associates with the P domain to form the catalytic site for ATP hydrolysis. A detail of the structure of the region of domain A of SERCA1 is illustrated in Fig. 7. In the E1.AMPPCP state, the protonated side chain of Arg164 is counterbalanced by the negatively charged Glu2. In addition, the Arg side chain forms extensive interactions with the carbonyl oxygen atoms of at least four surrounding residues (Ile165, The191, Lys7 and His5), acting as a central 'anchor point' for three different stretches of the A-domain fold, and is therefore probably central to proper folding. The substitution of the side chain of the arginine with the imidazole of the His residue, which is smaller and at physiologic pH can be neutral, could have a role in disfavoring a correct folding. This could affect the amount of SERCA that escapes proteolytic degradation to be correctly inserted into the SR bilayer.

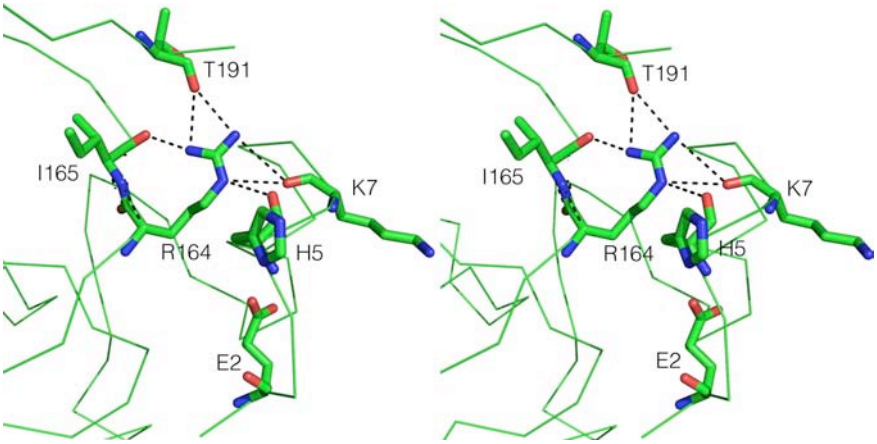

Fig. 7. Stereo view of a portion of domain A of E1.AMPPCP form of the bovine enzyme. Side chains of residues interacting with Arg164 are explicitly shown, along with Glu2. Potential H-bonds formed by Arg164 side chain are shown as dashed lines. The distance between Nε and NH1 of Arg164 and Oε2 of Glu2 are 6.2 Å and 8.0 Å, respectively.

2.5 CONCLUSIONS

The crystal structure of bovine SERCA1a presented in this paper shows that the overall conformation of the enzyme is well conserved between cattle and rabbit, that diverged several millions year ago (Hedges and Kumar, 2003). It is worth noticing that the binding sites for ions and for the nucleotide are very well conserved, and that the calcium binding constant is essentially the same for the two enzymes. By contrast, small differences can affect and modulate the transport activity, which relies on a complex concerted equilibrium between different conformational states. A few mutations have evidently rendered the bovine enzyme less efficient than the rabbit counterpart, as can be easily understood considering the different sizes and the different performances required by the muscle of the two animals. As demonstrated by pseudomyotonia in Chianina cattle, a single mutation is sufficient to perturb the three dimensional structure and induce a genetic disease.

2.6 ACCESSION NUMBERS

The coordinates and structure factors have been deposited in the Protein Data Bank (http://www.pdb.org) for immediate release under accession code 3TLM.

2.7 ACKNOWLEDGMENTS

We thank the staff of beamline ID29 of ESRF, Grenoble, for technical assistance during data collection. We acknowledge the precious help of Mr. Giovanni Caporale. We thank Anthea Rowlerson for carefully reading the manuscript. We are especially grateful to Giantin slaughterhouse, Fossò (VE) Italy. This work was supported by Foundation Cariparo (Calcium signalling in health and disease) and by the University of Padua Athenaeum Project (to F.M.).

2.8 SUPPLEMENTARY FIGURES

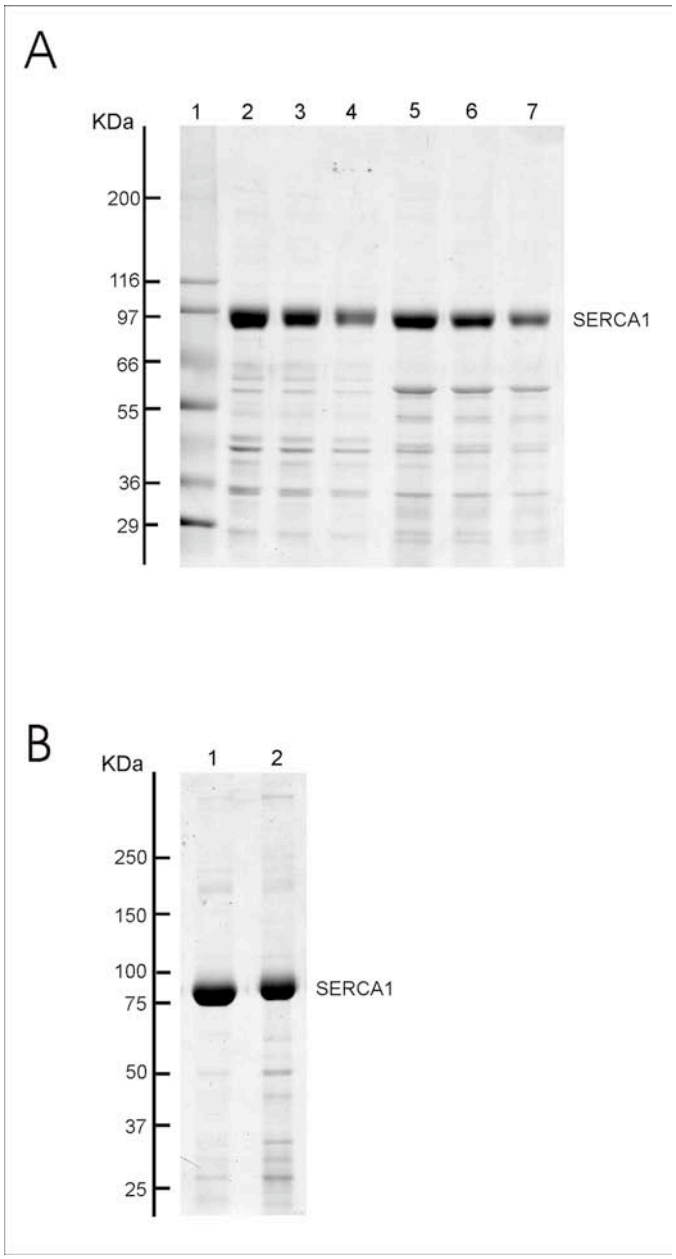

Fig. S1. A) SDS gel electrophoresis of rabbit and bovine SERCA used in the quantification of the enzymatic activity. Lanes 1, MW standards; lanes 2, 3 and 4 represent sarcoplasmic reticulum membranes extracted from rabbit muscle, following the procedure previously described (Sacchetto et al., 2005); lanes 5, 6 and 7 represent sarcoplasmic reticulum membranes of bovine SERCA extracted according to (De Meis and Hasselbach, 1971). B) Finally purified SERCA enzyme used for crystallization. The rabbit enzyme is in lane 1, bovine in lane 2.

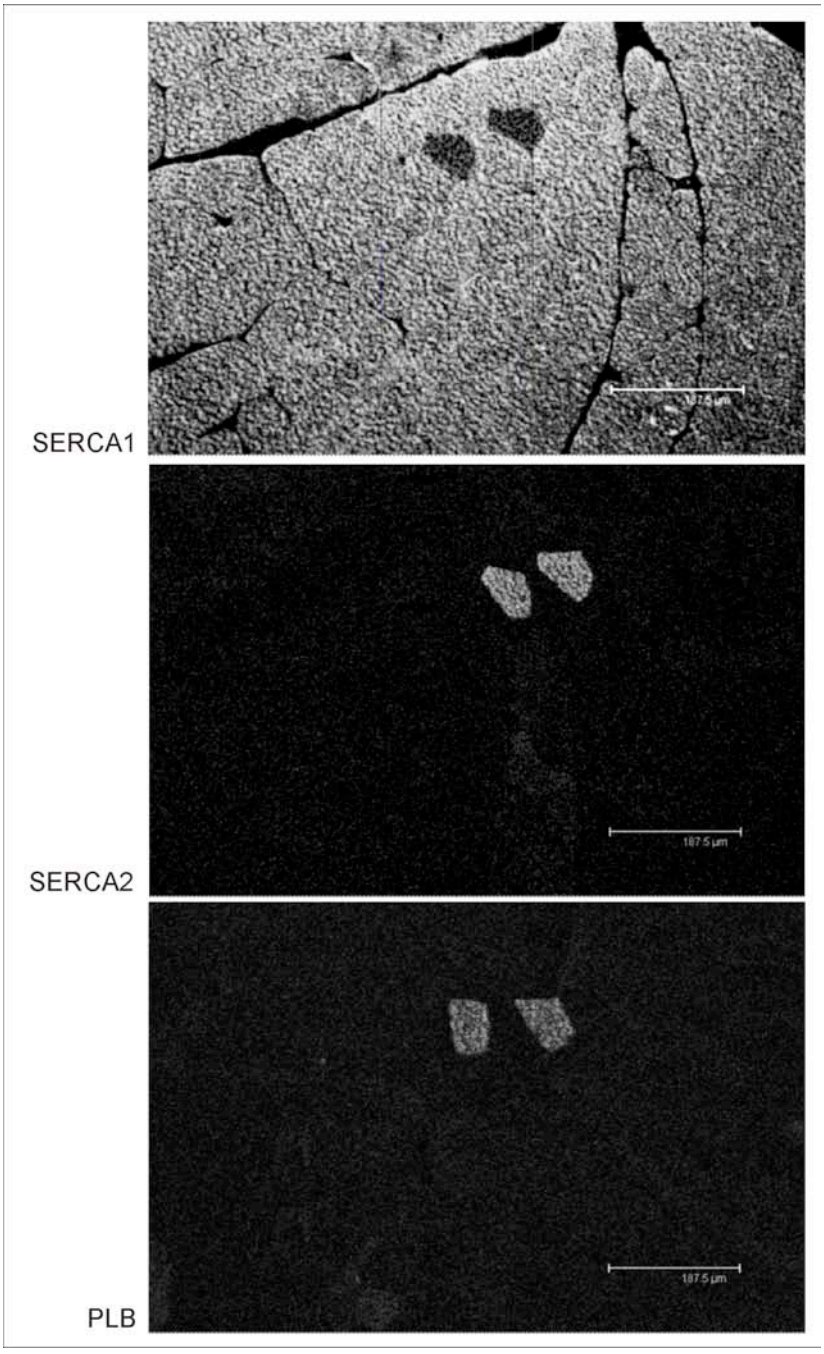

Fig. S2. Confocal microscopy of bovine cutaneus trunci muscle cryosections. Serial transverse sections were immunolabeled with monoclonal antibodies to SERCA1 and SERCA2 isoforms or phospholamban (PLB) (Thermo scientific) as indicated. Sections were then incubated with the appropriate secondary antibodies conjugated with tetramethylrhodamine isothiocyanate (TRITC) and examined using a Leica TCS-SP2 confocal scanning microscope. Scale bar: 187.5 mm.

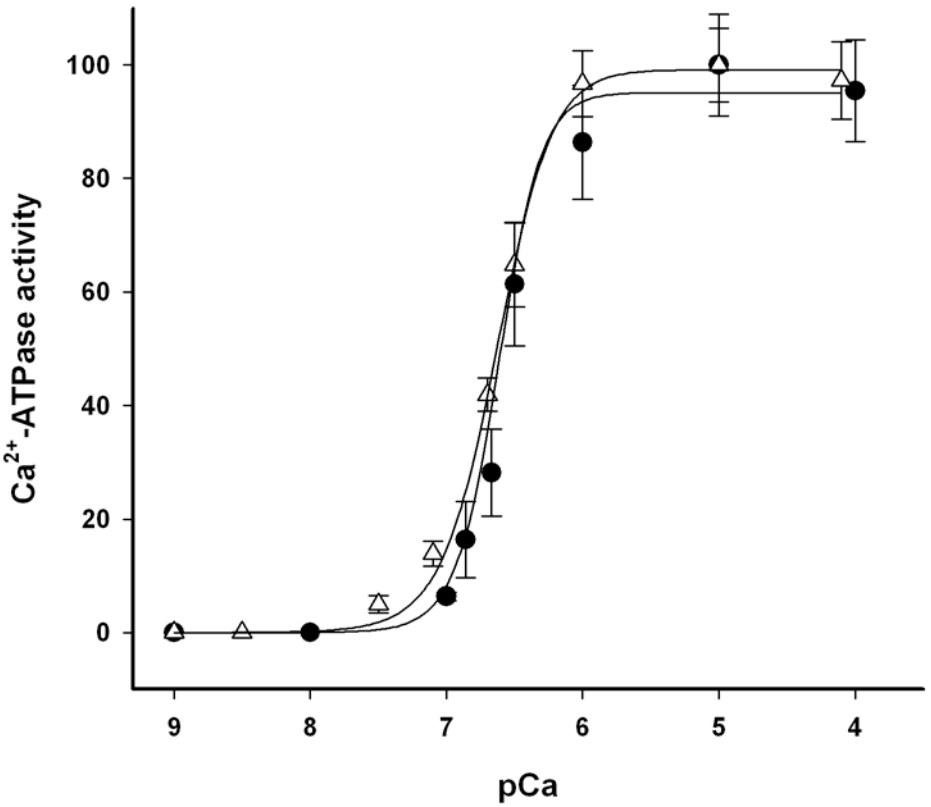

Fig. S3. Ca2+-ATPase activity of sarcoplasmic reticulum membranes, measured as a function of Ca2+ concentration. The Ca2+-ATPase activity was measured by spectrophotometric determination of NADH oxidation coupled to an ATP regenerating system at various concentration of free Ca2+. Data are expressed as percentage of maximun value (pCa 5) and are the mean + SD. Symbols: circle = bovine sarcoplasmic reticulum membranes; triangle = rabbit sarcoplasmic reticulum membranes.

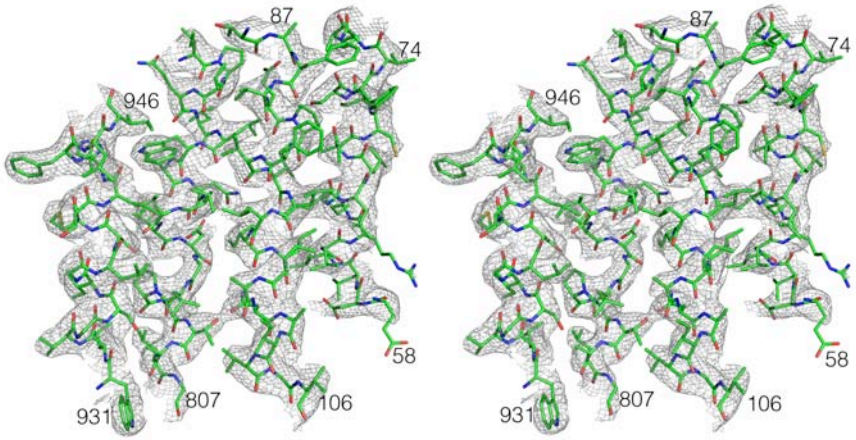

Fig. S4. Stereo view of a portion of the electron density map, showing four of the transmembrane helices. The map was calculated with (2Fobs-Fcalc) coefficients, contours are drawn at 1σ.

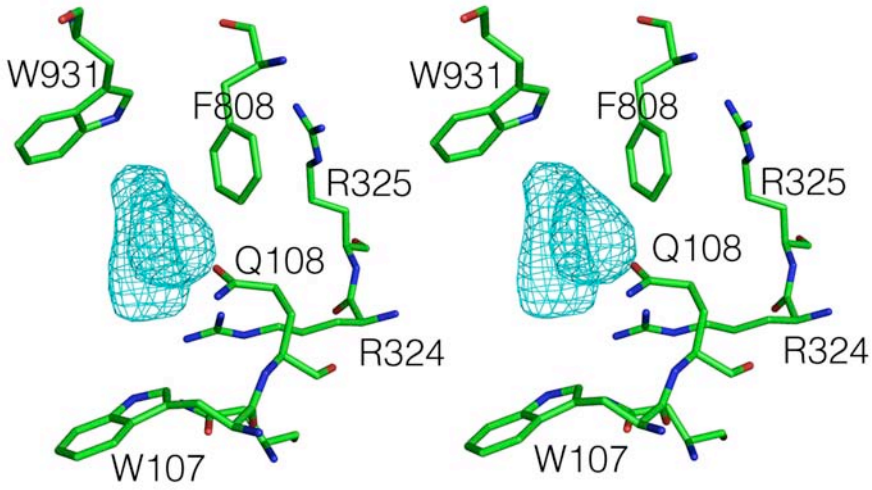

Fig. S5. Stereo view of the electron density map, calculated with coefficients (Fobs-Fcalc), of the region close to residue Q108. An electron density, possibly corresponding to a small ligand bound, is drawn at 4.5σ.

```
     *******:*********************************************:******
1    MEAAHSKTTEECLAYFGVSETTGLTPDQVKRHLEKYGHNELPAEEGKSLWELVLEQFEDL   60  BOVINE
1    MEAAHSKSTEECLAYFGVSETTGLTPDQVKRHLEKYGHNELPAEEGKSLWELVIEQFEDL   60  RABBIT

     ***********************:**********************************
61   LVRILLLAACISFVLAWFEEGEETVTAFVEPFVILLILIANAIVGVWQERNAENAIEALK  120  BOVINE
61   LVRILLLAACISFVLAWFEEGEETITAFVEPFVILLILIANAIVGVWQERNAENAIEALK  120  RABBIT

     ***********************************************:*************
121  EYEPEMGKVYRADRKSVQRIKARDIVPGDIVEVAVGDKVPADIRILTIKSTTLRVDQSIL  180  BOVINE
121  EYEPEMGKVYRADRKSVQRIKARDIVPGDIVEVAVGDKVPADIRILSIKSTTLRVDQSIL  180  RABBIT

     ***************************************:********.***********
181  TGESVSVIKHTEPVPDPRAVNQDKKNMLFSGTNIAAGKAIGIVATTGVGTEIGKIRDQMA  240  BOVINE
181  TGESVSVIKHTEPVPDPRAVNQDKKNMLFSGTNIAAGKALGIVATTGVSTEIGKIRDQMA  240  RABBIT

     ************************************************************
241  ATEQDKTPLQQKLDEFGEQLSKVISLICVAVWLINIGHFNDPVHGGSWIRGAIYYFKIAV  300  BOVINE
241  ATEQDKTPLQQKLDEFGEQLSKVISLICVAVWLINIGHFNDPVHGGSWIRGAIYYFKIAV  300  RABBIT

     ************************************************************
301  ALAVAAIPEGLPAVITTCLALGTRRMAKKNAIVRSLPSVETLGCTSVICSDKTGTLTTNQ  360  BOVINE
301  ALAVAAIPEGLPAVITTCLALGTRRMAKKNAIVRSLPSVETLGCTSVICSDKTGTLTTNQ  360  RABBIT

     **********::***:* *****:*****************:****:*************
361  MSVCKMFIIDRIDGDLCLLNEFSVTGSTYAPEGEVLKNDKPVRSGQYDGLVELATICALC  420  BOVINE
361  MSVCKMFIIDKVDGDFCSLNEFSITGSTYAPEGEVLKNDKPIRSGQFDGLVELATICALC  420  RABBIT

     ************:************************************************
421  NDSSLDFNETKGIYEKVGEATETALTTLVEKMNVFNTEVRNLSKVERANACNSVIRQLMK  480  BOVINE
421  NDSSLDFNETKGVYEKVGEATETALTTLVEKMNVFNTEVRNLSKVERANACNSVIRQLMK  480  RABBIT

     ********************** ************************************
481  KEFTLEFSRDRKSMSVYCSPAKS-RAAVGNKMFVKGAPEGVIDRCNYVRVGTTRVPMTGP  539  BOVINE
481  KEFTLEFSRDRKSMSVYCSPAKSSRAAVGNKMFVKGAPEGVIDRCNYVRVGTTRVPMTGP  540  RABBIT

     ****************************************::******************
540  VKEKILSVIKEWGTGRDTLRCLALATRDTPPKREEMVLDDSTKFMEYETDLTFVGVVGML  599  BOVINE
541  VKEKILSVIKEWGTGRDTLRCLALATRDTPPKREEMVLDDSSRFMEYETDLTFVGVVGML  600  RABBIT

     ************************************************:*************
600  DPPRKEVMGSIQLCRDAGIRVIMITGDNKGTAIAICRRIGIFGENEDVADRAYTGREFDD  659  BOVINE
601  DPPRKEVMGSIQLCRDAGIRVIMITGDNKGTAIAICRRIGIFGENEEVADRAYTGREFDD  660  RABBIT

     **********************:***********:*************************
660  LPLAEQREACRRACCFARVEPTHKSKIVEYLQSFDEITAMTGDGVNDAPALKKAEIGIAM  719  BOVINE
661  LPLAEQREACRRACCFARVEPSHKSKIVEYLQSYDEITAMTGDGVNDAPALKKAEIGIAM  720  RABBIT

     ************************************************************
720  GSGTAVAKTASEMVLADDNFSTIVAAVEEGRAIYNNMKQFIRYLISSNVGEVVCIFLTAA  779  BOVINE
721  GSGTAVAKTASEMVLADDNFSTIVAAVEEGRAIYNNMKQFIRYLISSNVGEVVCIFLTAA  780  RABBIT

     ****************************************:*****************
780  LGLPEALIPVQLLWVNLVTDGLPATALGFNPPDLDIMDRPPRTPKEPLISGWLFFRYMAI  839  BOVINE
781  LGLPEALIPVQLLWVNLVTDGLPATALGFNPPDLDIMDRPPRSPKEPLISGWLFFRYMAI  840  RABBIT

     ****************:****** *** ******:*:*. *.***:***:****:*****
840  GGYVGAATVGAAAWWFLYAEDGPHVTYSQLTHFMKCSEHSPDFEGVDCEVFEAPQPMTMA  899  BOVINE
841  GGYVGAATVGAAAWWFMYAEDGPGVTYHQLTHFMQCTEDHPHFEGLDCEIFEAPEPMTMA  900  RABBIT

     **********************:**********:*** **********************:
900  LSVLVTIEMCNALNSLSENQSLVRMPPWVNIWLVGSIGLSMSLHFLILYVDPLPMIFKLQ  959  BOVINE
901  LSVLVTIEMCNALNSLSENQSLMRMPPWVNIWLLGSICLSMSLHFLILYVDPLPMIFKLK  960  RABBIT

     **** :********************:******.
960  ALDLYHWLMVLKISLPVIGLDEILKFVARNYLEG                           993  BOVINE
961  ALDLTQWLMVLKISLPVIGLDEILKFIARNYLEG                           994  RABBIT
```

Fig. S6. Alignment of the amino acid sequence of bovine SERCAa1 pump (Q0VCY0) with that of the rabbit enzyme (Genbank M15158.1).

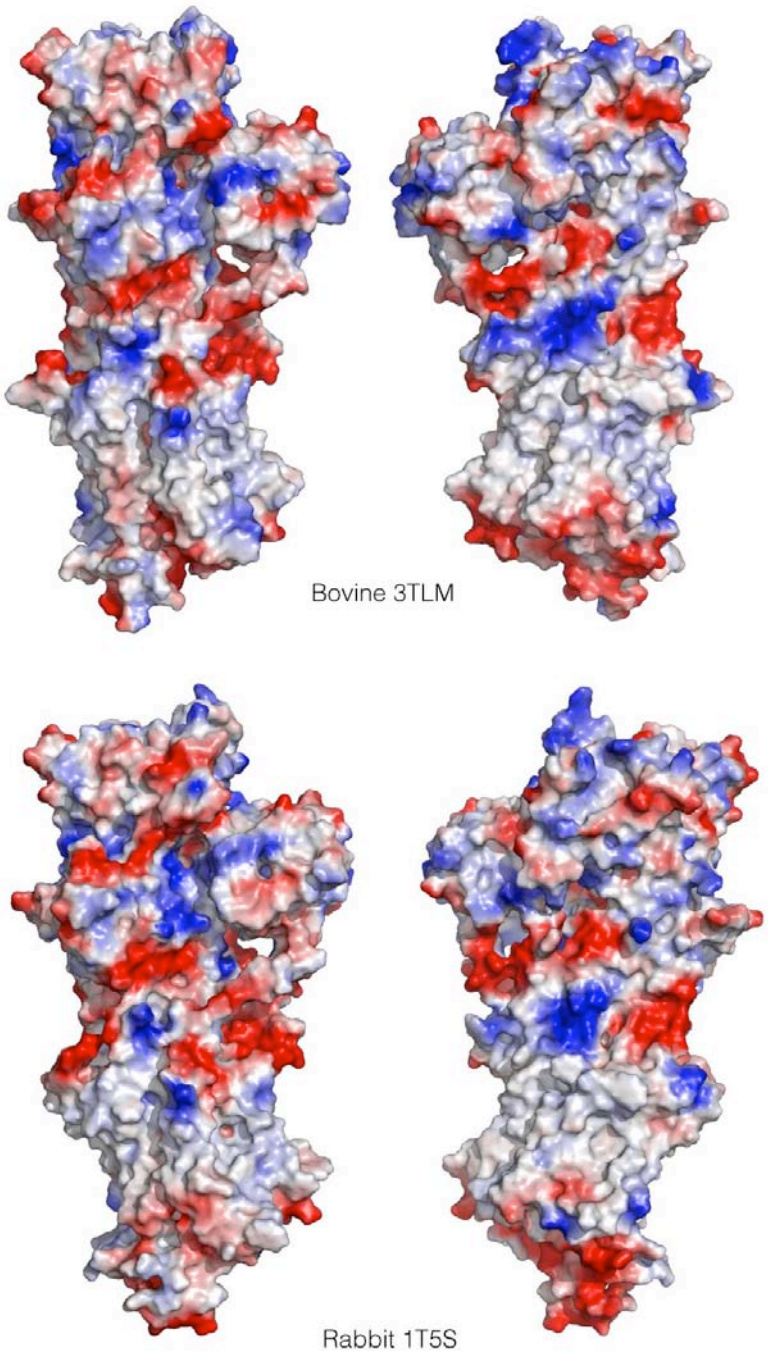

Fig. S7. Qualitative electrostatic potential surface (calculated by software Pymol) for bovine (top) and rabbit SERCA (bottom). The left and right views are rotated approximately 180° each other. Small differences can be observed at the bottom, corresponding to the area protruding into the lumen.

CHAPTER III

HETEROLOGOUS EXPRESSION AND AFFINITY PURIFICATION OF HUMAN SERCA 2A IN *SACCHAROMYCES CEREVISIAE*

CONTENTS

3.1 INTRODUCTION

The SERCA2a isoform is a membrane protein of about 115 kDa. As a member of the Ca^{2+} pumps family, it plays a key role in the control of calcium homeostasis in cardiac muscle, where its ability to remove calcium induces muscle relaxation. In humans, about 70% of the cytosolic Ca^{2+} reuptake into SR is regulated by the SERCA2a pump. Moreover, this pump indirectly controls the storage of Ca^{2+} into SR, which is responsible for the cardiac contraction activation. Consequently, the SERCA2a isoform represents the major player involved in the regulation of the excitation-contraction coupling of the heart (Konrad F. et al, 2003). Evidences from human and experimental models of heart failure have demonstrated that alterations in SR calcium handling are associated with an impaired contractility, probably due to decreased SERCA2a protein levels and/or increased inhibition by the phospolamban (PLN) regulatory protein (Elizabeth Vafiadaki, 2008). Other evidence also seems to suggest that mutations of the isoform 2a may predispose to cardiac diseases. Recently, SERCA2a pump gene transfer was demonstrated to be safe and effective in restoring contractile function via over-expression of SERCA2a under physiological and patho-physiological conditions (Gianni D. et al, 2005).

The involvement of the SERCA2a isoform in the control of calcium homeostasis in eukaryotic cells and consequently its role in the pathologies of cardiac muscle makes it an important target of research investigations. The determination of the crystal structure of the SERCA2a could help to elucidate the molecular mechanisms responsible for Ca^{2+} signaling dysfunction as well as to design and study specific inhibitors of the heart SERCA2a enzyme. For this reason, we have extended our investigations to the structural and functional study of SERCA2a and of the mutants responsible for Ca^{2+} signaling dysfunction.

In our work, the human SERCA2a was expressed in Saccharomyces cerevisiae as a recombinant protein with a biotin acceptor domain (BAD) linked to the C-terminus (hSERCA2a-BAD) by a thrombin cleavage site. Owing to the presence of a thrombin cleavage site within the protein sequence, a point mutant (R863G) was generated and the protein was

successfully expressed. In vivo yeast biotinylation of BAD added as a tag to SERCA2a has offered both a fast and efficient affinity purification strategy and a positive selection of the properly folded enzyme. To obtain sufficient amount of protein to perform crystallization trials, a protocol for batch fermentation of S. cerevisiae was optimized in a home made bioreactor, according to the method of Cardi. (Cardi D. et al, 2010). The protein was solubilized with a buffer containing n-dodecyl β-D-maltoside (DDM) at the appropriate CMC (critical micellar concentration). Finally, the enzyme was purified by avidin-affinity strategy, using two different purification tools (the avidin resin and the avidin magnetic nanoparticles).

3.2 MATERIALS AND METHODS

3.2.1 HETEROLOGOUS EXPRESSION OF HUMAN SERCA2AR863G IN S. CEREVISIAE

The c-DNA coding for human SERCA2a (Imagenes GmbH, Berlin, Germany) was amplified by PCR and cloned into pYeDP60 plasmid (kindly provided by Marc le Maire, (Université Paris-Sud, F-91405 Orsay, Institut de Biologie et Technologies de Saclay (iBiTec-S) Gif-sur-Yvette, and URA CNRS, France) in the same coding frame of thrombin cleavage site and BAD (biotin acceptor domain) sequences by the gap-repair cloning method (Chino, A. et al, 2010).

The forward (5'-ata ctt cta tag aca cgc aaa cac aaa tac aca cac taa att acc gaa ttc ATGGAGAACGCGCACACCAA-3') and the reverse primers (5'-TTTAGCGATATGTTCTGGTCT gct agc ttg gtt cca aga gga tcc acg gcg gct gct ccc ggg cct gct cct-3'), which were properly designed to allow the homologous recombination process in the yeast, were used to perform the gap-repair cloning as described by Kitazono. (Kitazono, A. A., 2009).

A mutant of hSERCA2a (R863G) was generated by PCR based on the QuickChange site-directed mutagenesis strategy (Stratagene) to eliminate a thrombin cleavage site within the protein sequence.

Competent S. cerevisiae cells (strain W303.1b Gal4–2 (a, leu2, his3, trp1: TRP1-GAL10-GAL4, ura3, ade2–1, canr, cir+) were transformed with the pYeDP60 vector containing

hSERCA-2aR863G and selected on minimal plates as described by Gietz and Woods (D. Gietz, R. and Woods, R. A.).

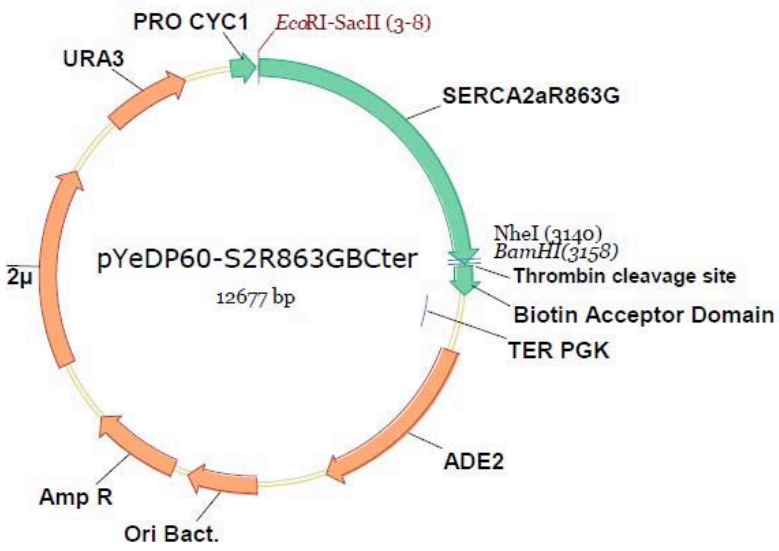

Fig. 1. Plasmid vector used for heterologous expression of hSERCA2aR863G-BAD in S. cerevisiae. Ori Bact., bacterial replication origin; ADE2 and URA, yeast selection markers; AmpR, bacterial selection marker; Pro GAL10-CYC1, galactose-inducible promoter; Ter PGK, phosphoglycerate kinase terminator sequence; BAD, biotin acceptor domain; Thr, thrombin cleavage site, EcoRI, SacII, NheI and BamHI, restriction enzyme sites.

Fig. 2. Alignment of the amino acid sequence of human SERCA2a pump with that of the SERCA2aR863G protein. The amino acids sequence of SERCA2aR863G after cloning was aligned with its wilt-type counterpart by using ClusterW software. The thrombin cleavage site is highlighted in light blue, whereas the point mutation is indicated by a blue arrow.

3.2.2 *PROTEIN EXPRESSION*

A total of 10 mL of minimal medium (0.1% w/v Bacto Casamino acids (BD Diagnostic Systems, NJ, U.S.A.), 0.7% w/v yeast nitrogen base, 2% w/v glucose, 20 µg/mL adenine) were inoculated with the selected clone and incubated at 28 °C for 24 h. The preculture was then diluted in 100 mL of fresh medium. The second pre-culture was used to start the culture in YPGE medium (1% w/v yeast extract, 0.5% w/v glucose, 1% w/v bactopeptone, 2.7% v/v ethanol). After 36 h of growth at 28 °C, the temperature of the culture was lowered to 20 °C. Expression was induced by adding galactose to a final concentration of 2% w/v. After overnight incubation at 20 °C, an additional induction with galactose was performed. The culture was stopped after 6 h. The culture was then collected and centrifuged at 1000g_{av} for 15 minutes. The pellet obtained was washed with sterile water, centrifuged at 1000 g_{av}, frozen and stored at -80 °C. The pellets weight was estimated prior to storage.

3.2.3 *ISOLATION OF YEAST MEMBRANES*

The pellet was thawed and resuspended in 50 mM TRIS-HCl, pH 7,5, 1mM EDTA, 0,6 M sorbitol, 0,1 M KCl, at a concentration of about 2 ml/g of yeast. Protease inhibitors were added to the suspension (Roche Diagnostics, Basel, Switzerland) (1 tablet of complete EDTA-free antiprotease cocktail for 100 ml) and the lysis was performed with a cell disruptor (One Shot Model, Constant Systems Ltd) at 2,4 kBar. The cell debris was separated from the suspension by centrifugation at 1000 g_{av} at 4 °C for 15 minutes. The supernatant (S1) was then centrifuged at 18,000 g_{av}. The pellet obtained (P2), containing the heavy membrane fraction, was resuspended in Hepes-sucrose buffer (20 mM Hepes-Tris, pH 7.4, 0,3 M sucrose, 0,1 mM $CaCl_2$), flash frozen and stored at -80 °C for further analysis. The supernatant (S2) was centrifuged at 29,000 g_{av} for 3 hour at 10 °C in order to recover the light membrane fraction (P3), which was resuspended in Hepes-sucrose buffer (0.2 mL/g of yeast) and stored at -80 °C after flash frozen.

3.2.4 SOLUBILIZATION OF MEMBRANE FRACTIONS

The total protein content was estimated by the bicinchoninic acid procedure. Light membranes (P3) were diluted at 5 mg/ml of total proteins in the pre-solubilization buffer (50 mM MOPS-Tris pH 7, 100 mM KCl, 20% Gycerol w/v, 1mM $CaCl_2$, 1mM PMSF, 1mM β-mercaptoethanol and protease inhibitors cocktail). After gentle stirring, the light membrane fraction was centrifuged at 29,000 g_{av} for 1 hour at 10 °C. The pellet was then resuspended using a Potter-type homogenizer in the solubilization buffer (same composition as pre-solubilization buffer) and *n*-dodecyl-β-d-maltoside (DDM) (detergent/protein ratio of 3:1). The suspension (T_{DM}) was kept under gentle stirring for 20 minutes at room temperature. Insoluble materials were removed by centrifugation for 1 hour at 10°C and 100,000 g_{av}. The supernatant contains the solubilized proteins (S_{DM}).

3.2.5 FORMATION OF PHOSPHO-INTERMEDIATE ENZYME ON MEMBRANE FRACTION

Formation of the phosphoenzyme intermediate from ATP on membrane fractions (10µg) was performed in a 100 µl reaction mixture containing 160 mM KCl, 17 mM Hepes, pH 7.0, 1 mM DTT, 5 mM NaN_3, and 0.1 mM $CaCl_2$, 50 mM EGTA, 1µM Thapsigargin.

The reaction, carried out on ice for 30 s, was started by the addition of 1µl of 2µCi/µl [γ-33P]ATP (Amersham Biosciences) and stopped by adding 6% trichloroacetic acid, 10 mM phosphoric acid, and 1 mM ATP. The samples were kept on ice for 15 min and then pelletted by centrifugation at 15,000 g_{av} for 3 min at 4°C. Pellets were washed two times in the same buffer and finally resuspended in modified SDS-PAGE sample buffer (100 mM Tris-HCl, pH 8, 1.4 M β-mercaptoethanol, 4% SDS, 1 mM EDTA, 8 M urea and 0.05% bromphenol blue). Phosphorylated proteins were separated by electrophoresis on SDS polyacrilamyde gradient gels (5-10%), according to Sarkadi et al. (Sarkadi, B. et al 1986). After fixation in 7.5% acetic acid and drying, the gels were analyzed by autoradiography through Cyclone Plus Phosphor Imager (PerkinElmer).

3.2.6 *PURIFICATION OF HSERCA2AR863G*

Purification of the hSerca2aR863G protein was carried out either by affinity chromatography with avidin agarose resin (Softlink Soft Release Avidin Resin, Promega) and with the use of avidin-coated magnetic nanoparticles (Magro, M. et al, 2012).

In this chapter, only the procedure of avidin-affinity chromatography is reported. For magnetic separator system with avidin-coated magnetic nanoparticles, see the paper in the appendix.

3.2.7 *BATCH PURIFICATION WITH AVIDINE AGAROSE*

The supernatant obtained after solubilization of the protein was applied to 5 ml of Softlink Soft Release Avidin Resin, previously equilibrated with the solubilization buffer and incubated overnight at 4 °C under gentle stirring. The supernatant was then collected and the resin was washed first with 10 column volume (CV) of high salt washing buffer (50 mM MOPS-Tris, pH 7.0, 1M KCl, 20% glycerol (w/w), 1mM $CaCl_2$ and 0,5 mg/ml DDM) and later with 10 CV of low salt washing buffer (50 mM MOPS-Tris, pH 7.0, 100 mM KCl, 20% glycerol (w/w), 2,5 mM CaCl2 and 0,5 mg/ml DDM). The resin was then resuspended in 2 ml of low salt washing buffer containing Thrombin (350 units, Sigma-Aldrich) and incubated overnight at 4 °C. The protease activity was stopped by adding 2.5 mM PMSF (phenylmethanesulfonylfluoride) and the supernatant was then collected.

3.2.8 *GEL-FILTRATION*

The affinity-purified hSERCA2aR863G obtained by avidin resin chromatography was concentrated by Vivaspin-20 (50,000 Mw cut off, Sartorius) and applied to a Superdex 200-HR 10/300 (GE Healthcare Bio-Sciences, Uppsala, Sweden) at 0.5 mL/min. The solvent was constituted of 50 mM Mops-Tris, pH 7.0, containing 100 mM KCl, 20% glycerol, 1mM $CaCl_2$, and 0.5 mg/ml of C12E8 (dodecyl octaethylene glycol monoether). The fractions were pooled and concentrated by Vivaspin-20 until reaching a volume of ≈ 50 μl. Fractions corresponding to monomeric hSerca2aR863G were therefore pooled and concentrated to 12 mg/ml.

3.2.9 PROTEIN RECONSTITUTION AND CRYSTALLIZATION TRIALS

Before crystallization trials, the sample containing the SERCA2a protein was supplemented with phospholipid DOPC (1,2-dioleoyl-sn-glicero-3-phosphocholine) to reach a C12E8/DOPC ratio of 3:1 (w/w), 10 mM $CaCl_2$, and 1mM AMPPCP (β-γ-methylenadenosine-5'-triphosphate). The sample was equilibrated overnight at 4 °C and then subjected to ultracentrifugation (180,000 g_{av} for 10 minutes) to remove aggregation. Crystallization trials were performed by the vapour diffusion method in 0.5 + 0.5 μl hanging drops equilibrating against 500 μl of buffer containing 220 mM sodium acetate, 4% t-butanol, 5 mM β-mercaptoethanol, 15% glycerol, 8-16% PEG 6000.

3.2.10 SODIUM DODECYL SULFATE-POLYACRYLAMIDE GEL ELECTROPHORESIS (SDS-PAGE)

SDS-PAGE was performed as described by Laemmli (Laemmli, U. et al, 1970), using a 10% polyacrylamide gel in a vertical slab gel apparatus (Hoefer Scientific Instrument). Protein samples were prepared in a denaturing sample buffer containing 1.4 M 2-mercaptoethanol, 8 M urea and 1 mM EDTA. The samples (20 μL) were diluted in an equal volume of denaturing sample buffer and boiled at 100 °C for 1 min. Electrophoresis was performed at 120 Volt and 25 mA for 1 h. The run was stopped when the dye front was 2 to 3 mm away from the bottom edge of the gel. The gel was then stained using the Coomassie Brilliant Blue (0.05% Coomassie blue R, 40% methanol, 10% acetic acid) (Neuhoff, V. et al, 1985). Destaining was performed by washing the gels several times with either water or 10% acetic acid.

3.2.11 WESTERN BLOTTING

Western blotting was performed according to the modified method of Towbin et al. (Towbin H. T. et al, 1979) After electrophoresis, the gel was soaked in cold transfer buffer (0.192 M glycine, 25 mM tris, pH 8.3, and 1.3 mM SDS) for 1 h to remove SDS and any excess of electrode buffer. A sheet of nitrocellulose membrane (pore size 0.45 μm) was used (15 × 15 cm) and then was immersed into the transfer buffer. To avoid contamination, forceps and

gloves were used when handling the membrane. Proteins transfer was obtained with a Mini-Trans-Blot Electrophoretic transfer Cell (Bio-Rad) at 100 V and 350 mA for 2 h. After the transfer, the nitrocellulose membrane was gently rocked in blocking buffer constituted of 3% (w/v) BSA in TBS buffer (20 mM Tris-HCl, pH 7.6, 150 mM NaCl) for 2 h at room temperature to block unoccupied sites. The membrane was then incubated with polyclonal antibody anti Serca (SERCA1/2/3 (H300) Santa-Cruz Biotechnology) at a 1:500 dilution in TBS overnight at 4°C in a rocking motion. The membrane was washed 3 times with the TBS buffer, containing 0.5% Tween 20. The membrane was then incubated with mouse antirabbit conjugated with horseradish peroxidase for 2 h at room temperature in a 1:2000 dilution in TBS. After an additional washing step (3 times with TBS and 0.5% Tween 20), the bound antibodies were revealed with Amersham ECL reagent (GE Helthcare and Life Science) in a Kodak Image Station 4000MM Pro (Kodak). The same procedure was performed for detecting all the biotynilated proteins, which was incubated with avidin peroxidase probe (AP) (Sigma Alderich) at a 1:2000 dilution.

3.3 Results and Discussion

3.3.1 Over-expression of hSERCA2aR863G in S. cerevisiae

Human SERCA isoform 2a (R863G) protein was expressed in *S. cerevisiae*, which was previously used for the expression of other Ca^{2+}-ATPases (Lenoir, G. et al, 2002) and for rabbit SERCA1a (Jidenko et al., 2006). This heterologous system appeared to be the more appropriate for the over-expression of functional mammalian membrane proteins, since both the post-translational modification system and the Ca^{2+} homeostasis mechanism are conserved in yeast.

Thanks to the pYeDP60 vector, the hSERCA2a gene was inserted in the same coding frame of Thr cleavage site and BAD (biotin acceptor domain) sequences by the Gap-repair-cloning (Homologous recombination) technique, to allow expression of fusion protein

Serca2a-BAD in *S. cerevisiae*. Later, a point mutation was generated to remove a further thrombin cleavage site within the sequence.

Thus, the recombinant protein was expressed under the control of a galactose-inducible promoter, whereas the biotinylation process of the protein, occurring directly in yeast, has provided a fast and efficient purification strategy. The expression of the protein was performed either in a home made bioreactor (Figure 3) or in 2 l flasks containing each not more than 500 ml, according to the protocol reported by Cardi. (Cardi, D. et al, 2010). We were able to recover about 50 grams of yeast for liter of culture. Since in vivo the biotinylation reaction only occurs with properly folded fusion protein, we have been able to select the active Ca^{2+}-ATPases molecules after yeast expression by using the avidin peroxidase probe. In addition, the ATP-ase activity was detected by autoradiography.

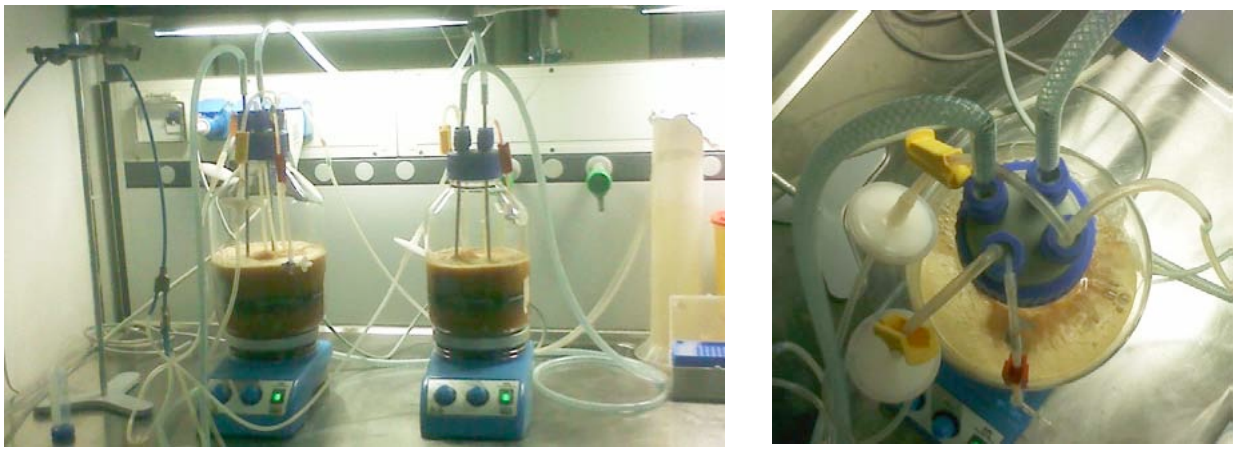

Fig. 3. Over-expression of hSERCA2aR863G in S. cerevisiae. Large-scale expression has been performed by using a home made reactor, allowing us to set the parameters of cell growth during the aerobic growing phase at 28 °C and the anaerobic expression phase at 18 °C.

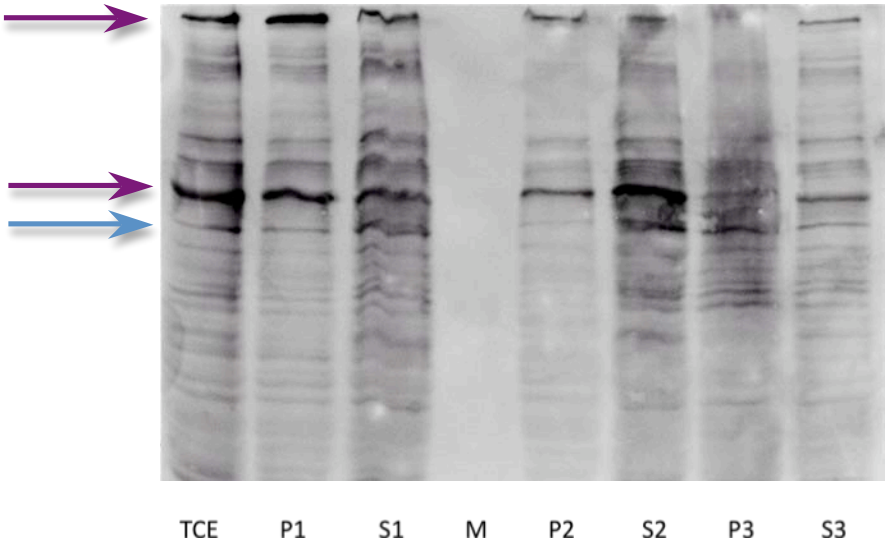

Fig. 4. Western blot analysis of fractions from the membrane preparation by using avidin-HRP probe. All the biotinylated proteins were detected by the probe, revealing two endogenous biotinylated proteins expressed in yeast (purple arrows). Samples were loaded as shown below: TCE, total crude extract; P1, pellet 1; S1, supernatant 1; P2, pellet 2, corresponding to the high membranes; S2, supernatant 2; P3, pellet 2, corresponding to the light membranes; S3, supernatant 3 and M, molecular weight marker. The yeast biotinylated proteins correspond to Acetyl-CoA carboxylase (AcoA. carb.) and pyruvate carboxilase (pyr. carb.). The blue arrow indicates the hSERCA2aR863G-BAD protein.

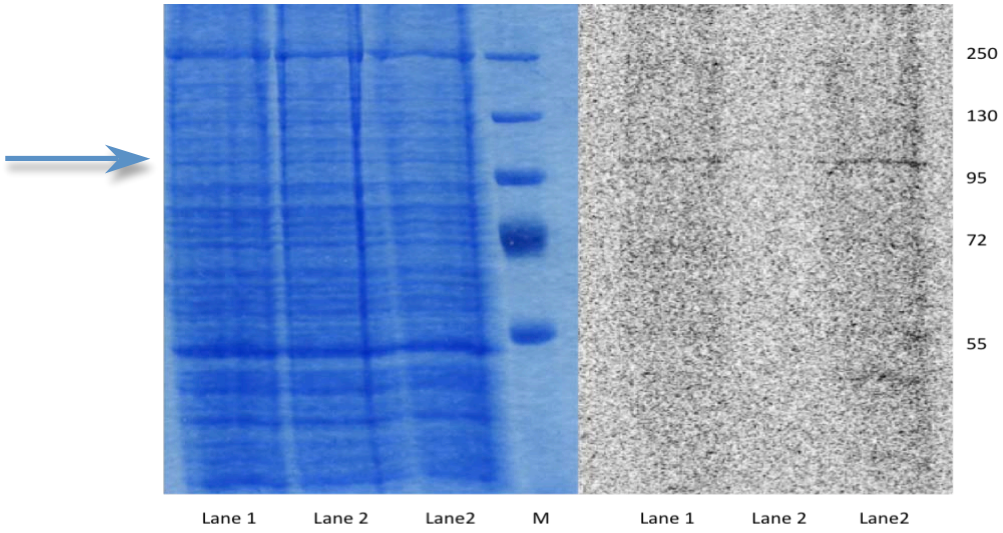

Fig. 5. Formation of phospho-intermediate enzyme on the membrane fraction. Coomassie blue stained SDS-PAGE (left) and autoradiogram (right) of the [γ-33P] ATP-phosphorylated hSerca2aR863G membranes in presence of 0.1 mM $CaCl_2$ (Lane 1), 50 mM EGTA (Lane 2), 1µM Thapsigargin (Lane 3).

3.3.2 HUMAN SERCA, ISOFORM 2A, PURIFICATION

About 4 L of yeast culture were used for each purification trial, from which about 200 g of dry cell pellet was recovered. The estimated total protein content in the light membrane fraction was about 26 mg.

Since recombinant human SERCA2a (hSERCA2aR863G-BAD) competes with the endogenous biotinylated proteins for the binding to avidin, an additional purification step was required in order to increase the recovery of the recombinant protein. Elution of the protein was achieved by overnight incubation of the protein-bound resin with thrombin. The fusion hSERCA2aR863G protein was then released in the supernatant, while the BAD domain remained immobilized onto the resin. About 1 mg of 50% purified protein was obtained from the affinity purification. Coomassie-stained PAGE-electrophoresis and Western blot followed the purification steps, from crude yeasts lysate to the gel-filtration purified product. As shown in Figure 6, a major band of about 80 kDa is visible in Coomassie-stained gels. This band was also detected by Western blot analyses with rabbit polyclonal anti-SERCA (Figure 7) and is therefore attributable to hSERCA2aR863G. The difference between the apparent molecular weight of purified SERCA2aR863G (80 kDa) and the expected weight reported in the literature (115 kDa) is attributable to the effect of the detergent on the electrophoretic mobility of the protein in SDS-PAGE, as often reported for hydrophobic proteins in the presence of detergents (Rath, A. et al, 2009). Finally, a gel-filtration step (Figures 8 and 9) was performed to increase protein purity and to exchange the detergent for crystallization trials. The final yield was about 500 µg of 70% purified protein. The amount of recombinant rabbit SERCA-1a was previously estimated to be about 3% of the total protein content in the membrane fraction of *S. cerevisiae* (Cardi, D. et al, 2010) Because of the high sequence similarity between rabbit SERCA1a and hSERCA2aR863G-BAD, it is possible to assume that the expression levels of the two proteins in yeast are the same. Therefore, based on this assumption, we calculated a yield in the purification process of about 64%.

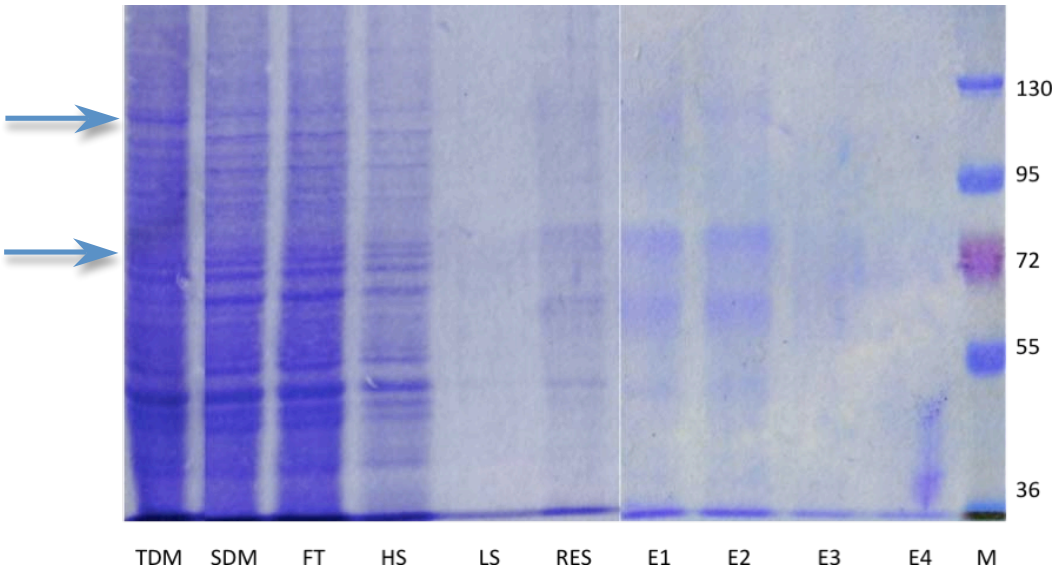

Fig. 6. Purification of hSERCA2aR863G by avidin affinity chromatography. Coomassie blue staining SDS-PAGE of samples collected during affinity purification. Samples for SDM to E4 fractions were 10-fold. Samples were loaded as shown below: TDM, membrane pellet. SDM, solubilized fraction. FT, flowthrought. HS and LS, washing at 1M and 50mM KCl, respectively. RES resin with bound SERCA2aR863G-BAD. E1, E2, E3 and E4, eluted fractions from affinity purification. M, molecular weight marker. Blue arrows indicate the position of the hSERCA2aR863G-BAD and hSERCA2aR863G proteins.

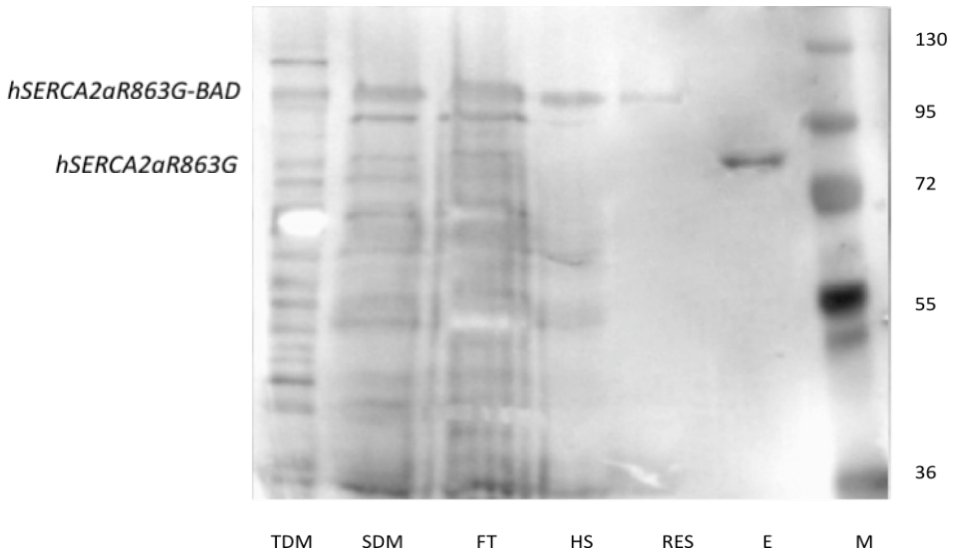

Fig. 7. Purification of hSERCA2aR863G by avidin affinity chromatography. Western blot and immunodetection using anti-SERCA1/2/3 antibody. Samples for SDM to RES fractions were 20-fold, eluted fractions samples (E) was pooled and 50-fold.

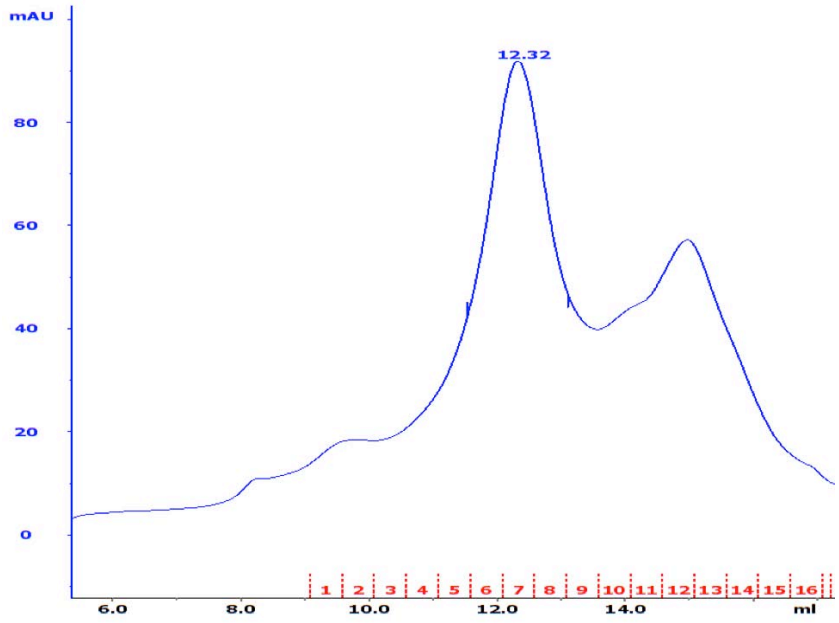

Fig. 8. SEC-FPLC purification step for crystallization attemps. The elution profile at 280 nm of hSERCA2aR863G from size exclusion chromatography after affinity chromatography. The absorption peaks correspond to hSERCA2aR863G and thrombin, respectively.

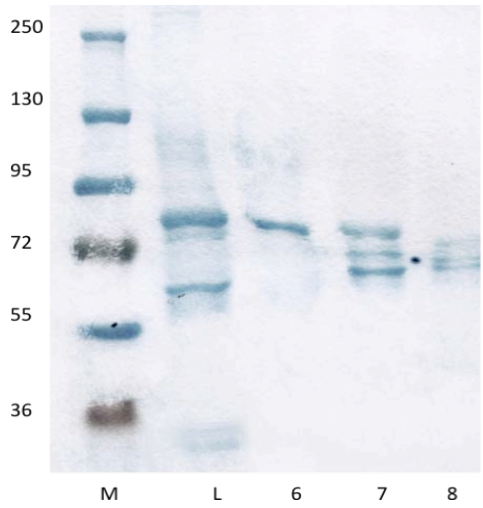

Fig. 9. SEC-FPLC purification step for crystallization attemps. Coomassie blue staining SDS-PAGE of the eluted fractions corresponding to the absorption peak shows that the hSERCA2aR863G pump is present in our protein solution at 70% of purity.

3.3.3 *CRYSTALLIZATION TRIALS*

Since the crystallization conditions for SERCA1a isoform are known and routinely used to obtain crystals of the native rabbit SERCA protein, and considering the very low amount of pure protein obtained, we decided to use these conditions to perform some trials by hanging-drop vapour-diffusion technique. Unfortunately, so far we are not able to obtain suitable crystals for diffraction analysis.

3.4 CONCLUSIONS

Despite significant and considerable recent improvements, the expression and the subsequent purification of functionally folded membrane proteins in sufficient amounts for functional and structural studies is still a challenging task; we used the proposed system to purify a membrane protein, the recombinant hSERCA2a. Few expression systems are successfully used to produce milligram quantities of membrane proteins. In recent years, yeast has become the second most popular membrane proteins expression system, after *E. coli*. It is more cost-effective than the expression in mammalian or insect cell lines and it often produces higher yields. Structural studies require that the purified membrane protein is chemically and conformationally homogeneous, stable at relatively high concentrations and available in milligram amounts. We have been able to purify the recombinant hSERCA2a, expressed in yeast, in the presence of other competitive biotinylated proteins and detergents. This system allowed us to reach the promising yield of 500 µg, a sufficient amount for the characterization of membrane proteins by in vitro approaches.

3.5 ACKNOWLEDGEMENTS

We want to address special thanks to Dr. Magro M., from Department of Comparative Biomedicine and Food Science, Padua, for kindly providing avidin@nanoparticles and to Dr. Venerando A. from Department of Biomedical Sciences, Padua, for performing γ-33P-ATPase Assay.

CHAPTER IV

EXPRESSION AND PURIFICATION OF SWIPROSIN1/EFHD2, A NOVEL HUMAN TAU-ASSOCIATED PROTEIN

CONTENTS

4.1 INTRODUCTION

EFhd2 is a novel calcium binding protein more conserved among the species. In fact there are traces from *C. elegans* to *H. sapiens*. Originally, the EFhd2 protein has been identified in CD4 and CD8 T cells and mast cells, but the highest expression of the protein has been detected in the central nervous system, where it has been found associated with pathological forms of the microtubule-associated protein tau. Specifically, EFhd2 forms a complex with the human TauP301L mutant in the JNPL3 tauopathy mouse model, which develops neurogeneration in age-dependent manner. This behaviour is absent in young JNPL3 mice, suggesting that this association is involved in the neurodegeneration process (Vega, I. E. et al, 2008). These data have been also validated in human affected by Alzheimer's disease, where the association between tau and the novel calcium-binding protein was found enhanced. The tau protein plays a key role in the appearance of tauophathies, which are described as a group of neurological disorders characterized by the aggregation of hyperphosphorylated and filamentous tau proteins organized in neurofibrillary tangles. The expression and aberrant modifications of tau proteins have been demonstrated to play a role in mediating the neurodegeneration process. Despite the tau phosphorylation process has been intensely studied, the molecular mechanism underlying the tau-mediated neurodegeneration is poorly understood. The identification of the new tau-associated protein EFhd2 and its structural characterization could help to elucidate the mechanisms responsible for tauopathies. Here we report the expression and purification of the EFhd2 protein aimed at performing structural studies.

4.2 MATERIALS AND METHODS

4.2.2 HETEROLOGOUS EXPRESSION OF HUMAN EFHD2 IN E. COLI

E. coli BL21(DE3) competent cells were transformed with a plasmid pet28b containing the EFhd2 coding sequence with a polyhistidine tag linked to the N-terminus. The plasmid

used was kindly provided by Irving Vega from the Department of Biology, University of Puerto Rico. After heat shock transformation, cells were grown in a selective LB medium supplemented with 100 µg/mL ampicillin. An overnight pre-inoculation was the starting point for a 1L culture performed at 37°C. When absorbance A_{600} reached the value 0.6, protein expression was induced with 0.5 mM IPTG and bacteria were grown for 1 additional hour at 37°C. The cells were harvested and the medium eliminated by centrifugation. The pellet was resuspended in a lysis buffer containing, 50 mM TRIS pH7.4, 150 mM NaCl, 1 mM CaCl2, supplemented with a protease inhibitor cocktail tablet (Roche). The lysis was carried out using the cell disruptor at 1,35 Kbar. Cells were then centrifuged at 18,000 g_{av} for 15 min in order to separate the supernatant from the insoluble fraction.

4.2.3 *IMAC PURIFICATION AND SIZE EXCLUSION CHROMATOGRAPHY*

The soluble fraction (crude protein mixture) was applied to a 1ml His-trap Ni-chelated column (GE Healtcare) for IMAC (Immobilized Metal Affinity Chromatography) purification. The column was firstly equilibrated with a buffer containing 50 mM TRIS pH 7.4, 150 mM NaCl, 1 mM CaCl2.Two subsequent washing steps were performed using the same buffer supplemented with 5 mM Imidazole. The EFhd2 protein was then eluted in a gradient ranging from 5 mM to 500mM imidazole. The fractions containing the EFhd2 protein were pooled, concentrated and further purified on a gel filtration column (Superdex 75 prep grade HR16/60; GE Healthcare) equilibrated with 150 mM NaCl, 50 mM TRIS pH 7.4 and 2 mM CaCl2 buffer.

4.2.4 *SDS-PAGE AND WESTER BLOT ANALYSIS*

SDS-PAGE was performed on a 14% polyacrylamide gel in a vertical slab gel apparatus (Hoefer Scientific Instrument). The samples (20 µL) were diluted in an equal volume of denaturing sample buffer containing 1.4 M 2-mercaptoethanol, 8 M urea and 1 mM EDTA and boiled at 100 °C for 1 min. After electrophoresis running at 120 Volt and 25 mA for 1 h, the gel was stained by using the Coomassie Brilliant Blue (0.05% Coomassie blue R, 40%

methanol, 10% acetic acid). Several washing with either water or 10% acetic acid destained the gel. After electrophoresis, the gel was transfers on a nitrocellulose membrane (pore size 0.45 µm) with a Mini-Trans-Blot Electrophoretic transfer Cell (Bio-Rad) at 100 V and 350 mA for 1 h in a 0.192 M glycine, 25 mM tris, pH 8.3, and 1.3 mM SDS buffer. After the transfer, the nitrocellulose membrane was blocked with a 3% (w/v) BSA in TBS buffer (20 mM Tris-HCl, pH 7.6, 150 mM NaCl) for 2 h at room temperature. The membrane was then incubated with mouse anti-His tag monoclonal antibody (Cell-Biolabs, Inc.) at a 1:1000 dilution in TBS overnight at 4°C in a rocking motion. The membrane was washed 3 times with the TBS buffer and was then incubated with mouse antirabbit conjugated with horseradish peroxidase for 2 h at room temperature in a 1:2000 dilution in TBS. After several washing steps, the bound antibodies were revealed with Amersham ECL reagent (GE Helthcare and Life Science) in a Kodak Image Station 4000MM Pro (Kodak).

4.2.5 LIMITED PROTEOLYSIS

The protein was incubated with Chimotripsin in a 1:1000 W/W ratio of protein: protease in 50mM Tris, pH 8.0, 0.5mM 2-ME, 150mM NaCl reaction buffer at 4 °C for 2, 15, 30 and 60 min. The total reaction volume was 1 ml. To test the activity of the proteolic enzyme on the protein in absence of calcium, the reaction buffer was supplemented with 0.2 mM EDTA. At the end of the digestion period, the reaction was stopped by adding the same amount of loading buffer. Finally, the samples containing the EFhd2 fragments were loaded on 14% SDS-PAGE and visualized by coomassie blue staining. The same procedure was used for testing Thermolysin activity in 1 ml of a buffer containing 50mM Tris, pH 8.0, 10mM $CaCl_2$, 0.5mM 2-ME and 150mM NaCl.

4.2.6 CRYSTALLIZATION

Crystallization trials were carried out using the vapour diffusion technique whit an Oryx8 crystallization device (Douglas Instruments). Different precipitant solutions from

several crystallization kits (Structure Screen I and II by Molecular Dimensions, PACT Suite, JCSG Suite, PEGs and PEGs II, by Qiagen) were screened by using the hanging drop technique.

In situ proteolysis with chimotripsin was performed to enhance the probability to obtain crystals starting from a more stable protein solution. Unfortunately crystals diffracting well have not been obtained yet. However, some small crystals formed in presence of 0.2 M calcium chloride, 0.1 M Na HEPES pH 7.5 and 28 % v/v PEG 400. They need further tests.

4.3 Results and Discussion

EFhd2 is a 240 amino-acid protein of 27 KDa that exhibit an apparent molecular weight of 33 KDa, as indicated by SDS-Page. The predicted secondary structure shows a protein consisting of a polyalanine motif located at the N-terminus, two EF-hand motifs and a coiled-coil domain at the C-terminus. The presence of polyalanine and coiled-coil are in agreement with the EFhd2 structural features to promote protein-protein interactions, whereas the two EF-hand motifs at the centre of the protein sequence mediate calcium binding. The protein stability is assured through the calcium binding, as described later. The recombinant EFHD2 protein was expressed in *E. coli* as polyhistidine-tagged fusion under the control of an IPTG-induced promoter. Affinity purification of Efhd2 was achieved though IMAC chromatography and yielded about 20 mg of protein per l of *E. Coli* culture. Initial purification trials showed that the protein in the absence of Calcium underwent proteolytic degradation. The addition of Calcium seamed to reduce the proteolytic degradation and to increase the purity of the protein after gel-filtration (see elution profile with and without Calcium). This behaviour, which is typical of calcium binging proteins (they undergo significant conformational changes upon calcium binding), is indicative of the correct folding of the protein. Nonetheless the presence of degradation bands in the SDS-PAGE after gel-filtration is hardly compatible with crystallization purposes. To identify exposed regions susceptible to protein degradation, a limited proteolysis strategy was performed. This procedure suggested Chimotripsin as the best enzyme able to remove disordered and unstable regions in order to recover a stable

protein subdomain, as shown by the presence of a single band in the SDS-PAGE (Figure 6). This allowed us to performed in situ proteolysis crystallization trials. Some small protein crystals have been observed in specific conditions of the Structure Screen kit, but unfortunately they do not diffract. Optimizing the crystal growth conditions, perhaps making use of additives, could enhance the probability to obtain suitable crystals for structure determination.

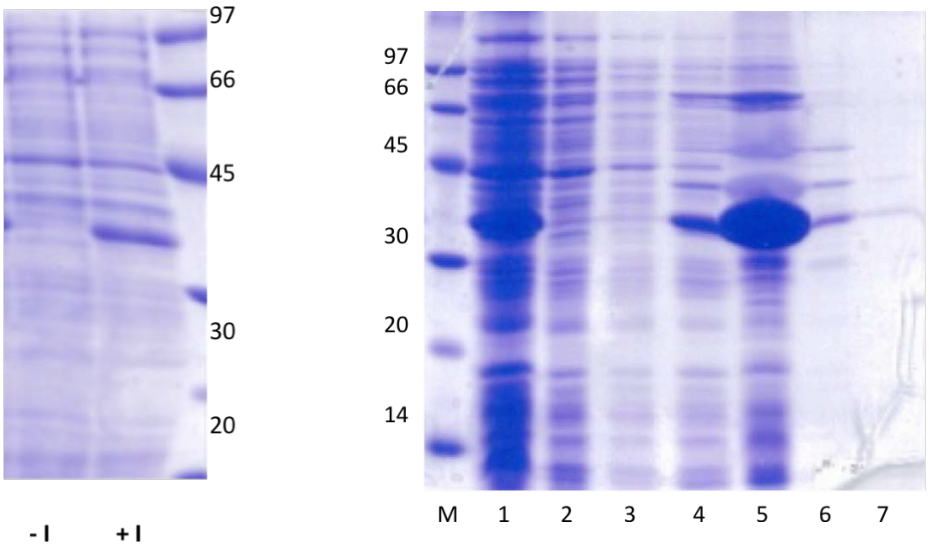

Fig 1. Expression and affinity purification of EFhd2. On the left: Coomassie blue staining SDS-PAGE of culture medium before (-I) and after (+I) induction via IPTG. Right: Coomassie blue staining SDS-PAGE of EFhd2 samples from Imac Affinity and after elution in imidazole steps gradient (0-500 mM). Samples were loaded as shown below: 1) Crude protein mixture, 2) flow through, 3) washing with 5mM imidazole, 4-7) eluted fractions from imidazole steps gradient.

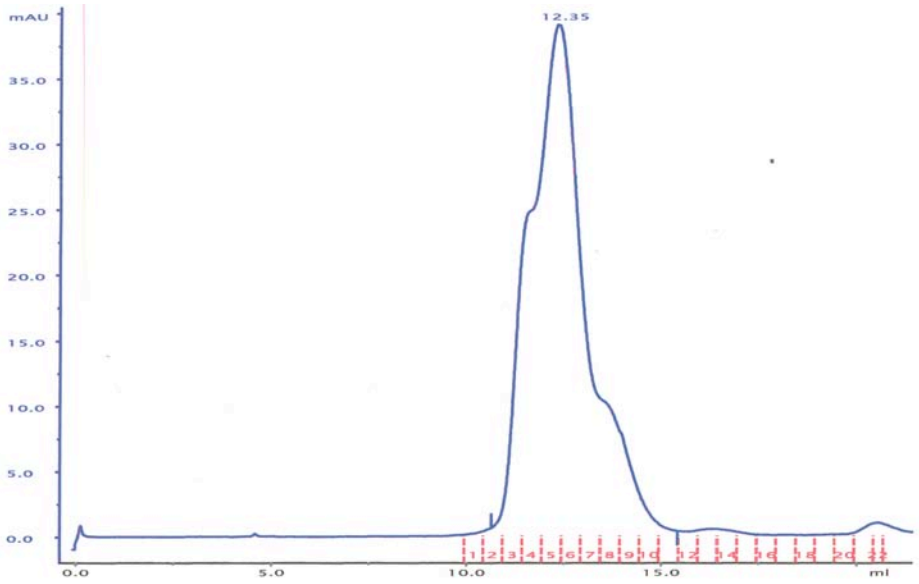

Fig. 2. SEC-FPLC purification step by using a buffer without Ca^{2+}. The elution profile at 280 nm of EFhd2 from size exclusion chromatography with a buffer without Ca^{2+}.

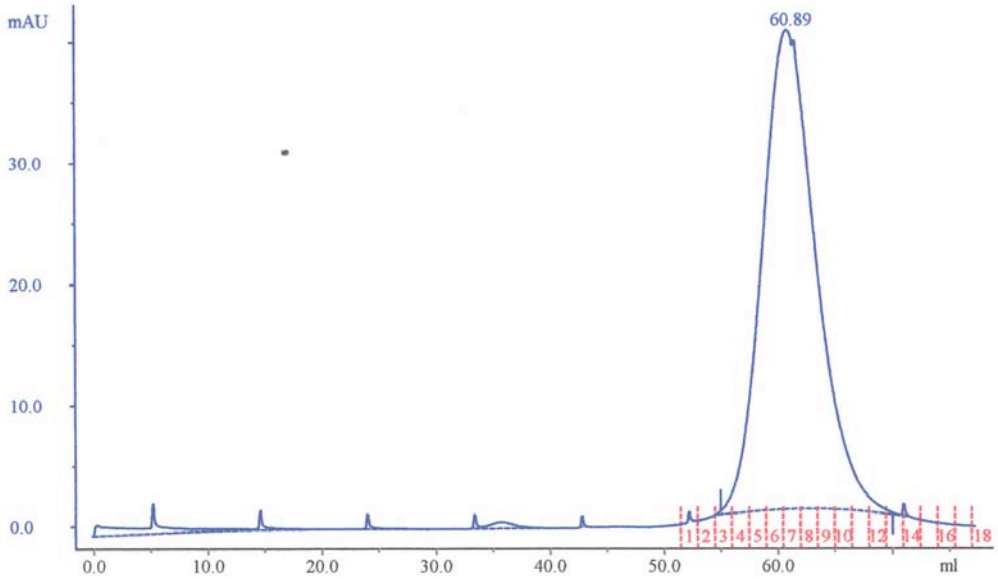

Fig. 3. SEC-FPLC purification step by using a buffer with Ca^{2+}. The elution profile at 280 nm of EFhd2 from size exclusion chromatography with a buffer containing Ca^{2+}.

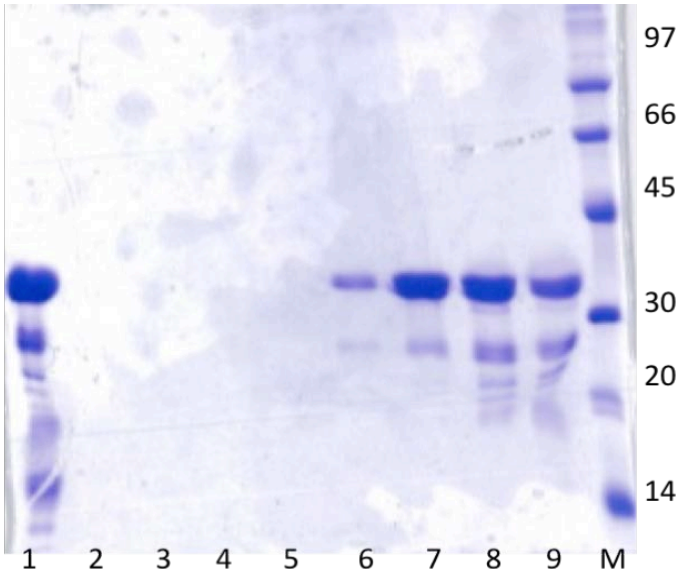

Fig. 4. SEC-FPLC purification step. Coomassie blue staining SDS-PAGE of the eluted fractions, corresponding to the EFhd2 absorption peak. (samples 6, 7, 8, 9).

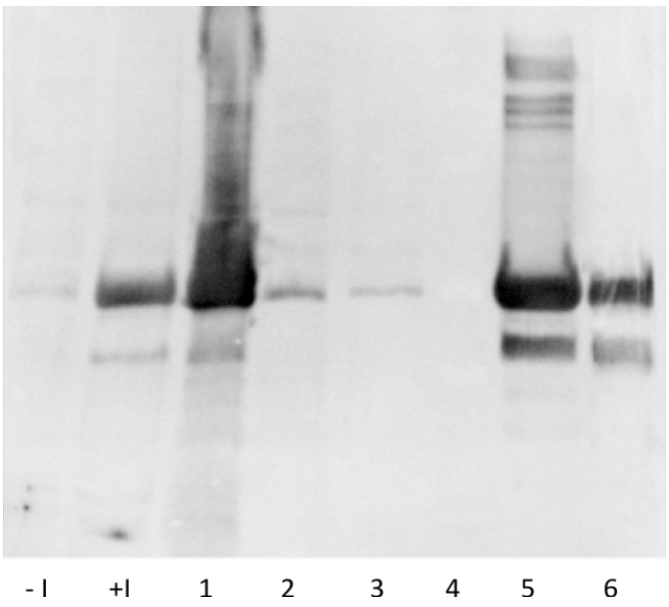

Fig. 5. Western blot and immunodetection using mouse anti-His tag monoclonal antibody. Samples were loaded as shown below: - I and + I) samples before and after induction via IPTG; 1) crude protein mixture; 2) flow through; 3) washing with 5mM imidazole; 4) molecular weight marker; 5) eluted fraction from IMAC purification; 6) eluted fraction from SEC-FPLC.

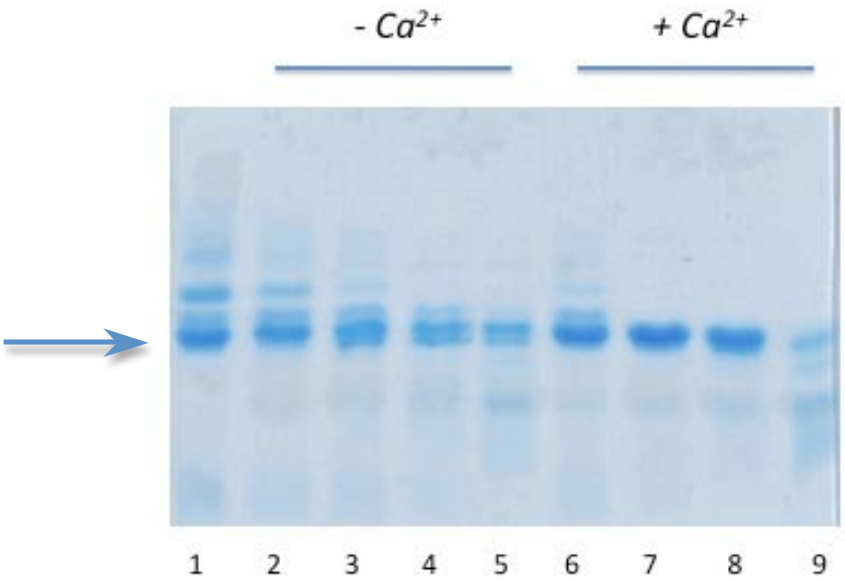

Fig. 6. Coomassie blue staining SDS-PAGE of EFhd2 samples after limited proteolysis. Samples were incubated with with Chimotripsin for 2, 15, 30 and 60 min, respectively. 1) Efhd2 sample after SEC-FPLC; 2-5) samples incubated in absence of Ca^{2+}; 6-9) samples incubated in presence of Ca^{2+}.

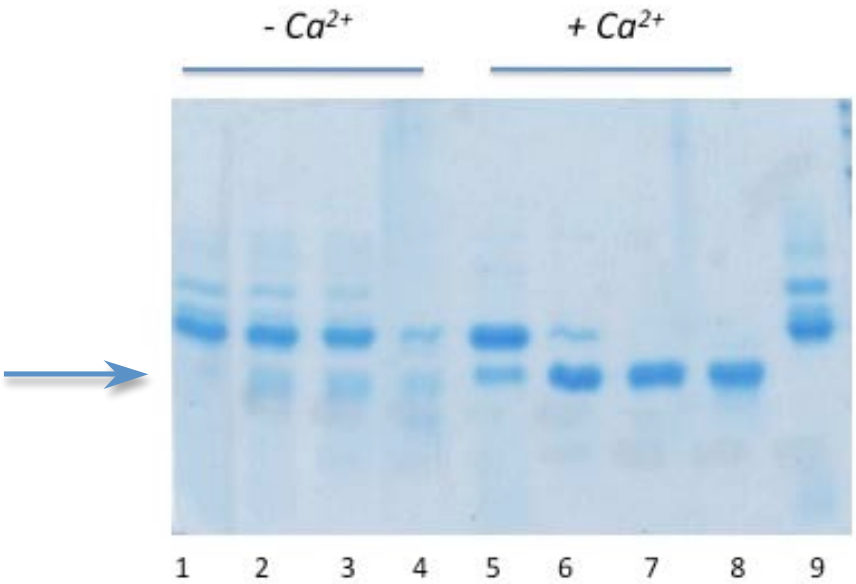

Fig. 7. Coomassie blue staining SDS-PAGE of EFhd2 samples after limited proteolysis. Samples were incubated with Thermolysin for 2, 15, 30 and 60 min, respectively. 1-4) Samples incubated in absence of Ca^{2+}; 5-8) samples incubated in presence of Ca^{2+}; 9) Efhd2 sample after SEC-FPLC.

APPENDIX

AVIDIN FUNCTIONALIZED MAGHEMITE NANOPARTICLES AND THEIR APPLICATION FOR RECOMBINANT HUMAN BIOTINYL-SERCA PURIFICATION

MASSIMILIANO MAGRO, ADELE FARALLI, DAVIDE BARATELLA, ILENIA BERTIPAGLIA, SARA GIANNETTI, GABRIELLA SALVIULO, RADEK ZBORIL AND FABIO VIANELLO

Langmuir 28 (2012) 15392-15401

Langmuir

Article

pubs.acs.org/Langmuir

Avidin Functionalized Maghemite Nanoparticles and Their Application for Recombinant Human Biotinyl-SERCA Purification

Massimiliano Magro,[†] Adele Faralli,[†] Davide Baratella,[†] Ilenia Bertipaglia,[‡] Sara Giannetti,[‡] Gabriella Salviulo,[§] Radek Zboril,[∥] and Fabio Vianello*[,†,∥]

[†]Department of Comparative Biomedicine and Food Science, [‡]Department of Biomedical Sciences, [§]Department of Geosciences, University of Padua, Italy

[∥]Regional Centre of Advanced Technologies and Materials, Department of Physical Chemistry, Faculty of Science, Palacky University in Olomouc, Czech Republic

Supporting Information

ABSTRACT: We report on the surface characterization, functionalization, and application of stable water suspensions of novel surface active maghemite nanoparticles (SAMNs), characterized by a diameter of 11 ± 2 nm and possessing peculiar colloidal properties and surface interactions. These features permitted the acquisition of titration curves and aqueous UV−vis spectra and suggested a role played by surface under-coordinated iron atoms. This new class of nanoparticles was obtained through an easy, inexpensive, one-step, green procedure and functionalized with ligands of high biotechnological interest, such as biotin and avidin, by simple incubation in aqueous solution. Bound avidin was determined by measuring the disappearance of free avidin absorbance at 280 nm, as a function of increasing nanoparticle concentration, showing the presence of 10 ± 3 avidin molecules per nanoparticle. The biological activity of the SAMN@avidin complex was evaluated and the number of available biotin binding sites was determined, using biotinyl-fluorescein as a probe, showing that each bound avidin molecule is able to bind 2.8 ± 0.8 biotin molecules, confirming the maintenance of biological activity and excellent binding capacity of the SAMN@avidin complex. Furthermore a Langmuir isotherm model was used to describe the biomolecule specific monolayer adsorption onto the particle surface, and in the case of avidin, the maximum adsorption capacity was 100 ± 27 μg avidin/mg SAMN, whereas the binding constant is 45.18 μL μg^{-1}. The SAMN@avidin complex was characterized by UV−vis spectroscopy, quartz crystal microbalance, FTIR spectroscopy, and transmission electron microscopy. Finally, SAMN@avidin was applied for the large scale purification of recombinant biotinylated human sarco/endoplasmic reticulum Ca^{2+}-ATPase (hSERCA-2a), expressed by *Saccharomyces cerevisiae*. The protein was magnetically purified, and about 500 μg of a 70% pure hSERCA-2a were recovered from 4 L of yeast culture, with a purification yield of 64%.

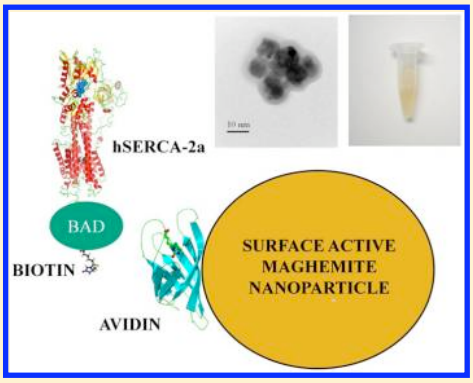

INTRODUCTION

The combination of nanotechnology, biochemistry, biotechnology, and molecular biology has developed into an emerging research area: nanobiotechnology, which offers exciting opportunities for developing new nanosized materials and technologies. In order to develop new hybrid nanostructures it is mandatory to understand surface nanostructure properties. Furthermore, hybrid nanostructures, which combine magnetic nanoparticles with bioelements, such as antibodies, proteins, or other functionalities, lead to superparamagnetic biofunctional nanoparticles exhibiting highly selective binding. As a result, these nanoparticles could have many applications in biology and medicine, including drug delivery, medical imaging, and protein purification.[1,2]

Recently, a number of aqueous magnetic nanoparticle dispersions have been reported, all coated by low or high molecular weight organic polymers or inorganic shells as steric stabilizers in order to prevent the particle aggregation and to maintain long-term stability, pH and electrolyte tolerance, and proper surface chemistry. Many of the polymeric stabilizers reported only bind weakly to nanoparticle surfaces and eventually desorb or exchange with bulk solution, affecting the stability of the resultant dispersions. Furthermore, processes to coat nanoparticles are often cumbersome, time-consuming, expensive, and with low yield and limiting massive productions. At last, nanoparticle coating reduces the average material magnetic moment by introducing nonmagnetic material in the final nanoparticles.[3,4]

Recently, we developed a novel synthesis of nanostructured superparamagnetic material, totally carried out in water, without any organic solvent or surfactant.[5,6] A wet reaction offers several advantages: simplicity, low cost, and high yield scale and, above all, it is an organic solvent free process and thus ecologically green. This nanomaterial is composed of

Received: August 3, 2012
Revised: October 5, 2012
Published: October 11, 2012

stoichiometric maghemite (γ-Fe_2O_3), with peculiar surface chemical behavior, called SAMNs (surface active magnetic nanoparticles).[5,6] SAMNs are synthesized in the dimension range around 10 nm without any superficial modification or coating derivatization. Bare SAMNs are dispersible in water, and their suspensions are stable for several months. Because of their unique physical and chemical properties, these bare iron oxide nanoparticles present a high average magnetic moment and can be easily used to immobilize specific organic molecules.[6] Functionalization is carried out in water, without any chemical reactant, and the total derivatization process is mild, minimizing alteration of ligand macromolecular structure, low cost, and ecologically green. In the present manuscript, SAMN surface properties were studied by titration curves, UV–vis spectroscopy, and ferrocyanide absorption, and we attributed the main responsibility in the distinctive SAMNs surface chemistry to under-coordinated iron atoms.

In biosciences and biotechnology, the isolation of proteins and peptides is usually performed using a variety of chromatographic, electrophoretic, ultrafiltration, or precipitation techniques, with affinity chromatography being the most important. Currently, affinity ligand techniques represent the most powerful tool available to the downstream processing both in terms of selectivity and recovery. The strength of column affinity chromatography has been shown in thousands of successful applications, especially in the laboratory scale.[7] However, the disadvantage of all standard column liquid chromatography procedures is the impossibility to cope with samples containing particulate material, so this technique is not suitable for work in early stages of the isolation/purification process, where suspended solid and fouling components are present in the sample.[8] Among the existing protein purification protocols, magnetic separation and purification seem to be convenient methods for selective and reliable capture of specific proteins.[4−9] Magnetic separation techniques have several advantages in comparison with standard separation procedures. These processes are usually very simple, with only a few handling steps. All of the purification steps can take place in one single test tube or vessel, even on very large volumes. There is no need for expensive liquid chromatography systems, centrifuges, filters, or other equipment. The separation process can be performed directly on crude samples, containing suspended solid material. Furthermore, separation of target proteins using standard chromatography techniques often leads to large volumes of diluted protein solutions. In this case, appropriate magnetic particles can be used for target protein concentration, instead of ultrafiltration, precipitation, etc.[9]

In order to propose a biotechnological application of SAMNs, we functionalized their surface with ligands of high biotechnological interest, such as biotin and avidin. Biotin and avidin represent an example of a molecular key-lock system in life processes, and their most important feature consists of the specificity and the strength of their interaction ($K_a \approx 10^{15}$ M^{-1}). We tested the functionality of SAMN@biotin and SAMN@avidin nanostructures, toward avidin and biotin, respectively. Subsequently, we applied the SAMN@avidin system for the purification of the recombinant sarcoplasmic reticulum Ca^{2+}-ATPase (SERCA-2a). This membrane protein, belonging to the family of P-types ATP-ases, plays a crucial role in the regulation of the excitation-contraction coupling in skeletal and cardiac muscle, thus making it an important target for research investigations.

MATERIALS AND METHODS

Chemicals. Chemicals were purchased at the highest commercially available purity, and they were used without further treatment. Iron(III) chloride hexahydrate (97%), sodium borohydride ($NaBH_4$), tetramethylammonium hydroxide (TMA), biotin, perchloric acid, biotinylated fluorescein, phenylmethanesulfonylfluoride (PMSF), and ammonia solution (35% in water) were obtained from Aldrich (Sigma-Aldrich, Italy). Egg's Avidin (cat. A9275; purity ≥98%) was from Aldrich (Sigma-Aldrich, Italy)

Instrumentation. Optical spectroscopy and fluorescence measurements were respectively performed in 1 cm quartz cuvettes using a Cary 50 spectrophotometer and a Cary Eclipse fluorescence spectrometer (Varian Inc., Palo Alto, CA, U.S.A.).

FT-IR spectra were acquired using a Thermo Nicolet Nexus 670 instrument. Nanoparticle samples were lyophilized, homogenized with KBr powder, and pelleted by an 8.0 tons hydraulic press.

Nanoparticles (2 g L^{-1}) were suspended in Milli-Q grade water (3.5 L) by treatment in an ultrasonic bath at 48 kHz, 50 W (Bransonic, mod. 221 at 48 kHz, 50 W), for at least 3 h, giving a stable colloidal suspension.

Microscopic characterizations of the native maghemite particles, as well as biotin and avidin coated particles, were performed by transmission electron microscopy (TEM) using a FEI Tecnai 12 microscope operating at 120 kV with a point-to-point resolution of 1.9 Å. Before measurements, SAMN were dispersed in ethanol (50 mg L^{-1}), and the suspension was treated by ultrasound for 10 min. A drop of a very dilute suspension was placed on a carbon-coated copper grid and allowed to dry by evaporation at room temperature.

Quartz crystal microbalance (QCMagic), from Elbatech (Marciana, LI, Italy), was interfaced to a driving PC by means of a USB port. QCMagic was equipped with a low-volume (20 μL) flow-through reaction chamber, which houses the oscillating crystal, tuned to work at 9.5 MHz.

Derivatization of the Piezoelectric Crystal. Piezoelectric crystals (Elbatech, Marciana, LI, Italy) consist of a thin quartz disk with gold electrodes plated on it, in which the acoustic wave propagates in a direction perpendicular to the crystal surface. As shown by Sauerbrey in 1959,[10] changes in resonant frequency are simply related to the mass accumulated on the crystal by the following equation:

$$\Delta f = -2\Delta m n f_0^{\,2} \eta_q \rho_q \qquad (1)$$

where η_q and ρ_q are the density and the viscosity of the quartz, n is the overtone number, $f_0^{\,2}$ is the basic oscillator frequency of the quartz, and Δm is the mass adsorbed on the surface per unit/area. For an AT-cut quartz crystal, $\Delta f = -2.26 \times 10^{-6} f_0^{\,2} \Delta m$.

Before the immobilization, the electrode surface of the quartz crystal was cleaned with ethanol and Milli-Q water. The gold electrodes, plated on piezoelectric crystals, were derivatized as follows: freshly cleaned crystals were immersed in an unstirred ethanolic solution of 10 mM 2-mercaptoethylamine at room temperature, in the dark, for 14 h. Crystals were then washed with ethanol and Milli-Q water to remove the excess of the thiol. In order to immobilize biotin on amine derivatized piezoelectric crystals, carbodiimide chemistry was used. In particular, amine modified crystals were incubated in the presence of 10 mM biotin, 50 mM *N*-hydroxysuccinimide, and 200 mM EDC in water for 2 h. This solution must be prepared immediately before the use. The crystals were finally washed with Milli-Q water to remove the excess of reactants.

Derivatized piezoelectric crystals were inserted in a flow injection analysis system (P-500 pump, MV-7 injection valve and LC-500 controller by Pharmacia, Uppsala, Sweden), equipped with a 200 μL loop, at a flow rate of 100 μL min^{-1}. In this way, a QCM sensor, bearing solvent exposed biotin molecules on the surface, was prepared. The biotin modified sensor was tested with SAMN@avidin complex. Alternatively, by injecting an avidin solution (50 μg/mL) in the flow QCM system, containing the biotinylated crystal, the crystal surface was covered by a monomolecular layer of avidin. Due to the presence of 4 biotin binding sites on avidin molecules, the resulting crystal

dx.doi.org/10.1021/la303148u | *Langmuir* 2012, 28, 15392−15401

surface exposed biotin binding sites to the solvent.[11,12] In this last case, the avidin modified sensor was tested with SAMN@biotin complex.

Synthesis of SAMNs. A typical nanoparticles synthesis was already described[5,6] and can be summarized as follows: $FeCl_3 \cdot 6H_2O$ (10.0 g, 37 mmol) was dissolved in Milli-Q grade water (800 mL) under vigorous stirring at room temperature. $NaBH_4$ solution (2 g, 53 mmol) in ammonia (3.5%, 100 mL, 4.86 mol/mol Fe) was then quickly added to the mixture. Soon after the reduction reaction occurrence, the temperature of the system was increased to 100 °C and kept constant for 2 h under stirring. The material was cooled at room temperature and aged in water, as prepared, for other 12 h. This product was separated by imposition of an external magnet, as described in Method, for 60 min, and washed several times with water. This material can be transformed into a red brown powder (final synthesis product) by drying and curing at 400 °C for 2 h, obtaining individual nanoparticles after thermal treatment. The resulting nanopowder showed a magnetic response upon exposure to a magnetic field. The final mass of product was 2.0 g (12.5 mmol) of Fe_2O_3 and a yield of 68% was calculated.

The obtained nanomaterial was characterized by zero field and in field (5 T) Mössbauer spectroscopy, FTIR spectroscopy, high resolution transmission electron microscopy, XRPD, magnetization measurements[5,6] and resulted constituted of stoichiometric maghemite (γ-Fe_2O_3) with a mean diameter of 11 ± 2 nm (see Figure S1), which can lead to the formation, upon sonication in water (Bransonic, model 221, 48 kHz, 50 W) of a stable colloidal suspension, without any organic or inorganic coverage. Notwithstanding, the surface of these bare maghemite nanoparticles shows peculiar binding properties and can be reversibly derivatized with selected organic molecules. We called these bare nanoparticles suface active maghemite nanoparticles (SAMNs).

Magnetic Separation. A series of Nd−Fe−B magnets (N35, 263−287 kJ/m3 BH, 1170−1210 mT flux density by Powermagnet, Germany) were used for the magnetic separations. Magnets were applied on the bottom of the reaction flasks, and depending on the flask volume, supernatants were separated by suction after 30−60 min.

Derivatization of SAMNs with Avidin. SAMNs can be superficially derivatized by simple incubation in water solutions in the presence of avidin. In the present case avidin binding was carried out in 50 mM tetramethylammonium perchlorate, pH 7.0. The amount of bound avidin was calculated from the disappearance of the absorbance at 280 nm in the supernatants ($\varepsilon_{280nm} = 6.99 \times 10^4\ M^{-1}\ cm^{-1}$). Alternatively, bound avidin was released from nanoparticle surface by treatment with 0.5 M ammonia. The released protein was evaluated by spectrophotometry.

Heterologous Expression of Human SERCA-2a in *S. cerevisiae*. The c-DNA coding for human SERCA-2a (Imagenes GmbH, Berlin, Germany) was amplified by PCR and cloned into pYeDP60 plasmid (kindly provided by Marc le Maire, (Université Paris-Sud, F-91405 Orsay, Institut de Biologie et Technologies de Saclay (iBiTec-S) Gif-sur-Yvette, and URA CNRS, France) in the same coding frame of thrombin cleavage site and BAD (biotin acceptor domain) sequences. A mutant of hSERCA-2a (R863G) was generated by PCR based on the QuickChange site-directed mutagenesis strategy (Stratagene) to eliminate a thrombin cleavage site within the protein sequence.

Competent *S. cerevisiae* cells (strain W303.1b Gal4−2 (a, leu2, his3, trp1::TRP1-GAL10-GAL4, ura3, ade2−1, canr, cir+) were transformed with the pYeDP60 vector containing hSERCA-2a (R863G) and selected on minimal plates as described by Gietz and Woods.[13]

Protein Expression. A total of 10 mL of minimal medium (0.1% w/v Bacto Casamino acids (BD Diagnostic Systems, NJ, U.S.A.), 0.7% w/v yeast nitrogen base, 2% w/v glucose, 20 μg/mL adenine) were inoculated with the selected clone and incubated at 28 °C for 24 h. The preculture was then diluted in 100 mL of fresh medium. The second preculture was used to start the culture in YPGE medium (1% w/v yeast extract, 0.5% w/v glucose, 1% w/v bactopeptone, 2.7% v/v ethanol). After 36 h of growth at 28 °C, the temperature of the culture was lowered to 20 °C. Expression was induced by adding galactose to a final concentration of 2% w/v. After overnight incubation at 20 °C, an additional induction with galactose was performed. The culture was stopped after 6 h.[14]

Isolation and Solubilization of Membrane Fractions. Membranes were separated as described by Cardi et al.[15] and the total protein content was estimated by the bicinchoninic acid procedure.[16] Protein solubilization was performed in a buffer containing 50 mM MOPS-Tris, pH 7.0, containing 100 mM KCl, 20% v/v glycerol, 1 mM $CaCl_2$, 1 mM PMSF, 1 mM 2-mercaptoethanol, complete EDTA-free antiprotease cocktail (Roche Diagnostics, Basel, Switzerland) and *n*-dodecyl-β-D-maltoside (DDM) (detergent/protein ratio of 3:1). The suspension was kept under gentle stirring for 20 min at room temperature. Insoluble materials were removed by centrifugation at 100,000*g*.

Purification of hSERCA-2a and Its Mutant. The supernatant (180 mL) was mixed with SAMN@avidin (40 mL, 3.12 g/L) and gently stirred overnight at 4 °C. The magnetic nanoparticles were separated by exposure to an external magnet for 1 h at 4 °C and washed twice with 80 mL of buffer containing 0.05 M Tris, pH 7.0, 1 M NaCl, 20% (w/v) glycerol, 1 mM $CaCl_2$, 1 mM 2-mercaptoethanol, and 0.05% w/v DDM) to remove nonspecifically bound proteins. A further washing step was carried out with 80 mL of the buffer containing 0.05 M Tris-HCl, pH 7.0, containing 0.15 M NaCl, 20% v/v glycerol, 2.5 mM $CaCl_2$, 1 mM 2-mercaptoethanol, 0.05% w/v DDM. The removal of the BAD domain was achieved by thrombin cleavage. The protease activity was stopped by adding 2.5 mM PMSF (phenylmethanesulfonylfluoride). The nanoparticles were removed by magnetic separation.

Gel-Filtration. The affinity-purified hSERCA-2a, obtained by SAMN@avidin purification, was concentrated by Vivaspin-20 (50 000 M_w cut off, Sartorius) and applied to a Superdex 200-HR 10/300 (GE Healthcare Bio-Sciences, Uppsala, Sweden) at 0.5 mL/min. The solvent was constituted of 50 mM Mops-Tris, pH 7.0, containing 100 mM KCl, 20% glycerol, 1 mM $CaCl_2$, and 0.5 g L^{-1} dodecyloctaethylene glycol ether. The gel-filtration was performed in order to increase the protein purity.

Sodium Dodecyl Sulfate-Polyacrylamide Gel Electrophoresis (SDS-PAGE). SDS-PAGE was performed as described by Laemmli,[17] using a 12% polyacrylamide gel in a vertical slab gel apparatus (Hoefer Scientific Instrument). Protein samples were prepared in a denaturing sample buffer containing 1.4 M 2-mercaptoethanol, 8 M urea and 1 mM EDTA. The samples (20 μL) were diluted in an equal volume of denaturing sample buffer and boiled at 100 °C for 1 min. Electrophoresis was performed at 120 mA and 25 mA for 1 h. The run was stopped when the dye front was 2 to 3 mm away from the bottom edge of the gel. The gel was then stained using the Coomassie Brilliant Blue (0.05% Coomassie blue R, 40% methanol, 10% acetic acid).[18] Destaining was performed by washing the gels several times with either water or 10% acetic acid.

Western Blotting. Western blotting was performed according to the modified method of Towbin et al.[19] After electrophoresis, the gel was soaked in cold transfer buffer (0.192 M glycine, 25 mM tris, pH 8.3, and 1.3 mM SDS) for 1 h to remove SDS and any excess of electrode buffer. A sheet of nitrocellulose membrane (pore size 0.45 μm) was used (15 × 15 cm) and then was immersed into the transfer buffer. To avoid contamination, forceps and gloves were used when handling the membrane.

Proteins transfer was obtained with a Mini-Trans-Blot Electrophoretic transfer Cell (Bio-Rad) at 100 V and 350 mA for 2 h. After the transfer, the nitrocellulose membrane was gently rocked in blocking buffer constituted of 3% (w/v) BSA in TBS buffer (20 mM Tris-HCl, pH 7.6, 150 mM NaCl) for 2 h at room temperature to block unoccupied sites. The membrane was then incubated with polyclonal antibody anti Serca (SERCA1/2/3 (H300) Santa-Cruz Biotechnology) at a 1:500 dilution in TBS overnight at 4 °C in a rocking motion. The membrane was washed 3 times with the TBS buffer, containing 0.5% Tween 20. The membrane was then incubated with mouse antirabbit conjugated with horseradish peroxidase for 2 h at room temperature in a 1:2000 dilution in TBS. After an additional washing step (3 times with TBS and 0.5% Tween 20), the bound

dx.doi.org/10.1021/la303148u | *Langmuir* 2012, 28, 15392−15401

antibodies were revealed with Amersham ECL reagent (GE Helthcare and Life Science) in a Kodak Image Station 4000MM Pro (Kodak).

RESULTS

In order to characterize the surface of nanomaterials and to propose new nanobiotechnological applications, it is of fundamental importance to work with stable colloidal water suspensions and the excellent colloidal behavior of SAMNs permitted some informative characterizations. In the present case, maghemite nanoparticles (SAMNs), synthesized according to an innovative, already described method,[5,6] were used. The synthetic mechanism of maghemite formation under our experimental conditions, briefly described in the Materials and Methods section, comprises the reduction of iron(III) by borohydride in water, leading to zerovalent iron. The reaction is conducted in an ammonia containing, alkaline solution, which generates very easily an unstable intermediate. This intermediate, right after its formation, is heated at 100 °C and aged in water, giving maghemite nanoparticles, with no traces of other iron compounds. After curing this material at 400 °C, we obtain the final product, characterized for being stoichiometric crystalline maghemite nanoparticles with peculiar surface properties. The synthetic mechanism of maghemite formation under our experimental conditions is under detailed study.

The resulting nanoparticles were suspended in bidistilled water by using an ultrasonic bath (Bransonic, model 221 at 48 kHz, 50 W). Once formed, this colloidal suspension of bare maghemite nanoparticle was stable, without precipitation or aggregation phenomena, for more than 6 months, in contrast with other maghemite nanoparticles described in literature.[20,21]

The remarkable aqueous suspensions stability of SAMNs was exploited to obtain information on nanoparticle surface behavior by pH titration. An aliquot of SAMN colloidal water suspension (50 mL, 200 mg/L) was brought at pH above 10.5 with tetramethylammonium hydroxide and retro-titrated with 1 M perchloric acid. Two different pK_a were evidenced (pK_{a1} = 5.0 and pK_{a2} = 8.5), demonstrating the presence of different ionizable groups on SAMN surface, differently to data reported in literature.[22] From the same titration curve, 2.5 meq/g SAMNs for each ionizable group were estimated.

In order to obtain deeper information on the nature of nanoparticle surface, SAMNs (500 mg/L) were suspended in 0.10 M $K_4Fe(CN)_6$ (50 mL) and stirred for about 30 min. Then, under continuous stirring, few drops of 6 M HCl were added, till pH 3.5. The resulting mixture turned to blue in few seconds (see Figure 1A), forming the typical Prussian blue color, demonstrating the presence of under-coordinated Fe^{3+} functionalities on SAMN surface. In Figure 1B, the UV−vis spectrum of bare and $Fe(CN)_6^{4-}$ modified SAMNs is presented. The electronic absorption spectrum of bare SAMNs, acquired in water, shows a wide band with a maximum at about 400 nm (Figure 1B) characterized by an extinction coefficient of 1520 $M^{-1}cm^{-1}$, expressed as Fe_2O_3 molar concentration. Furthermore, we noticed that optical properties of SAMNs depend on the presence of salts and on the pH of the suspension. In fact, the SAMN UV−vis spectrum acquired in 50 mM tetramethylammonium perchlorate, pH 7.0, resulted different from the spectrum acquired in pure water see Figure 2A. The SAMN spectrum in tetramethylammonium perchlorate, pH 7.0, shows a wide absorption band characterized by two peaks, at 450 and 500 nm, respectively. Optical properties of SAMN suspensions were also analyzed as a function of pH, in the 200−800 nm spectral range. It was noticed that the wavelength of the absorption maximum was constant, at 450 nm, in the 3.5 − 8.8 pH range, and it decreased to 380 nm increasing the pH value from 8.0 to 11.0 (see Figure 2B). The second peak, at 500 nm, gradually disappears with the increasing of pH, confirming the involvement of surface properties on optical SAMN behavior.

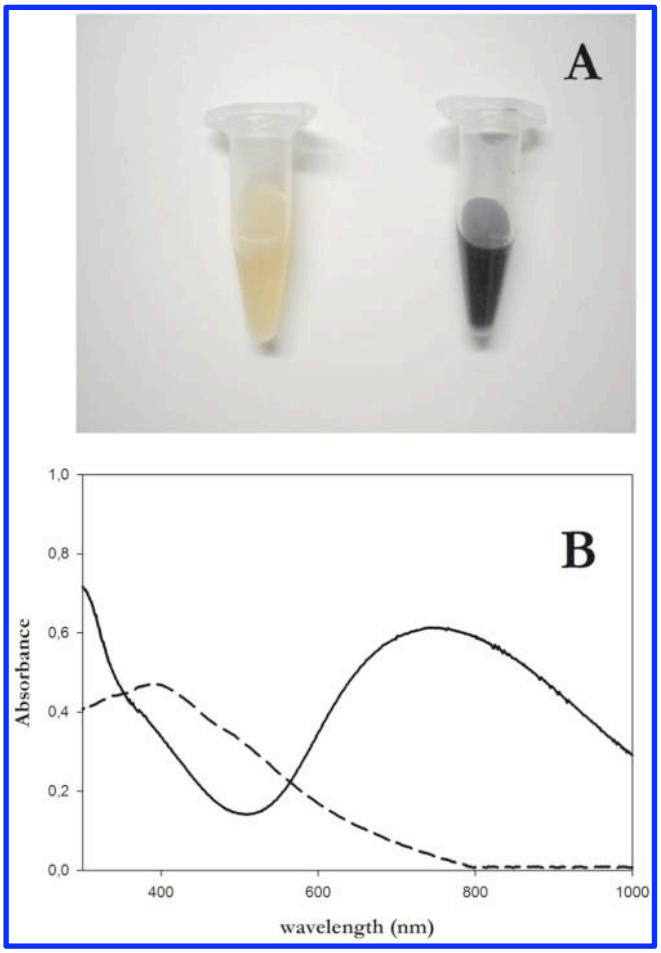

Figure 1. SAMNs superficially derivatized with $Fe(CN)_6^{4-}$. Photograph of bare SAMNs and SAMN@$Fe(CN)_6^{4-}$ suspensions. Optical spectrum of bare SAMN and SAMN@$Fe(CN)_6^{4-}$ suspension acquired in a 1 cm quartz cuvette in water. (---) bare SAMN; (——) SAMN@$Fe(CN)_6^{4-}$.

SAMN Surface Functionalization with Biotin and Avidin. SAMN surface functionalization was accomplished with biotin and avidin by simple incubation of reactants in 50 mM tetramethylammonium perchlorate, at pH 7.0. In particular, SAMN colloidal dispersion (50 mg/L) were incubated with avidin (100 mg/L) or biotin (100 μM), under overnight end-over-end mixing at 4.0 °C. After the incubation period, nanoparticles were separated by the application of an external magnetic field and the presence of the biomolecule in the supernatant was checked by spectrophotometry. SAMN@biotin or SAMN@avidin complexes were magnetically isolated and washed several times with 50 mM tetramethylammonium perchlorate, pH 7.0, and water. Biomolecule coverage on SAMNs was stable, without any loss in solution of biotin or avidin, as checked by spectrophotometry. Even the interaction of avidin and biotin with SAMN surface produced an alteration of nanoparticle optical properties. In this case, both the shape and the position of maximum absorption were altered, further demonstrating the influence of SAMN surface properties on optical characteristics. In water, SAMN@avidin presents a

dx.doi.org/10.1021/la303148u | *Langmuir* 2012, 28, 15392−15401

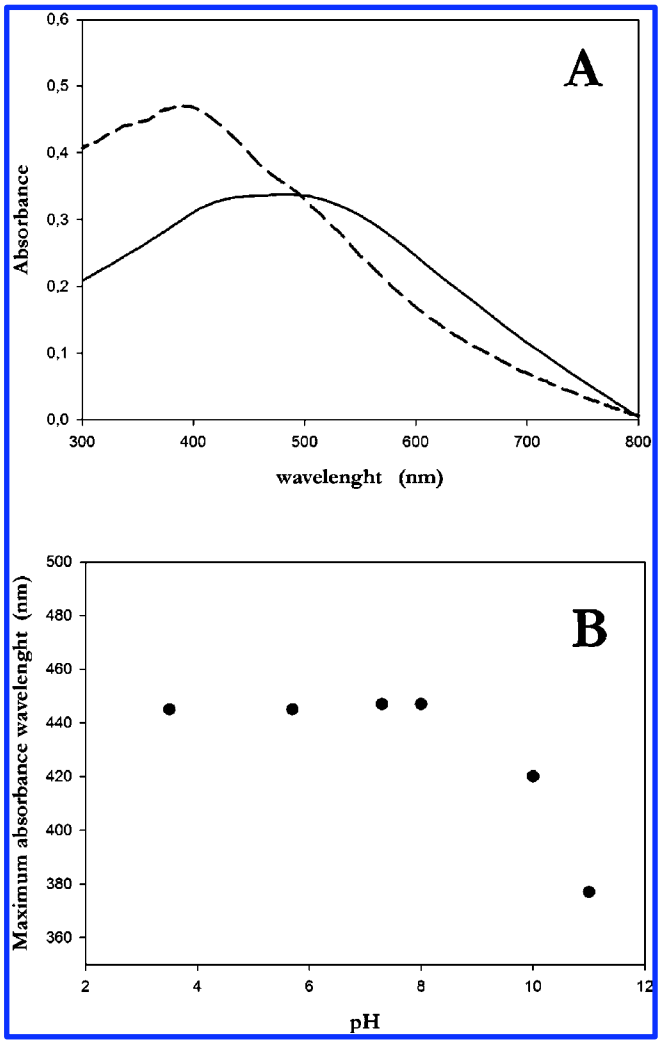

Figure 2. Optical spectrum of SAMN suspension. Spectrum of nanoparticles (50 mg/L), dispersed by sonication, acquired in a 1 cm quartz cuvette. (---) SAMN in water, pH 7.0; (——) SAMN in 50 mM tetramethylammonium perchlorate, pH 7.0. Dependence of the wavelength of maximum absorption of a nanoparticle colloidal dispersion as a function of pH. Nanoparticle colloidal dispersion (100 mg/L) was prepared in 50 mM tetramethylammonium perchorate. The pH was controlled by small additions of perchloric acid and tetramethylammonium hydroxide.

single broad absorption peak, red-shifted by about 10 nm with respect to bare SAMNs, whereas the spectrum of SAMN@biotin is characterized by two peaks, at 450 and 510 nm (see Figure S2).

SAMN@biomolecule complexes were also studied by transmission electron microscopy (TEM) and FTIR. TEM microscopy images of the SAMN@biotin complex indicate the presence of an organic matrix, as a 2−3 nm sized shell around iron oxide nanoparticles, characterized by a lower electron density, attributable to biotin bound molecules on the SAMN surface.

SAMN@biotin complex was characterized by FTIR spectroscopy and compared with underivatized SAMNs. A remarkable change in the FTIR spectrum of SAMNs upon biotin binding, recorded in the 400−4000 cm^{-1} range, confirms the binding of biotin on the SAMN surface (see Figure 3). The FTIR spectrum of free biotin shows two strong bands in the region around 1700 cm^{-1}: The most intense band at 1706 cm^{-1}

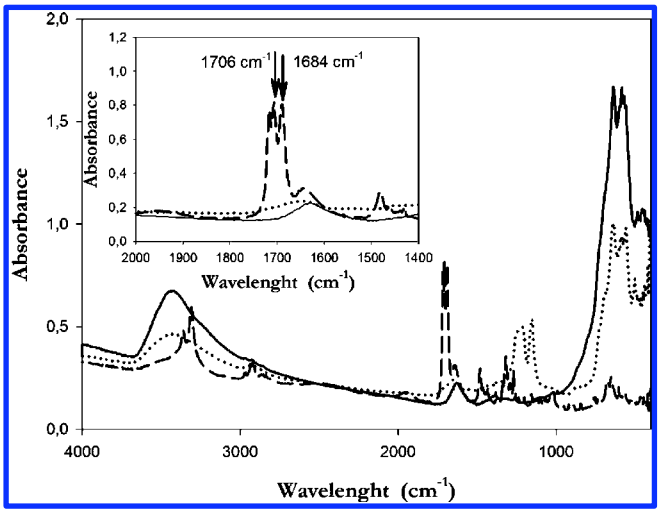

Figure 3. FTIR spectrum of the SAMN@biotin complex. Nanoparticles samples were lyophilized, homogenized with KBr powder and pelleted by an 8.0 tons hydraulic press. (——) SAMN, (---) biotin, and (····) SAMN@biotin. Inset: Detail of the FTIR spectrum of SAMN@biotin complex.

is assigned to the asymmetric C═O stretching of the protonated carboxylate group, whereas the band at 1684 cm^{-1} is due to the C═O stretching vibration of the ureido group.[23,24] It can be observed that the IR spectrum of the SAMN@biotin complex does not show any of the two IR bands, suggesting that both the carboxyl terminal group of the valeric acid chain and the carbonyl of the ureido group are involved in the binding,[25] possibly with under-coordinated iron(III) sites, as discussed by Chen and co-workers.[26]

As a low molecular weight ligand, such as biotin, could completely adhere to the surface of nanoparticles, hindering its recognition by avidin, SAMN@biotin complex was tested by quartz crystal microbalance (QCM). In this case, the gold surface of the piezoelectric crystal was derivatized with avidin, then 50 μg/mL SAMN@biotin complex was injected in the QCM flow-through system. No variation of the resonance frequency acquired by QCM was observed, confirming that the binding capacity of SAMN@biotin toward avidin was compromised, and bound biotin cannot be recognized by avidin, as suggested by FTIR measurements. The unavailability of bound biotin for avidin binding lead us to exclude SAMN@biotin for the development of any further application.

SAMN@avidin complex was prepared as already described and characterized by TEM, FTIR spectroscopy and QCM.

TEM images of SAMN@avidin showed the presence of an organic shell coverage around the iron oxide nanoparticle (see Figure 4), characterized by a shell thickness of about 5 nm, and a lower contrast of particles themselves, which are more embedded in the organic matrix. The shell thickness is in good agreement with avidin size (5.6 × 5.0 × 4.0 nm).[27] The aggregation phenomenon showed by the coated nanoparticles is probably due to TEM sample pretreatment and drying on the copper grid. In water suspensions SAMN@avidin still maintain their stable colloidal behavior.

From the FTIR spectrum of SAMN@avidin (see Figure 5), the presence of typical IR bands, attributable to protein vibrational frequencies of C═C, C═O, and CH_2− groups, in the 1000−1700 cm^{-1} range, appeared,[28] confirming the presence of avidin bound on nanoparticle surface. In particular, the characteristic protein amide I and amide II IR bands at 1654

dx.doi.org/10.1021/la303148u | *Langmuir* 2012, 28, 15392−15401

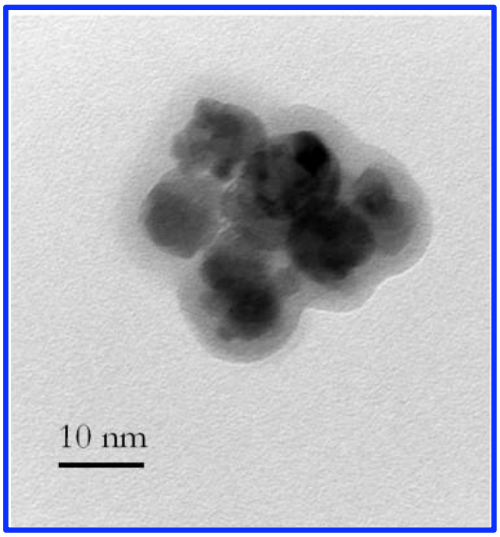

Figure 4. TEM image of the SAMN@avidin complex.

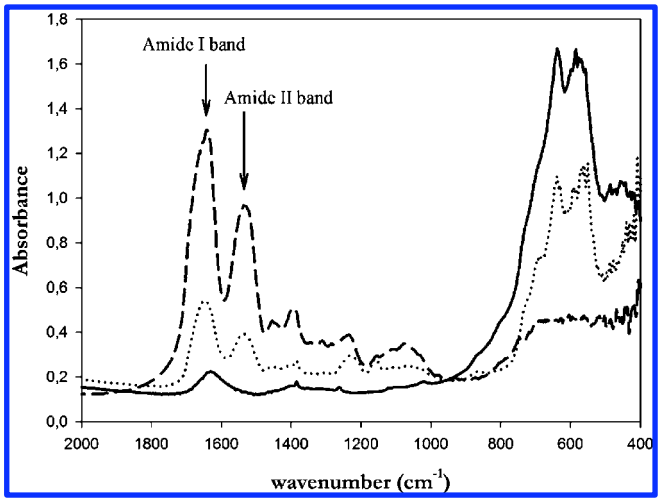

Figure 5. FTIR spectrum of the SAMN@avidin complex. Nanoparticles samples were lyophilized, homogenized with KBr powder and pelleted by an 8.0 tons hydraulic press. (——) SAMN, (---) avidin, and (····) SAMN@avidin.

and 1544 cm^{-1}[29] are present in the SAMN@avidin FTIR spectrum (see Figure 5).

As the interactions between proteins and solid surfaces could lead to significant changes in protein structure[30] and,[31] possibly altering protein functionality and biological activity, as well as modifying ligand accessibility due to unproper orientation of bound protein, SAMN@avidin binding properties were tested by quartz crystal microbalance (QCM), in which the gold surface of the piezoelectric crystal was derivatized with biotin, as described in Methods. Upon injection of 100 μL of 100 mg L^{-1} SAMN@avidin suspension in the flow-through QCM system, a 40 Hz decrease in the resonance frequency of the biotin derivatized crystal was observed, indicating the binding occurrence and confirming the binding capacity of the SAMN@avidin complex.

Furthermore, data on avidin binding on SAMN surface were analyzed according to the Langmuir isotherm model.[32] The analysis was carried out on the assumptions that each binding site acts independently of other sites.[33] The surface fractional coverage of protein was calculated using the following saturation function:[34,35]

$$\theta = \frac{\Gamma}{\Gamma_{max}} = \frac{K[P]}{1 + K[P]} \quad (2)$$

where θ is the surface fractional coverage of bound protein, Γ_{max} is the surface concentration of protein at the full monolayer coverage, K is the apparent binding constant, and Γ is the surface concentration of associated proteins when the bulk concentration of protein is [P]. A linear plot of the experimentally determined $\theta - 1$ as a function of [P] $-$ 1 yields the value of the binding constant, K. In the case of the SAMN@avidin complex, Γ_{max} was 100 μg mg^{-1} and K was 45.18 μL μg^{-1}. The comparison with literature on nanoparticle surface binding of proteins showed comparable results.[36] A value of Γ_{max} 100 μg mg^{-1} corresponds to 17 avidin molecules in a close packed geometry. Bound avidin was also determined by measuring the disappearance of free avidin absorbance at 280 nm ($\varepsilon_{280\ nm} = 6.99 \times 10^4\ M^{-1}\ cm^{-1}$), as a function of increasing nanoparticle concentration, in the range 200−1800 mg L^{-1}, in 50 mM tetramethylammonium perchlorate, pH 7.0. Experimental data showed the presence of 12 ± 3 (n = 5) avidin molecules per nanoparticle, in good agreement with the maximum coverage capacity calculated according to the Langmuir isotherm model. As a comparison, the possible theoretical number of avidin molecules on SAMN surface, considering the geometry of the protein on a sphere of 5.5 nm radius, gives 11−16 avidin molecules per nanoparticle (considering different protein orientations).

The biological activity of SAMN@avidin complex was evaluated and the number of available biotin binding sites was determined, using biotinyl-fluorescein as a probe, showing that each bound avidin molecule is able to bind 2.8 ± 0.8 biotin molecules, confirming the maintenance of biological activity and excellent binding capacity of SAMN@avidin.

Human SERCA, Isoform 2a, Purification. Yeast culture (4 L) was used for each purification trial, from which about 115 g of dry cell pellet was recovered. The estimated total protein content in the membrane fraction was of about 26 mg.

Since recombinant human SERCA-2a (hSERCA-2a-(R863G)-BAD) competes with the endogenous biotinylated proteins for the binding to avidin, a large excess (134 mg) of SAMN@avidin was used for the purification. Furthermore the Coomassie stained gels showed that a significant amount of the recombinant protein was still present in the supernatant after incubation with the nanoparticles (Figure 6). Therefore an additional purification step with SAMN@avidin was performed, by incubating the supernatant previously recovered with fresh nanoparticles, to increase the recovery of the recombinant protein. Elution of the protein was achieved by overnight incubation of the nanoparticles with thrombin. The fusion hSERCA-2a(R863G) protein was then released in the supernatant, while the BAD domain remained immobilized onto the SAMN@avidin surface. About 1 mg of protein was obtained from magnetic affinity purification with SAMN@avidin. The purification steps were followed by Coomassie stained PAGE-electrophoresis and Western blot, from the crude yeasts lysate to the gel filtration purified product. As shown in Figure 6, a major band of about 80 kDa was visible in Coomassie stained gels. This band was also detected by Western blot analyses with rabbit polyclonal anti-SERCA (Figure 7) and is therefore attributable to hSERCA-2a(R863G). The difference between

dx.doi.org/10.1021/la303148u | Langmuir 2012, 28, 15392−15401

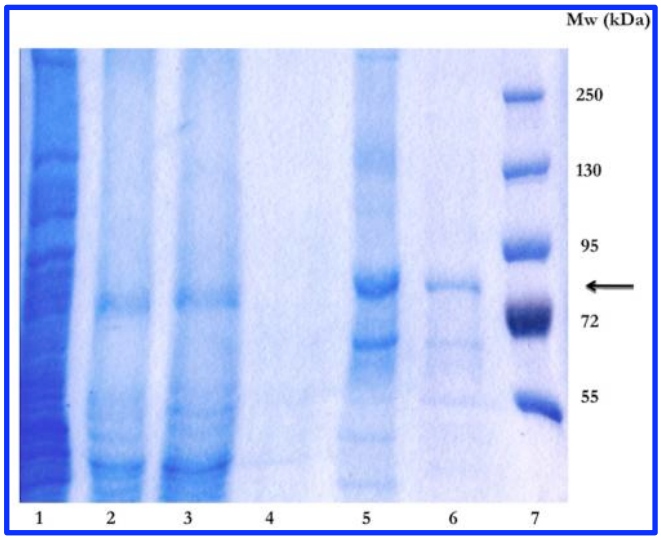

Figure 6. Coomassie stained SDS-PAGE of the different purification steps of hSERCA-2a(R863G) with SAMN@avidin. Collected samples were diluted in SDS-PAGE loading buffer (20 μL of sample diluted in 20 μL loading buffer) and 20 μL of the resulting mixture were loaded on a 10% polyacrylamide gel as follow. 1: membrane pellet; 2: solubilized fraction; 3: supernatant after incubation with SAMN@avidin; 4: washing fraction (with 1 M KCl); 5: eluted fraction from the magnetic purification with SAMN@avidin; 6: eluted fraction from SEC-FPLC (size-exclusion chromatography-fast protein liquid chromatography); 7: molecular weight markers.

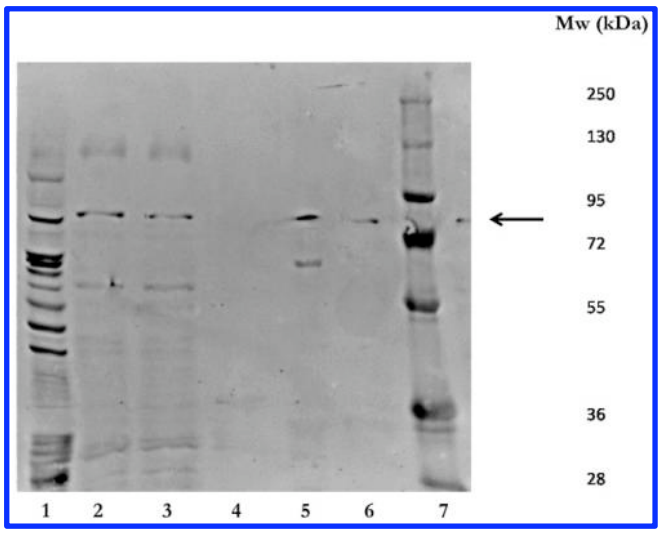

Figure 7. Western blotting analyses of purified fractions. Samples of the eluted fractions were diluted in loading buffer (as previously described) and loaded on an SDS-PAGE acrylamide gel. After electrophoresis, the proteins were transferred to nitrocellulose membranes and hSERCA-2a was detected with rabbit polyclonal antibodies against SERCA (SERCA1/2/3, Santa Cruz Biothecnology) as primary antibody, and with mouse antirabbit conjugated with horse radish peroxidase (AMS Biotechnology ltd). 1: membrane pellet; 2: solubilized fraction; 3: supernatant after incubation with SAMN@avidin; 4: washing fraction (with 1 M KCl); 5: eluted fraction from the magnetic purification with SAMN@avidin; 6: eluted fraction from SEC-FPLC (size-exclusion chromatography-fast protein liquid chromatography); 7: molecular weight markers.

the apparent molecular weight of purified SERCA-2a(R863G) (80 kDa) and the expected weight, reported in the literature (115 kDa), is attributable to the effect of the detergent on the electrophoretic mobility of the protein in SDS-PAGE, as often reported for hydrophobic proteins in the presence of detergents.[36] Finally, a gel-filtration step (Figure S3) performed to increase protein purity and to eliminate excess thrombin yielded to 500 μg of purified protein. The amount of recombinant rabbit SERCA-1a was previously estimated to be about 3% of the total protein content in the membrane fraction of *S. cerevisiae*.[15] Because of the high sequence similarity between rabbit SERCA-1a and hSERCA-2a(R863G)-BAD, it is possible to assume that the expression levels of the two proteins in yeast are the same. Therefore, based on this assumption, we calculated a yield in the purification process of about 64%.

The stability of the SAMN@avidin complex was verified. SAMN@avidin complex was stored in sterile 50 mM tetramethylammonium perchlorate, pH 7.0, at 4 °C, and it was successfully applied for hSERCA-2a(R863G) purification within 6 months.

SAMN@avidin Regeneration. After hSERCA-2a(R863G) purification, the biotin binding domain (BAD) remains bound SAMN@avidin (SAMN@avidin-BAD). The regeneration of SAMN@avidin was successfully accomplished by using a modification of the method proposed by Promega Corporation for the Softlink Soft Release Avidin Resin. Briefly, SAMN@avidin-BAD was incubated in 10% acetic acid, containing an excess of biotin (1 mM), under continuous stirring at 4 °C, in order to partially denature immobilized avidin and to compete with bound biotin binding domain (BAD) and other biotinylated proteins, derived by the yeast colture. A large amount of biotin had been used in order to guarantee the total and irreversible protein removal. After SAMN@avidin washing twice with 1 mM biotin in 10% acetic acid, biotin was removed by washing SAMN@avidin twice with 10% acetic acid. Immobilized avidin was refolded in 0.1 M potassium phosphate buffer, pH 7.0. The biological activity of the regenerated SAMN@avidin was tested by titration of biotin binding sites with biotinylated fluorescein, as described in Methods. After regeneration, each avidin molecule bound to SAMN surface is able to bind 2.0 ± 0.4 biotin molecules, indicating that after hSERCA-2a purification and regeneration, SAMN@avidin maintain 60% of its purification efficiency.

■ DISCUSSION

Surface characteristics of bare SAMNs confer the peculiar ability to form colloidal suspensions, stable for months, suggesting a network of interactions with water molecules and repulsive forces, inhibiting nanoparticle aggregation. At the same time, nanoparticle surface is able to interact with organic molecules in solution. In our previous work we presented a simple electrostatic model to explain SAMN peculiar surface properties[6] and in a following paper we used rhodamine isothiocyanate, as a fluorescent surface probe, suggesting a multiple point binding, involving both electrostatic interactions and complex formation with under-coordinated iron atoms on SAMNs surface, generated by crystal truncation.[38] In the present report we found further evidence of the involvement of under-coordinated iron atoms on SAMN surface in the binding with biological molecules. A strong evidence of the presence of under-coordinated iron atoms on SAMN surface was obtained by Prussian Blue formation after incubation of SAMNs in $K_4Fe(CN)_6$ containing solutions. The UV−vis spectrum of the SAMN@$Fe(CN)_6^{4-}$ was similar to that presented by Zhao et al.[39] (Figure 1) on magnetite nanoparticles covered by Prussian Blue. In our case no addiction of Fe^{3+} was necessary for the

reaction taking place, confirming both the presence of under-coordinated Fe^{3+} on SAMN surface and their availability toward chelating molecules. Up to author knowledge few reports can be found in literature about optical characteristics of water suspensions of bare nanocrystalline maghemite,[40] probably because it is unusual to obtain stable colloidal suspensions of this kind of material. According to Sherman et al.[41] iron oxide optical properties, peculiar of semiconductor metal oxides, can be explained considering that the valence band consists mostly of O(2p)-like orbitals, together with the occupied Fe(3d) orbitals, and the conduction band consists of unoccupied Fe(3d) orbitals. Thus, the band gap corresponds to a ligand-to-metal charge-transfer (LMCT) transition, O(2p) → Fe(3d). Although the band gap of maghemite is 2.01 eV (611 nm), the visible transitions are thought to be indirect transitions (d → d type).[38] Depending on the iron oxide material, direct transitions from O(2p) valence band orbitals to the conduction band edge occur in the range comprised between 3 and 4.7 eV (257−413 nm).[42] As consequence, in agreement with literature prediction, our 400 nm maximum absorption wavelength is attributable to the direct transitions from O(2p) valence band orbitals to the conduction band edge. Furthermore, optical properties of metal oxide in the nanometer range size are expected to be sensitive to surface characteristics.[43] Conversely, the modification of nanoparticle surface will reflect on optical spectrum, as we observed on SAMNs upon salt addition, pH variations and biomolecule binding (see Figures 1, 2, and S2).

Rajh et al[43] found a comparable binding behavior of TiO_2, ZrO_2, and Fe_2O_3 toward chelating ligands. The phenomenon is exclusively characteristic of metal oxide systems displaying colloidal stability, high crystallinity, dimensions below 20 nm, and SAMNs perfectly adhere to these requirements. In this size domain the surface atoms adjust their coordination environment to form under-coordinated metal sites and ligand binding is favored because of the stability gained from ligand adsorption induces a restructuration of the nanoparticle surface. As a consequence, surface modification of nanocrystalline metal oxide particles alters nanoparticle optical properties.[43] Avidin and biotin probably adjust the coordination geometry of the surface Fe^{3+} atoms and shift the onset of absorption band toward the visible region of the spectrum, compared to unmodified SAMNs. The solvent, as well, influences SAMN optical absorption, by interacting with the under-coordinated sites on SAMNs surface.

The possibility to form stable interactions with selected organic molecules leads us to propose the avidin−biotin couple for SAMN derivatization. In particular, SAMN@biotin resulted unuseful for biotechnological application, even if informative about nanoparticle surface properties, possibly confirming the presence of under-coordinated iron(III) atoms on nanoparticle surface, as already suggested.[23] The higher complexity of FTIR spectrum of avidin did not allow us to distinguish about the involvement of specific protein functional groups in SAMN binding. Nevertheless, avidin binds on nanoparticle surface by a monomolecular layer effectively and quickly, by simple incubation in aqueous solution without any expensive reagent or cumbersome procedure, thus reducing the overall unoccupied surface area and, as a consequence, reducing nonspecific protein absorption phenomena and achieving a high specificity.

Protein structural changes upon binding on a solid surface are well documented.[31] These protein conformational modification may negatively affect ligand accessibility and, in the case of avidin, the biotin binding site recognition properties and availability. For this reason, the biological activity of SAMN@avidin complex was studied, in terms of number of biotinylable sites, by using a fluorescent probe, namely biotinyl-fluorescein. From the experimental data, each avidin molecule immobilized on SAMN surface is able to bind 2.8 ± 0.8 biotin molecules, indicating a good binding capacity of SAMN@avidin, and, as consequence, the absence of significant changes in protein structure and of its binding sites.

Furthermore, SAMN@avidin complex was successfully applied to the purification of a membrane protein, namely recombinant human SERCA-2a(R863G), previously biotinylated in *S. cerevisiae*, which present a still unknown structure. The proposed system enabled the magnetic affinity isolation of human SERCA-2a(R863G), from yeast lysate, with an estimated 64% yield and SAMN@avidin, after the purification procedure, was regenerated by an optimized method.

The high specificity exhibited by SAMN on protein separation suggests that these magnetic nanoparticles could be successfully used as a general and versatile system for protein isolation, possibly feasible for other biological targets.

CONCLUSIONS

A new category of maghemite nanoparticles (SAMNs), with a size of about 10 nm, has been proposed and applied. Despite XRD, low-temperature, and in-field Mössbauer and FTIR spectroscopic data, confirm that SAMNs are composed of stochiometric maghemite,[5,6] these particles, easily matching with the interest in biotechnology, revealed different surface characteristics from other reported maghemite nanoparticles. Beyond the peculiar dispersion properties, giving stable water colloidal suspensions without any organic or inorganic coverage, and the possibility to adsorb organic molecules, we first evidenced a unique titration behavior and peculiar UV−vis spectrum. We pointed out the accessibility and availability of under-coordinated Fe^{3+} by a simple reaction with $K_4Fe(CN)_6$ leading to Prussian Blue formation, and we illustrated that SAMN spectral parameters appear to depend on the buffer, on suspension pH and on coupling biomolecules, indicating that nanoparticle optical characteristics are governed by surface properties, in agreement with surface reconstruction theory,[43] probably justifying the peculiar behavior of SAMN suspensions, their high stability in water and their ability of adsorbing biomolecules, features that lead us to propose a new biotechnological device, such as SAMNs@avidin, which can be successfully used to isolate and purify biotinylated proteins.

Despite significant and considerable recent improvements, the expression and the subsequent purification of functionally folded membrane proteins in sufficient amounts for functional and structural studies is still a challenging task; we used the proposed system to purify a hydrophobic membrane protein, the recombinant hSERCA-2a, expressed for the first time in yeast. Few expression systems are successfully used to produce milligram quantities of membrane proteins, in recent years, yeasts have become the second most popular membrane proteins expression system, after *E. coli*, more cost-effective than expression in mammalian or insect cell lines and often showing higher yields. Structural studies require that purified membrane proteins should be chemically and conformationally homogeneous, stable at relatively high concentrations and available in milligram amounts, as consequence, high expression rates are necessary. In this report we were able to purify for the first time recombinant hSERCA-2a, expressed in yeast, in the

dx.doi.org/10.1021/la303148u | *Langmuir* 2012, 28, 15392−15401

presence of a great amount of fouling agents, other competitive biotinylated proteins and detergents. Our system allowed us to reach the promising yield of 500 μg, a sufficient amount for the characterization of membrane proteins by in vitro approaches. Moreover, the complete purification process, from SAMNs synthesis to their application, is cost-effective, fast and ecologically green.

■ ASSOCIATED CONTENT

Supporting Information

Size distribution of SAMNs (Figure S1), optical spectra of SAMN@avidin and SAMN@biotin suspension (Figure S2), and chromatographic exclusion profile from SEC-FPLC of hSERCA-2a(R863G) (Figure S3). This material is available free of charge via the Internet at http://pubs.acs.org.

■ AUTHOR INFORMATION

Corresponding Author

*Tel.: 0039-049-8276863. Fax: 0039-049-8073310. E-mail: fabio.vianello@unipd.it.

Notes

The authors declare no competing financial interest.

■ ACKNOWLEDGMENTS

The authors gratefully acknowledge the support by the Operational Program Research and Development for Innovations, European Regional Development Fund (Project CZ.1.05/2.1.00/03.0058), the Operational Program Education for Competitiveness, European Social Fund (Project CZ.1.07/2.3.00/20.0155) of the Ministry of Education, Youth and Sports of the Czech Republic, and the Grant Agency of the Academy of Sciences of the Czech Republic (KAN115600801 and KAN200380801). The present experimental work was partially funded by Italian Institutional Ministry Grants Cod. 60A06-7411 and 60A06-8055.

■ REFERENCES

(1) Gupta, A. K.; Gupta, M. Synthesis and surface engineering of iron oxide nanoparticles for biomedical applications. *Biomaterials* **2005**, *26*, 3995−4021.
(2) Thorek, D. L.; Chen, A. K.; Czupryna, J.; Tsourkas, A. Superparamagnetic iron oxide nanoparticle probes for molecular imaging. *Ann. Biomed. Eng.* **2006**, *34*, 23−38.
(3) Mackay, M. E.; Tuteja, A.; Duxbury, P. M.; Hawker, C. J.; Van Horn, B.; Guan, Z.; Chen, G.; Krishnan, R. S. General Strategies for Nanoparticle Dispersion. *Science* **2006**, *311*, 1740−1743.
(4) Horak, D.; Babic, M.; Mackova, H.; Benes, M. J. Preparation and properties of magnetic nano- and microsized particles for biological and environmental separations. *J. Sep. Sci.* **2007**, *30*, 1751−1772.
(5) Magro, M.; Valle, G.; Russo, U.; Nodari, L.; Vianello, F. Maghemite nanoparticles and method for preparing thereof. Patent no. PCT/EP2010/060486, 2010.
(6) Magro, M.; Sinigaglia, G.; Nodari, L.; Tucek, J.; Polakova, K.; Marusak, Z.; Cardillo, S.; Salviulo, G.; Russo, U.; Stevanato, R.; Zboril, R.; Vianello, F. Charge binding of rhodamine derivative to OH−stabilized nanomaghemite: universal nanocarrier for construction of magnetofluorescent biosensors. *Acta Biomater.* **2012**, *8*, 2068−2076.
(7) Hage, D. S.; Cazes, J. *Handbook of Affinity Chromatography*, 2nd ed.; CRC Press, Taylor and Francis Group: Boca Raton, FL, 2005.
(8) Turkova, J. *Affinity chromatography*; Elsevier Scientific Publishing Company: Amsterdam, The Netherlands, 1978.
(9) Safarik, I.; Safarikova, M. Magnetic techniques for the isolation and purification of proteins and peptides. *Biomagn. Res. Technol.* **2004**, *2*, 7−24.
(10) Sauerbrey, G. Verwendung von Schwingquarzen zur Wagung dunner Schichtenund Microwagung. *Z. Phys.* **1959**, *155*, 206−222.
(11) Laitinen, O. H.; Nordlund, H. R.; Hytönen, V. P.; Kulomaa, M. S. Brave new (strept)avidins in biotechnology. *Trends Biotechnol.* **2007**, *25*, 269−277.
(12) Livnah, O.; Bayer, E. A.; Wilchek, M.; Sussman, J. L. Three-dimentional structures of avidin and the avidin-biotin complex. *Proc. Natl. Acad. Sci. U.S.A.* **1993**, *90*, 5076−5080.
(13) Gietz, R. D.; Woods, R. A. Transformation of yeast by Liac/SS carrier DNA/PEG method. *Meth. Enzymol.* **2002**, *350*, 87−96.
(14) Jidenko, M.; Lenoir, G.; Fuentes, J. M.; le Maire, M.; Jaxel, C. Expression in yeast and purification of a membrane protein, SERCA1a, using a biotinylated acceptor domain. *Prot. Expr. Purif.* **2006**, *48*, 32−42.
(15) Cardi, D.; Montigny, C.; Arnou, B.; Jidenko, M.; Marchal, E.; le Maire, M.; Jaxel, C. Heterologous expression and affinity purification of eukaryotic membrane protein in view of functional and structural studies: The example of the sarcoplasmic reticulum Ca^{2+}-ATPase. *Methods Mol. Biol.* **2010**, *601*, 247−267.
(16) Smith, P. K.; Krohn, R. I.; Hermanson, G. T.; Mallia, A. K.; Gartner, F. H.; Provenzano, M. D.; Fujimoto, E. K.; Goeke, N. M.; Olson, B. J.; Klenk, D. C. Measurement of protein using bicinchoninic acid. *Anal. Biochem.* **1985**, *150*, 76−85.
(17) Laemmli, U. K. Cleavage of structural proteins during the assembly of the heat of bacteriophage T4. *Nature* **1970**, *227*, 680−685.
(18) Neuhoff, V.; Stamm, R.; Eibl, H. Clear background and highly sensitive protein staining with Coomassie Blue dyes in polyacrylamide gels: A systematic analysis. *Electrophoresis.* **1985**, *6*, 427−448.
(19) Towbin, H. T.; Staehelin, T.; Gordon, T. Electrophoretic transfer of protein from polyacrylamide gels to nitrocellulose sheets: Procedure and applications. *Proc. Natl. Acad. Sci. U.S.A.* **1979**, *76*, 4350−4354.
(20) Harris, L. A.; Goff, J. D.; Carmichael, A. Y.; Riffle, J. S.; Harburn, J. J.; Pierre, T. G., St.; Saunder, S. M. Magnetite Nanoparticle Dispersions Stabilized with Triblock Copolymers. *Chem. Mater.* **2003**, *15*, 1367−1377.
(21) Jain, N.; Wang, Y.; Jones, S. K.; Hawkett, B. S.; Warr, G. G. Optimized Steric Stabilization of Aqueous Ferrofluids and Magnetic Nanoparticles. *Langmuir* **2010**, *26*, 4465−4472.
(22) Simmons, G. W.; Beard, B. C. Characterization of Acid-Base Properties of the Hydrated Oxides on Iron and Titanium Metal Surfaces. *J. Phys. Chem.* **1987**, *91*, 1143−1148.
(23) Shindo, H.; Brown, T. L. Infrared Spectra of Complexes of L-Cysteine and Related Compounds with Zinc(II), Cadmium(II), Mercury(II), and Lead(II). *J. Am. Chem. Soc.* **1965**, *87*, 1904−1909.
(24) Bellamy, L. J. *Advances in infrared group frequencies*; Methuen Co. Ltd.: London, 1968.
(25) Hegde, S.; Kapoor, S.; Joshi, S.; Mukherjee, T. Self-assembly of Ag nanoparticle−biotin composites into long fiberlike microstructures. *J. Colloid Interface Sci.* **2006**, *297*, 637−643.
(26) Chen, L. X.; Liu, T.; Thurnauer, M. C.; Csencsits, R.; Rajh, T. Fe_2O_3 nanoparticle structures investigated by X-ray absorption near-edge structure, surface modifications, and model calculations. *J. Phys. Chem. B* **2002**, *106*, 8539−8546.
(27) Pugliese, L.; Coda, A.; Malcovati, M.; Bolognesi, M. Three-dimensional structure of the tetragonal crystal form of egg-white avidin in its functional complex with biotin at 2.7A° resolution. *J. Mol. Biol.* **1993**, *231*, 698−710.
(28) Stuart, B. H. *Infrared Spectroscopy: fundamentals and applications*; John Wiley & Sons: Hoboken, NJ, 2004.
(29) Haris, P. I.; Severcan, F. FTIR spectroscopic characterization of protein structure in aqueous and non-aqueous media. *J. Mol. Catal. B: Enzymatic* **1999**, *7*, 207−221.
(30) Aubin-Tam, M. E.; Hamad-Schifferli, K. Structure and function of nanoparticle−protein conjugates. *Biomed. Mater.* **2008**, *3*, 034001.
(31) Fenoglio, I.; Fubini, B.; Ghibaudi, E. M..; Turci, F. Multiple Aspects of the interaction of biomacromolecules with inorganic surfaces. *Adv. Drug Delivery Rev.* **2011**, *63*, 1186−1209.

(32) Langmuir, I. The adsorption of gases on plane surfaces of glass, mica and platinum. *J. Am. Chem. Soc.* **1918**, *40*, 1361−1403.
(33) Yang, J.; Swaminathan, C. P.; Huang, Y.; Guan, R.; Cho, S.; Kieke, M. C.; Kranz, D. M.; Mariuzza, R. A.; Sundberg, E. J. Dissecting Cooperative and Additive Binding Energetics in the Affinity Maturation Pathway of a Protein-Protein Interface. *J. Biol. Chem.* **2003**, *278*, 50412−50421.
(34) Pisarchick, M. L.; Thompson, N. L. Binding of a monoclonal antibody and its Fab fragment to supported phospholipid monolayers measured by total internal reflection fluorescence microscopy. *Biophys. J.* **1990**, *58*, 1235−1249.
(35) Hong, M. Y.; Lee, D.; Kim, H. S. Kinetic and Equilibrium Binding Analysis of Protein-Ligand Interactions at Poly(amidoamine) Dendrimer Monolayers. *Anal. Chem.* **2005**, *77*, 7326−7334.
(36) Sun, S.; Ma, M.; Qiu, N.; Huang, X.; Cai, Z.; Huang, Q.; Hu, X. Affinity adsorption and separation behaviors of avidin on biofunctional magnetic nanoparticles binding to iminobiotin. *Coll. Surf. B: Biointerfaces* **2011**, *88*, 246−253.
(37) Rath, A.; Glibowicka, M.; Nadeau, V. G.; Chen, G.; Deber, C. M. Detergent binding explains anomalous SDS-PAGE migration of membrane proteins. *Proc. Natl. Acad. Sci.* **2009**, *106*, 1760−1765.
(38) Sinigaglia, G.; Magro, M.; Miotto, G.; Cardillo, S.; Agostinelli, E.; Zboril, R.; Bidollari, E.; Vianello, F. Catalytically active bovine serum amine oxidase bound to fluorescent and magnetically drivable nanoparticles. *Int. J. Nanomed.* **2012**, *7*, 1−11.
(39) Zhao, G.; Feng, J.; Zhang, Q.; Li, P.; Chen, H. Y. Synthesis and Characterization of Prussian Blue Modified Magnetite Nanoparticles and Its Application to the Electrocatalytic Reduction of H_2O_2. *Chem. Mater.* **2005**, *17*, 3154−3159.
(40) Cherepy, N. J.; Liston, D. B.; Lovejoy, J. A.; Deng, H.; Zhang, J. Z. Ultrafast Studies of Photoexcited Electron Dynamics in γ- and α-Fe_2O_3 Semiconductor Nanoparticles. *J. Phys. Chem. B* **1998**, *102*, 770−776.
(41) Sherman, D. M. Electronic structures of Fe^{3+} coordination sites in iron oxides; applications to spectra, bonding and magnetism. *Phys. Chem. Miner.* **1985**, *12*, 161−175.
(42) Sherman, D. M.; Waite, T. D. Electronic spectra of Fe^{3+}oxides and oxide hydroxides in the near-IR to near-UV. *Am. Mineral.* **1985**, *70*, 1262−1269.
(43) Rajh, T.; Chen, L. X.; Lukas, K.; Liu, T.; Thurnauer, M. C.; Tiede, D. M. Surface Restructuring of Nanoparticles: An Efficient Route for Ligand-Metal Oxide Crosstalk. *J. Phys. Chem. B* **2002**, *106*, 10543−10552.

REFERENCES

Adachi, T., Welsbrod, R.M., Pimentel, D.R., Ying, J., Sharov, V.S., et al., 2004. S-Glutathiolation by peroxynitrite activates SERCA during arterial relaxation by nitric oxide. Nature Med. 10, pp. 1200-1207.

Adams, P.D., Afonine, P.V., Bunkoczi, G., Chen, V.B., Davis, I.W., et al. 2010. PHENIX: a comprehensive Python-based system for macromolecular structure solution. Acta Crystallogr. Sect. D-Biol. Crystallogr. 66, pp. 213-221

Albers, R. W., 1967. Biochemical aspects of active transport. Annu. Rev. Biochem. 36, 727−756.

Asahi, M., Sugita, Y., Kurzydlowski, K., De Leon, S., Tada, M. et al., 2003. Sarcolipin regulates sarco(endo)plasmic reticulum Ca2+-ATPase (SERCA) by binding to transmembrane helices alone or in association with phospholamban. Proc. Natl Acad. Sci. USA, 100, pp. 5040–5045.

Avramidou, A., Kroczek, C., Lang, C., Schuh, W., Jack, H. M., & Mielenz, D. (2007). The novel adaptor protein swiprosin-1 enhances BCR signals and contributes to BCR-induced apoptosis. Cell Death Differ, 14, 1936-1947.

Ballatore, C., Lee, V. M., & Trojanowski, J. Q. (2007). Tau-mediated neurodegeneration in alzheimer's disease and related disorders. Nat Rev Neurosci, 8, 663-672.

Berridge, M. J., 1997. Elementary and global aspects of calcium signalling. J. Physiol., 499, pp. 291–306.

Berridge, M. J., Bootman, M. D., & Lipp, P. (1998). Calcium--a life and death signal. Nature, 395, 645-648.

Berridge, M. J., Bootman, M. D., Roderick, H. L., 2003. Calcium signalling: dynamics, homeostasis and remodeling. Nat. Rev. Mol. Cell Biol., 4, pp. 517–529.

Berridge, M. J., Bootman, M.D., Lipp, P., 1998. Calcium – a life and death signal. Nature, 395, pp. 645–648.

Berridge, M. J., Lipp, P., & Bootman, M. D. (2000). The versatility and universality of calcium signalling. Nat Rev Mol Cell Biol, 1, 11-21.

Brandl, C. J., deLeon, S., Martin, D. R. & MacLennan, D. H., 1987. Adult forms of the Ca2+ ATPase of sarcoplasmic reticulum. Expression in developing skeletal muscle. J. Biol. Chem. 262, 3768−3774.

Brini, M., Carafoli, E., 2009. Calcium pumps in health and disease. Physiol. Rev. 89, pp. 1341-1378.

Brunger, A.T., Adams, P.D., Clore, G.M., DeLano, W.L., Gros, P., et al., 1998. Crystallography & NMR system: A new software suite for macromolecular structure determination. Acta Crystallogr. Sect. D-Biol. Crystallogr. 54, pp. 905-921.

Buffy, J. J., Buck-Koehntop, B. A., Porcelli, F., Traaseth, N. J., Thomas, D. D. et al., 2006. Defining the intramembrane binding mechanism of sarcolipin to calcium ATPase using solution NMR spectroscopy. J. Mol. Biol. 358, pp. 420–429.

Carafoli, E., & Brini, M. (2000). Calcium pumps: Structural basis for and mechanism of calcium transmembrane transport. Current Opinion in Chemical Biology, 4(2), 152-161.

Carafoli, E., Santella, L., Branca, D., & Brini, M. (2001). Generation, control, and processing of cellular calcium signals. Crit Rev Biochem Mol Biol, 36, 107-260.

Cardi, D., Montigny, C., Arnou, B., Jidenko, M., Marchal, E., le Maire, M., et al. (2010). Heterologous expression and affinity purification of eukaryotic membrane proteins in view of functional and structural studies: The example of the sarcoplasmic reticulum ca(2+)-ATPase. Methods in Molecular Biology (Clifton, N.J.), 601, 247-267.

Charlier C, Coppieters W, Rollin F, Desmecht D, Agerholm JS, et al., 2008. Highly effective SNP-based association mapping and management of recessive defects in livestock. Nat Genet. 40, pp. 449-454.

Chen, L., Sumbilla, C., Lewis, D., Zhong, L., Strock, C., Kirtley, M. E., and Inesi, G., 1996. J. Biol. Chem. 271, 10745−10752.

Chen, Z., Akin, B. L., & Jones, L. R. (2007). Mechanism of reversal of phospholamban inhibition of the cardiac Ca2+-ATPase by protein kinase A and by anti-phospholamban monoclonal antibody 2D12. Journal of Biological Chemistry, 282(29), 20968-20976.

Chen, Z., Akin, B. L., & Jones, L. R. (2010). Ca2+ binding to site I of the cardiac Ca2+ pump is sufficient to dissociate phospholamban. Journal of Biological Chemistry, 285(5), 3253-3260.

Chen, Z., Akin, B. L., Stokes, D. L., & Jones, L. R. (2006). Cross-linking of C-terminal residues of phospholamban to the Ca2+ pump of cardiac sarcoplasmic reticulum to probe spatial and functional interactions within the transmembrane domain. Journal of Biological Chemistry, 281(20), 14163-14172.

Chino, A., Watanabe, K., & Moriya, H. (2010). Plasmid construction using recombination activity in the fission yeast schizosaccharomyces pombe. PloS One, 5(3), e9652.

Chu, A., Saito, A., Fleischer, S., 1987. Preparation and characterization of longitudinal tubules of sarcoplasmic reticulum from fast skeletal muscle. Arch. Biochem. Biophys. 258, pp. 13-23.

Clapham D.E. 1995. Calcium signalling. Cell, 80, pp. 259–268.

Clarke, D. M., Loo, T. W. & MacLennan, D. H., 1990. Functional consequences of mutations of conserved amino acids in the beta-strand domain of the Ca2+-ATPase of sarcoplasmic reticulum. J. Biol. Chem. 265, 14088−14092.

Collaborative Computational Project, Number 4, 1994. The CCP4 suite: programs for protein crystallography. Acta Crystallogr. D Biol. Crystallogr. 50, pp. 760-763.

Daiho, T., Yamasaki, K., Saino, T., Kamidochi, M., Satoh, K., et al. 2001. Mutations of either or both Cys876 and Cys888 residues of sarcoplasmic reticulum Ca2+-ATPase result in a complete loss of Ca2+ transport activity without a loss of Ca2+-dependent ATPase activity. Role of the CYS876-CYS888 disulfide bond. J. Biol.Chem. 276, pp.32771-32778.

Daniel Gietz, R., & Woods, R. A. Transformation of yeast by lithium acetate/single-stranded carrier DNA/polyethylene glycol method. Methods in enzymology (pp. 87-96) Academic Press.

De Meis, L., Hasselbach, W., 1971. Acetyl phosphate as substrate for Ca2+ uptake in skeletal muscle microsomes. Inhibition by alkali ions. J. Biol. Chem. 246, pp. 4759-4763.

Dutting, S., Brachs, S., & Mielenz, D. (2011). Fraternal twins: Swiprosin-1/EFhd2 and swiprosin-2/EFhd1, two homologous EF-hand containing calcium binding adaptor proteins with distinct functions. Cell Communication and Signaling, 9(1), 2.

Emsley, P., Cowtan, K., 2004. Coot: model-building tools for molecular graphics. Acta Crystallogr. Sect. D-Biol. Crystallogr. 60, pp. 2126-2132.

Evans, P., 2006. Scaling and assessment of data quality. Acta Crystallogr. D Biol. Crystallogr. 62, pp. 72-82.

Foggia, L., & Hovnanian, A. (2004). Calcium pump disorders of the skin. American Journal of Medical Genetics.Part C, Seminars in Medical Genetics, 131C(1), 20-31.

Frank, K. F., Bölck, B., Erdmann, E., & Schwinger, R. H. G. (2003). Sarcoplasmic reticulum Ca2+-ATPase modulates cardiac contraction and relaxation. Cardiovascular Research, Vol. 57(1), pp. 20-27.

Gianni, D., Chan, J., Gwathmey, J. K., del Monte, F., Hajjar, R. J., 2005. SERCA2a in heart failure: role and therapeutic prospects. J Bioenerg Biomembr, Vol. 37(6), pp. 375-80.

Glaves, J. P., Trieber, C. A., Ceholski, D. K., Stokes, D. L., & Young, H. S. (2011). Phosphorylation and mutation of phospholamban alter physical interactions with the sarcoplasmic reticulum calcium pump. Journal of Molecular Biology, 405(3), 707-723.

Godic, A., Korosec, B., Miljkovic, J., Kansky, A., & Glavac, D. (2010). Four novel ATP2A2 mutations in slovenian patients with darier disease. Journal of the American Academy of Dermatology, 62(5), 819-823.

Gould, G.W., East, J.M., Froud, R.J., McWhirter, J.M., Stefanova, et al., 1986. A kinetic model for the Ca2+ + Mg2+-activated ATPase of sarcoplasmic reticulum. Biochem. J. 237, pp. 217-227.

Grabarek, Z. (2006). Structural basis for diversity of the EF-hand calcium-binding proteins. Journal of Molecular Biology, 359(3), 509-525.

Grünberg W., Sacchetto R., Wijnberg I., Neijenhuis K., Mascarello F., et al., 2010. Pseudomyotonia, a muscle function disorder associated with an inherited ATP2A1 (SERCA1) defect in a Dutch Improved Red and White cross-breed calf. Neuromusc. Disord. 20, pp. 467-470.

Hedges S.B., Kumar, S., 2003. Genomic clocks and evolutionary timescales. TRENDS in Genetics 19, pp. 200-206.

Inesi, G., Prasad, A. M., & Pilankatta, R. (2008). The Ca2+ ATPase of cardiac sarcoplasmic reticulum: Physiological role and relevance to diseases. Biochemical and Biophysical Research Communications, 369(1), 182-187.

Jencks, W. P. Utilization of binding energy and coupling rules for active transport and other coupled vectorial processes. Methods Enzymol. 171, 145–164 (1989)

Jensen, A.L., Sorensen, T.L., Olesen, C., Moller, J.V., Nissen, P., 2006. Modulatory and catalytic modes of ATP binding by the calcium pump. EMBO J. 25, pp. 2305-2314.

Jidenko, M., Lenoir, G., Fuentes, J. M., le Maire, M., & Jaxel, C. (2006). Expression in yeast and purification of a membrane protein, SERCA1a, using a biotinylated acceptor domain. Protein Expression and Purification, 48(1), 32-42.

Jidenko, M., Nielsen, R. C., Sorensen, T. L., Moller, J. V., le Maire, M., Nissen, P., et al. (2005). Crystallization of a mammalian membrane protein overexpressed in saccharomyces cerevisiae. Proceedings of the National Academy of Sciences of the United States of America, 102(33), 11687-11691.

Kawasaki, H., & Kretsinger, R. H. (1995). Calcium-binding proteins 1: EF-hands. Protein Profile, 2, 297-490.

Kho, C., Lee, A., Jeong, D., Oh, J.G., Chaanine, et al., 2011. SUMO1-dependent modulation of SERCA2a in heart failure. Nature 477, pp. 601-606.

Kitazono, A. A. (2009). Improved gap-repair cloning method that uses oligonucleotides to target cognate sequences. Yeast, 26(9), 497-505.

Knyushko, T.V., Sharov, V.S., Williams, T.D., Schöneich, C., Bigelow, D.J. 2005. 2-Nitrotyrosine modification of SERCA2a in the aging heart: a distinct signature of the cellular redox environment. Biochemistry 44, pp. 13071-13081.

Kroczek, C., Lang, C., Brachs, S., Grohmann, M., Dutting, S., Schweizer, A., et al. (2010). Swiprosin-1/EFhd2 controls B cell receptor signaling through the assembly of the B cell receptor, syk, and phospholipase C gamma2 in membrane rafts. J Immunol, 184, 3665-3676.

Kühlbrandt, W., 2004. Biology, structure and mechanism of P-type ATPases. Nature Rev. Mol. Cell Biol. 5, 282–295.

Laskowski, R.A., Macarthur, M.W., Moss, D.S., Thornton, J.M., 1993. Procheck - a Program to Check the Stereochemical Quality of Protein Structures. J. Appl. Crystallogr. 26, pp. 283-291.

Laursen, M., Bublitz, M., Moncoq, K., Olesen, C., Möller, et al., 2009. Cyclopiazonic acid is complexed to a divalent metal ion when bound to the sarcoplasmic reticulum Ca2+-ATPase. J. Biol. Chem. 284, pp. 13513-13518.

Lee, V. M., Goedert, M., & Trojanowski, J. Q. (2001). Neurodegenerative tauopathies. Annu Rev Neurosci, 24, 1121-1159.

Lenoir, G., Menguy, T., Corre, F., Montigny, C., Pedersen, P. A., Thines, D., et al. (2002). Overproduction in yeast and rapid and efficient purification of the rabbit SERCA1a ca(2+)-ATPase. Biochimica Et Biophysica Acta, 1560(1-2), 67-83.

Leslie, A.G.W., 2006. The integration of macromolecular diffraction data. Acta Crystallogr. D Biol. Crystallogr. 62, pp. 48-57.

Levy, D., Seigneuret, M., Bluzat, A., Rigaud, J.-L. Evidence for proton countertransport by the sarcoplasmic reticulum Ca2+-ATPase during calcium transport in reconstituted proteoliposomes with low ionic permeabilità. J Biol Chem, 265 (1990), pp. 19524–19534

Lowry, O.H., Rosebrough, N.J., Farr, A.L., Randall, R.J., 1951. Protein measurement with the Folin phenol reagent. J. Biol. Chem. 193, pp. 265-275.

Ma, H., Lewis, D., Xu, C., Inesi, G., & Toyoshima, C. (2005). Functional and structural roles of critical amino acids within the"N", "P", and "A" domains of the Ca2+ ATPase (SERCA) headpiece. Biochemistry, 44(22), 8090-8100.

MacLennan, D. H. (2000). Ca2+ signalling and muscle disease. European Journal of Biochemistry / FEBS, 267(17), 5291-5297.

MacLENNAN, D. H., ASAHI, M., & TUPLING, A. R. (2003). The regulation of SERCA-type pumps by phospholamban and sarcolipin. Annals of the New York Academy of Sciences, 986(1), 472-480.

MacLennan, D. H., Brandl, C. J., Korczak, B. & Green, N. M., 1985. Amino-acid sequence of a Ca2+ + Mg2+-dependent ATPase from rabbit muscle sarcoplasmic reticulum, deduced from its complementary DNA sequence. Nature 316, 696−700

MacLennan, D.H. & Kranias, E.G., 2003. Phospholamban: a crucial regulator of cardiac contractility. Nat Rev Mol. Cell Biol., 4, pp. 566–577.

MacLennan, D.H., Brandl, C.J., Korczak, B., Green, N.M., 1985. Amino-acid sequence of a Ca2+ + Mg2+-dependent ATPase from rabbit muscle sarcoplasmic reticulum, deduced from its complementary DNA sequence. Nature 316, pp. 696-700.

Magro, M., Faralli, A., Baratella, B., Bertipaglia, I., Giannetti, S., Salviulo, G., Zboril, R., and Vianello F, 2012. Avidin Functionalized Maghemite Nanoparticles and Their Application for Recombinant Human Biotinyl-SERCA Purification. Langmuir 28 (43), 15392-15401.

Maruyama, K., MacLennan, D.H., 1988. Mutation of aspartic acid-351, lysine-352, and lysine-515 alters the Ca2+ transport activity of the Ca2+-ATPase expressed in COS-1 cells. Proc. Natl. Acad. Sci. U. S. A. 85, pp. 3314-3318.

McCoy, A.J., Grosse-Kunstleve, R.W., Adams, P.D., Winn, M.D., Storoni, L.C., et al., 2007. Phaser crystallographic software. J. Appl. Crystallogr. 40, pp. 658-674.

Meissner, G., Conner, G.E., Fleischer, S., 1973. Isolation of sarcoplasmic reticulum by zonal centrifugation and purification of Ca2+-pump and Ca2+-binding proteins. Biochim. Biophys. Acta 298, pp. 246-269.

Moller, J. V., Lenoir, G., Le Maire, M., Juul, B. S., & Champeil, P. (2003). Proteolytic studies on the transduction mechanism of sarcoplasmic reticulum Ca2+-ATPase: Common features with other P-type ATPases. Annals of the New York Academy of Sciences, 986, 82-89.

Moller, J. V., Lenoir, G., Marchand, C., Montigny, C., le Maire, M., Toyoshima, C., et al. (2002). Calcium transport by sarcoplasmic reticulum ca(2+)-ATPase. role of the A domain and its C-terminal link with the transmembrane region. The Journal of Biological Chemistry, 277(41), 38647-38659.

Moller, J. V., Nissen, P., Sorensen, T. L., & le Maire, M. (2005). Transport mechanism of the sarcoplasmic reticulum Ca2+ -ATPase pump. Current Opinion in Structural Biology, 15(4), 387-393.

Moncoq, K., Trieber, C.A., Young, H.S., 2007. The molecular basis for cyclopiazonic acid inhibition of the sarcoplasmic reticulum calcium pump. J. Biol. Chem. 282, pp. 9748-9757.

Obara, K., Miyashita, N., Xu, C., Toyoshima, I., Sugita, Y., et al., 2005. Structural role of countertransport revealed in Ca(2+) pump crystal structure in the absence of Ca(2+). Proceedings of the National Academy of Sciences of the United States of America 102, pp. 14489-14496.

Odermatt, A., Barton, K., Khanna, V.K., Mathieu, J., Escolar, D., et al., 2000. The mutation of Pro789 to Leu reduces the activity of the fast-twitch skeletal muscle sarco(endo)plasmic reticulum Ca2+ ATPase (SERCA1) and is associated with Brody disease. Hum. Genet. 106, pp. 482-491.

Olesen, C., Picard, M., Winther, A. M., Gyrup, C., Morth, J. P., Oxvig, C., et al. (2007). The structural basis of calcium transport by the calcium pump. Nature, 450(7172), 1036-1042.

Olesen, C., Picard, M., Winther, A. M., Gyrup, C., Morth, J. P., Oxvig, C., et al. (2007). The structural basis of calcium transport by the calcium pump. Nature, 450(7172), 1036-1042.

Olesen, C., Picard, M., Winther, A.M., Gyrup, C., Morth, J.P., et al., 2007. The structural basis of calcium transport by the calcium pump. Nature 450, pp. 1036-1042.

Olesen, C., Sorensen, T. L., Nielsen, R. C., Moller, J. V. & Nissen, P., 2004. Dephosphorylation of the calcium pump coupled to counterion occlusion. Science 306, 2251–2255.

Picard, M., Jensen, A. M., Sorensen, T. L., Champeil, P., Moller, J. V., & Nissen, P. (2007). Ca2+ versus Mg2+ coordination at the nucleotide-binding site of the sarcoplasmic reticulum Ca2+-ATPase. Journal of Molecular Biology, 368(1), 1-7.

Picard, M., Jensen, L.A.-M., Sørensen, T. L.-M., Champeil, P., Møller, J.V. et al. 2007. Ca2+ versus Mg2+ coordination at the nucleotide-biding site of the sarcoplasmic reticulum Ca2+-ATPase. J. Mol. Biol. 368, pp. 1-7.

Post, R. L., Hegyvary, C. & Kume, S., 1972. Activation by adenosine triphosphate in the phosphorylation kinetics of sodium and potassium ion transport adenosine triphosphatase. J. Biol. Chem. 247, 6530−6540.

Rath, A., Glibowicka, M., Nadeau, V. G., Chen, G., & Deber, C. M. (2009). Detergent binding explains anomalous SDS-PAGE migration of membrane proteins. Proceedings of the National Academy of Sciences, 106(6), 1760-1765.

Sacchetto, R., Bertipaglia, I., Giannetti, S., Cendron, L., Mascarello, F., Damiani, E., et al. (2012). Crystal structure of sarcoplasmic reticulum Ca2+-ATPase (SERCA) from bovine muscle. Journal of Structural Biology, 178(1), 38-44.

Sacchetto, R., Bovo, E., Donella-Deana, A., Damiani, E., 2005. Glycogen- and PP1c-targeting subunit GM is phosphorylated at Ser48 by sarcoplasmic reticulum-bound Ca2+-calmodulin protein kinase in rabbit fast twitch skeletal muscle. J. Biol. Chem. 280, pp. 7147-7155.

Sacchetto, R., Testoni, S., Gentile, A., Damiani, E., Rossi, et al., 2009. A defective SERCA1 protein is responsible for congenital pseudomyotonia in Chianina cattle. Am. J. Pathol. 174, pp. 565-573.

Sacchetto, R., Testoni, S., Gentile, A., Damiani, E., Rossi, M., Liguori, R., et al. (2009). A defective SERCA1 protein is responsible for congenital pseudomyotonia in chianina cattle. The American Journal of Pathology, 174(2), 565-573.

Sarkadi, B., Enyedi, A., Földes-Papp, Z., & Gárdos, G. (1986). Molecular characterization of the in situ red cell membrane calcium pump by limited proteolysis. Journal of Biological Chemistry, 261(20), 9552-9557.

Sharov, V.S., Galeva, N.A., Knyushko, T.V., Bigelow, D.J., Williams, T.D., et al., 2002. Two-dimensional separation of the membrane protein sarcoplasmic reticulum Ca-ATPase for high-performance liquid chromatography-tandem mass spectrometry analysis of posttranslational protein modifications. Anal. Biochem. 308, pp. 328-335

Sørensen, T. L., Møller, J. V. & Nissen, P., 2004.Phosphoryl transfer and calcium ion occlusion in the calcium pump. Science 304, 1672−1675.

Sorensen, T., Moller, J.V., Nissen, P., 2004. Phosphoryl transfer and calcium ion occlusion in the calcium pump. Science 304, pp. 1672-1675.

Takahashi, M., Kondou, Y., Toyoshima, C., 2007. Interdomain communication in calcium pump as revealed in the crystal structures with transmembrane inhibitors. Proc. Natl. Acad. Sci. U. S. A. 104, pp. 5800-5805.

Thylur, R. P., Kim, Y. D., Kwon, M. S., Oh, H. M., Kwon, H. K., Kim, S. H., et al. (2009). Swiprosin-1 is expressed in mast cells and up-regulated through the protein kinase C beta I/eta pathway. J Cell Biochem, 108, 705-715.

Totland, G.K., Kryvi, H., 1991. Distribution patterns of muscle fibre types in major muscles of the bull (Bos taurus). Anat. Embryol. (Berl) 184, pp. 441-450.

Toyoshima, C. (2009). How Ca2+-ATPase pumps ions across the sarcoplasmic reticulum membrane. Biochimica Et Biophysica Acta, 1793(6), 941-946.

Toyoshima, C. & Mizutani, T., 2004.Crystal structure of the calcium pump with a bound ATP analogue. Nature 430, 529−535.

Toyoshima, C. & Nomura, H., 2002. Structural changes in the calcium pump accompanying the dissociation of calcium. Nature 418, 605−611.

Toyoshima, C., & Inesi, G. (2004). Structural basis of ion pumping by Ca2+-ATPase of the sarcoplasmic reticulum. Annual Review of Biochemistry, 73, 269-292.

Toyoshima, C., & Mizutani, T. (2004). Crystal structure of the calcium pump with a bound ATP analogue. Nature, 430(6999), 529-535.

Toyoshima, C., Inesi, G., 2004. Structural basis of ion pumping by CA(2+)-ATpase of the sarcoplasmic reticulum. Annu. Rev. Biochem. 73, pp. 269-292.

Toyoshima, C., Mizutani, T., 2004. Crystal structure of the calcium pump with a bound ATP analogue. Nature 430, pp. 529-535.

Toyoshima, C., Nakasako, M., Nomura, H. & Ogawa, H., 2000. Crystal structure of the calcium pump of sarcoplasmic reticulum at 2.6 Å resolution. Nature 405, 647–655.

Toyoshima, C., Nakasako, M., Nomura, H., Ogawa, H., 2000. Crystal structure of the calcium pump of sarcoplasmic reticulum at 2.6 Å resolution. Nature 405, pp. 647-655.

Toyoshima, C., Nomura, H., 2002. Structural changes in the calcium pump accompanying the dissociation of calcium. Nature 418, pp. 605-611.

Toyoshima, C., Yonekura, S., Tsueda, J., Iwasawa, S., 2011. Trinitrophenyl derivatives bind differently from parent adenine nucleotides to Ca2+-ATPase in the absence of Ca2+. Proc. Natl. Acad. Sci. U. S. A. 108, pp. 1833-1838.

Vafiadaki, E., Papalouka, V., Arvanitis, D., A., Kranias, E., G., Sanoudou, D., 2009. The role of SERCA2a/PLN complex, Ca2+ homeostasis, and anti-apoptotic proteins in determining cell fate. Pflügers Archiv - European Journal of Physiology, Vol. 457(3), pp 687-700.

Vandecaetsbeek, I., Christensen, S. B., Liu, H., Van Veldhoven, P. P., Waelkens, E., Eggermont, J., et al. (2011). Thapsigargin affinity purification of intracellular P(2A)-type ca(2+) ATPases. Biochimica Et Biophysica Acta,

Vega, I. E., Traverso, E. E., Ferrer-Acosta, Y., Matos, E., Colon, M., Gonzalez, J., et al. (2008). A novel calcium-binding protein is associated with tau proteins in tauopathy. J Neurochem, 106, 96-106.

Vuadens, F., Rufer, N., Kress, A., Corthesy, P., Schneider, P., & Tissot, J. D. (2004). Identification of swiprosin 1 in human lymphocytes. Proteomics, 4, 2216-2220.

Wang, S. -Q., Song, L. -S., Lakatta, E. G. & Cheng, H. Ca2+ signalling between single L-type Ca2+ channels and ryanodine receptors in heart cells. Nature 410, 592–596 (2001).

Winther, A.L., Liu, H., Sonntag, Y., Olesen, C., Le Maire, M., et al., 2010. Critical roles of hydrophobicity and orientation of side chains for inactivation of sarcoplasmic reticulum Ca2+-ATPase with thapsigargin and thapsigargin analogs. J. Biol. Chem. 285, pp. 28883-28892.

Xu, C., Rice, W.J., He, W., Stokes, D.L., 2002. A structural model for the catalytic cycle of Ca(2+)-ATPase. J. Mol. Biol. 316, pp. 201-211.

Zuo, S., & Lundahl, P. (2000). A micro-bradford membrane protein assay. Analytical Biochemistry, 284(1), 162-164.

ACKNOWLEDGMENTS

I would like to express my sincere gratitude to my supervisor Prof. Giuseppe Zanotti for his invaluable support and assistance during my PhD program. I can never thank him enough for the opportunity to know and enter into the amazing world of crystallography.

I want to extend my special thanks to Dr Ilenia Bertipaglia for shared her personal experience with me and for all nice time spent together. Without her constant support and encouragement, this dissertation could not have been written. Thank you!

A special thank to Dr. Laura Cendron for the great help in assisting my research experiments with enthusiasm and kindness.

Thanks to all the colleagues with whom I had the opportunity to work: Sandra, Giorgia, Lorenza, Munan, Sara, and Marco. I would like to thanks also Laura Dondini for her physiological and technical assistance during the achievement of this dissertation.

I finally want to thank my parents and friends that have always encouraged me to pursue my scientific career.